Scale coupling and upscaling techniques in elastostatics and elastodynamics in random media

Régis Cottereau

Université Pierre et Marie Curie (Paris-6)

Habilitation à Diriger des Recherches

présentée en vue de l'obtention du diplôme par

Régis COTTEREAU

Couplages et transitions entre échelles en élastostatique et élastodynamique en milieu aléatoire

Scale coupling and upscaling techniques in elastostatics and elastodynamics in random media

Thèse soutenue le 1er septembre 2016 devant le jury composé de :

M.	Claude Boutin	ENTPE	(Examinateur)
M.	Yann Capdeville	Université de Nantes	(Rapporteur)
Mme	Lori Graham-Brady	Johns Hopkins University (USA)	(Rapporteur)
M.	Djimédo Kondo	Université Pierre et Marie Curie	(Président)
M.	Anthony Nouy	École Centrale de Nantes	(Rapporteur)
M.	Serge Prudhomme	École Polytechnique Montréal (Canada)	(Examinateur)
M.	Karam Sab	Ecole des Ponts-ParisTech & IFFSTAR	(Examinateur)
M.	Julien Yvonnet	Université Paris-Est	(Examinateur)

Contents

Introduction 1

The mechanical behavior of homogeneous solids and structures is well understood, at least in the low frequency range, for regular geometries and limited loading amplitudes. Only a few mechanical parameters are required and computations can be performed very efficiently with Finite Element methods, for instance. When mechanical properties are heterogeneous and smaller geometrical details appear, the parameterization of the mechanical problems becomes more intricate, both in terms of number of degrees of freedom and number of parameters to be defined. The computational cost increases dramatically and many engineering systems cannot be simulated. In particular regimes, however, homogenization or other asymptotic behaviors come into play. Coarser (and well justified mathematically) models can then be used, providing both for cheaper computational approaches and simpler physical analyses of the behavior of the mechanical systems.

This manuscript discusses some of these particular situations, referred to as multiscale mechanical problems. Two aspects will be considered: (i) construction of upscaled (homogenized) models and parameters from the knowledge of a micro-scale model, and (ii) numerical coupling of a given micro-scale model with its upscaled counterpart. This report focuses mainly on stochastic models, for which parameters, geometry, loading and/or boundary conditions are modeled as random fields or variables. The solutions of the micro-scale models are then stochastic, although the upscaled models are often deterministic.

The main objective of this document is to present the research I conducted during the last thirteen years (from the beginning of my Ph.D. studies). However, this research needed to be put in perspective. A lot of the work presented in this document is therefore not mine, but necessary to fill the gaps in between aspects and research areas I considered. The final overall impression is therefore maybe closer to a general review in the fields of coupling and upscaling of stochastic models rather than a report on the research I personally conducted. To balance this impression, my personal publications are highlighted in blue color and listed in a separate bibliography.

1.1 Examples of stochastic multiscale problems

Before defining more precisely the notion of multiscale problems (Section 1.2), we describe in this section a few examples of multiscale engineering problems. They should be seen as the motivation for the development of the mathematical and numerical techniques described in the remainder of the document. We introduce for each of them the governing equations and the scientific and technological issues, as well as the characteristic dimensions that control their multiscale character: the wave length λ, the characteristic size over which the material properties fluctuate ℓ_c (or correlation length in a stochastic setting) and the propagation length L (or source-observation distance).

1.1.1 Wave propagation in geophysical media

Wave propagation in geophysical media has a wide range of applications. At the global scale (see Figure 1.1), where $\lambda \approx 100$ km, $\ell_c \approx 100 - 10000$ km and $L \approx 10000$ km, geophysicists are interested in understanding the nature, properties and evolution of the deep Earth, locating the epicenter of earthquakes and estimating the large scale influence of seismic events. At the regional scale (see Figure 1.2), where $\lambda \approx 100$ m, $\ell_c \approx 0.1 - 1000$ m and $L \approx 1000$ m, seismic tomography is heavily used by the petroleum and mining industries to locate potential exploitation sites.

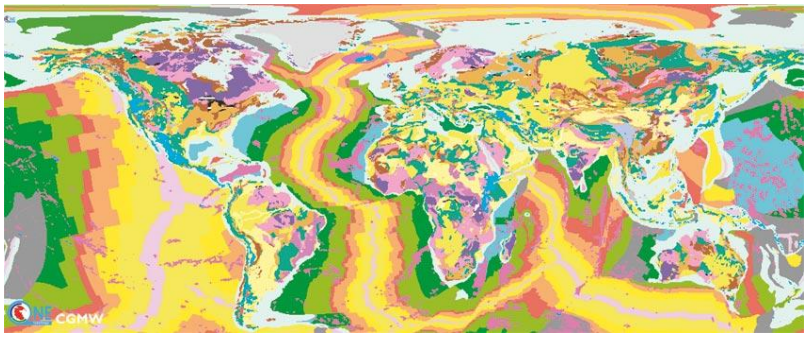

Figure 1.1 – *Example of horizontal heterogeneity at the global scale: geology map of the surface of the Earth. Taken from Charles (2008).*

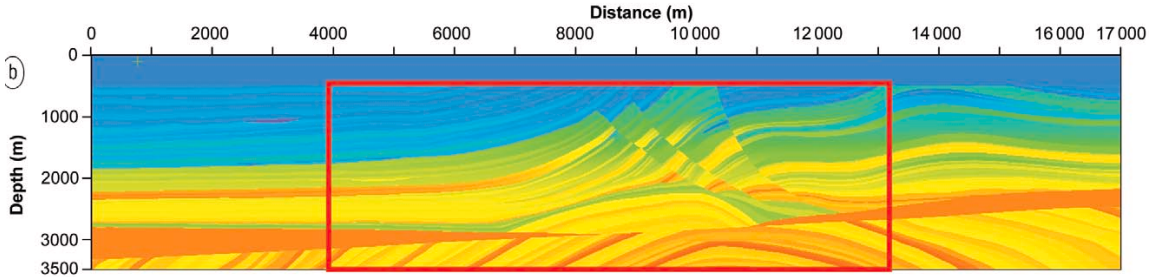

Figure 1.2 – *Example of vertical heterogeneity at the local scale: P-wave velocity for the Marmousi2 model. Taken from Martin et al. (2006). The red box indicates the correspondance with a previous Marmousi model.*

Elastic wave propagation describes the evolution (in a domain Ω and over a time interval $(0, T)$) of a displacement field $\mathbf{u}(\mathbf{x}, t)$ driven by the following equation:

$$\rho(\mathbf{x})\ddot{\mathbf{u}}(\mathbf{x}, t) - \nabla \cdot \sigma(\mathbf{x}, t) = \mathbf{f}(\mathbf{x}, t) \tag{1.1}$$

when submitted to loading $\mathbf{f}(\mathbf{x}, t)$ and initial conditions $\mathbf{u}(\mathbf{x}, t = 0) = \mathbf{u}_0(\mathbf{x})$ and $\dot{\mathbf{u}}(\mathbf{x}, t = 0) = \mathbf{v}_0(\mathbf{x})$. The stress tensor $\sigma(\mathbf{x}, t) = \mathbb{C}(\mathbf{x}) : \epsilon(\mathbf{x}, t)$ is related to the strain tensor $\epsilon = \nabla \otimes_s \mathbf{u}(\mathbf{x}, t)$ through the constitutive tensor $\mathbb{C}(\mathbf{x})$. At the free surface Γ_{fs}, a homogeneous Neumann boundary condition $\sigma \cdot \mathbf{n} = \mathbf{0}$ is considered. The material behavior is often considered as isotropic. The wave equation is then parameterized with the P-wave velocity c_P and S-wave velocity c_S. Based on laboratory experiments for materials composing the continental crust (Christensen and Mooney 1995, Christensen 1996, Kenter et al. 2007), characteristic values of the parameters in the crust are $c_P/c_S = 1.768 \approx \sqrt{3}$. Using piecewise-homogeneous models, and after inverting for the wave velocities, experimental observations of the initial phase of the seismograms and the low frequency part of their spectrum (below approximately 1 Hz) can often be well reproduced (Nolet 2008, Weber and Münch 2014).

However, higher frequency signals and the later portions of the seismograms have proven more difficult to model. Indeed, the composite mineralogy of the crust and the presence of fractures of various sizes induce large fluctuations around the average values of the mechanical parameters (Simmons and Wang 1971, Moos and Zoback 1983). For instance, values greater than $c_P/c_S = 2.4$ have been found in some sedimentary rocks (Kenter et al. 2007). These heterogeneities at different scales have a complex influence on the waveforms (Hong et al. 2005). Scatterers transfer part of the coherent energy into incoherent signal. This results in an apparent attenuation (Wu 1982, Frenje and Juhlin 2000) and the creation of a seemingly random wave train behind the coherent pulses: the so-called *coda* (Herraiz and Espinosa 1987). As can be observed on Figure 1.3, the duration of this coda is much larger than that of the seismic event that created it and its shape is relatively independent of the seismic source. Whereas the first arrivals are different from one station to the other, the amplitude of the signals at long lapse times is identical for all source-to-station distances. The directionality of the coda is also more isotropic than that of the coherent pulses (Paul et al. 2005, Schisselé et al. 2005, Imperatori and Mai 2013, Galluzzo et al. 2015). The scattering character of the coda was first identified in the pioneering works of Aki (1969) and Aki and Chouet (1975). Considering the characteristic dimensions mentionned

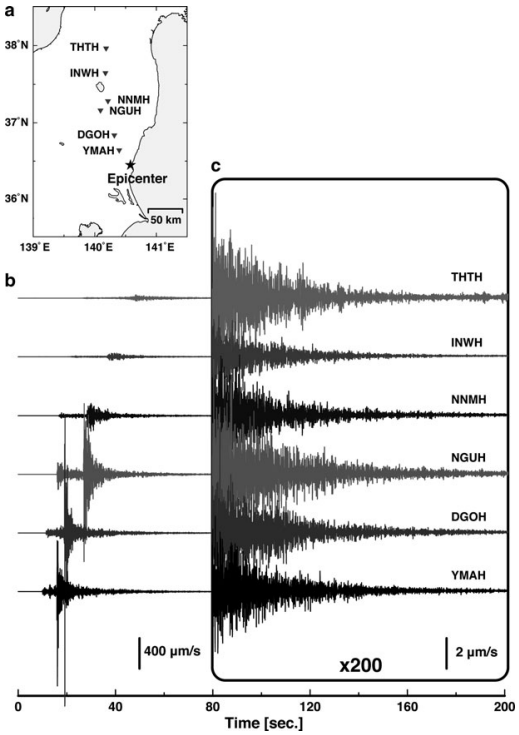

Figure 1.3 – *(a) Epicenter (star) of an MW* 4.8 *earthquake with* 55.3 *km in focal depth and Hi-net stations (reversed triangles) in Honshu, Japan. (b) Velocity seismograms (horizontal transverse component) arranged from bottom to top by increasing epicentral distance, where the gain is the same for all the traces. (c) Magnification of 200 times. Taken from Sato et al. (2012).*

above, random models offer a powerful tool for parameterizing the heterogeneity and discussing their influence on the wave field.

Using well-log data collected in various areas of the world, several authors (Wu et al. 1994, Kneib 1995, Holliger 1996, Shiomi et al. 1997) have constructed random models for these fields of mechanical properties (see Fig. 1.4), including correlation models between P- and S-wave velocities (Birch 1961). Most of these authors measure a relative standard deviation close to 5%, but the consensus is not so clear about the correlation length, which is measured between 1 m and 100 m. Besides this direct evidence based on well-log data, hundreds of travel-time tomography campaigns over the years have proven that the crust is heterogeneous on scales of 1 km to 10 km (Schilt et al. 1979, Aki and Lee 1976, Aki et al. 1976, Zhang and Thurber 2003, Zhao et al. 2009, Takemura et al. 2015). Combining regional and global methods, Meschede and Romanowicz (2015) identified the power-spectrum of heterogeneities over the range 200-20000 km, while Nakata and Beroza (2015) fit a power-spectrum centered on 100 m. In geotechnics, Cone Penetrometer Tests (Fenton 1999) and Spectral Analysis of Surface Waves tests (Schevenels et al. 2008) have identified correlation lengths of the order of 1 m in the vertical direction and of $10 - 100$ m in the horizontal direction (see a review of various studies in Phoon and Kulhawy (1999)). Using these random models and powerful 3D elastic wave propagation solvers, it becomes possible to obtain reliable wave fields for increasingly higher frequency and larger distances (see for instance Pitarka and Ichinose (2009), O'Brien and Bean (2009), Hartzell et al. (2010), Kumagai et al. (2011), Takemura and Furumura (2013), Imperatori and Mai (2013), Takemura et al. (2015)). Unfortunately, these direct methods remain too expensive to use for the characteristic dimensions mentioned at the beginning of this section.

From both experimental observations and numerical simulations, it is clear that the displacement field in the coda is extremely sensitive to small fluctuations of the mechanical parameters, geometry and loading. It hence cannot be considered a relevant parameter for identification. Contrarily, the amplitude of the coda appeared over the years as a stable regional feature, and researchers focused their attention on the diffusion model originally proposed by Aki and Chouet (1975). In the single scattering approximation, this model describes the evolution of the energy density $a(\mathbf{x}, t, \omega)$ in a unit frequency band around ω as a diffusion equation with diffusivity D

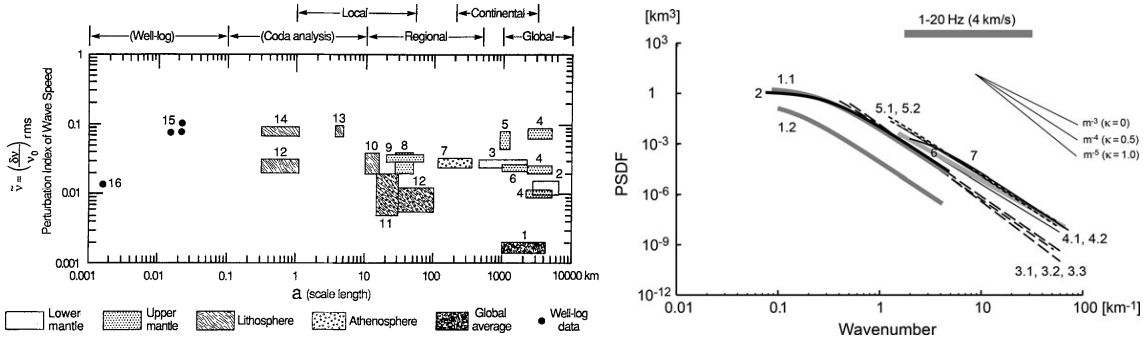

Figure 1.4 – *(left) Strength-scale distribution of heterogeneities in the Earth (taken from Wu and Aki (1988b), based on data from the literature, see Wu and Aki (1988b) for the full list of references, indicated by small numbers). (Right) Measurements of the power spectral density function of the fractional velocity fluctuation in the lithosphere and mantle in different regions of the world and at different depths, based on P and S waves envelopes (taken from Sato et al. (2012), based on data taken from a variety of papers, see Sato et al. (2012) for details).*

and intrinsic attenuation Q_i:

$$\frac{\partial a}{\partial t} = \nabla \cdot D \nabla a - \frac{\omega}{Q_i} a. \tag{1.2}$$

Its solution (in 3D) reads $a(\mathbf{x}, t, \omega) = a_0(\omega) \exp(-|\mathbf{x}|^2/4Dt - \omega t/Q_i)/(4\pi Dt)^{3/2}$, where $a_0(\omega)$ is the total input energy. More complex models have also been proposed based on a multiple scattering setting. In particular, the so-called radiative transfer equations, as well as multiple-scattering diffusion model have been widely studied (see Ryzhik et al. (1996) for the theory, Gaebler et al. (2015) for an example of identification and Shearer (2007) for the specific case of the deep Earth). Subsequently, many experimental campaigns have focused on the exponential decay rate of the envelopes, denoted as coda attenuation Q_c^{-1} (see for instance (Nishigami 2000, Calvet et al. 2013) and a review of identified values in (Sato et al. 2012, Chapter 3)). These models proved very efficient to simulate wave envelopes at large distances (Sato et al. 2012)).

Scientifically, there remains to clarify the relation between the diffusion parameters and the statistics of the wave velocities, in particular when considering fully elastic models, for which P- and S-wave energies are coupled, or when scale separation cannot be assumed, as well as to derive comprehensive inversion schemes that take into account both the coherent and incoherent parts of the signal. Also, due to geological formation processes and other phenomena, anisotropy is very important in the crust (Helbig and Thomsen 2005, Tsvankin et al. 2010). This makes the relation between wave propagation parameters and diffusion parameters much more complex. As we have observed enormous differences between propagation in isotropic and anisotropic media for the same level of fluctuation of the constitutive tensor (Ta et al. 2010), this feature can however not be ignored. Indeed, Fig. 1.5 illustrates wave fields obtained by propagation within two heterogeneous media, with similar average isotropic behavior and fluctuations levels, but locally isotropic or anisotropic. The description of the two wave fields is clearly different although the difference between the two media is extremely small in amplitude.

1.1.2 Vibrations in a ballasted railway track

The ballast is the uppermost layer of the railway track superstructure (Fig. 1.6). It is made of coarse crushed stone, whose size distribution lies in the range $\ell_c \approx 25 - 50$ mm (Fig. 1.7). Depending on the velocity of the trains, the wavelength in the ballast lies in the range $\lambda \approx 1 - 10$ m. This ballast layer plays an important role in the transmission and repartition of static and dynamic train loads ($L \approx 40$ cm), the absorption of mechanical and acoustical vibrations ($L \approx 100$ m), and the drainage of rain water (Indraratna et al. 2011). The noise and vibration impact on the environment can be important for all types of trains: heavy freight coaches, whose low frequency influence in the soil carries far away; high-velocity trains, that generate high amplitude excitations; and even tramways, which stand very close to surrounding buildings. With time and the repeated passage of trains, the ballast layer settles down. This induces a leveling defect of the track and may force the train companies to locally reduce the velocity of the passing trains for the comfort and security of passengers. These defects are therefore regularly controlled, and

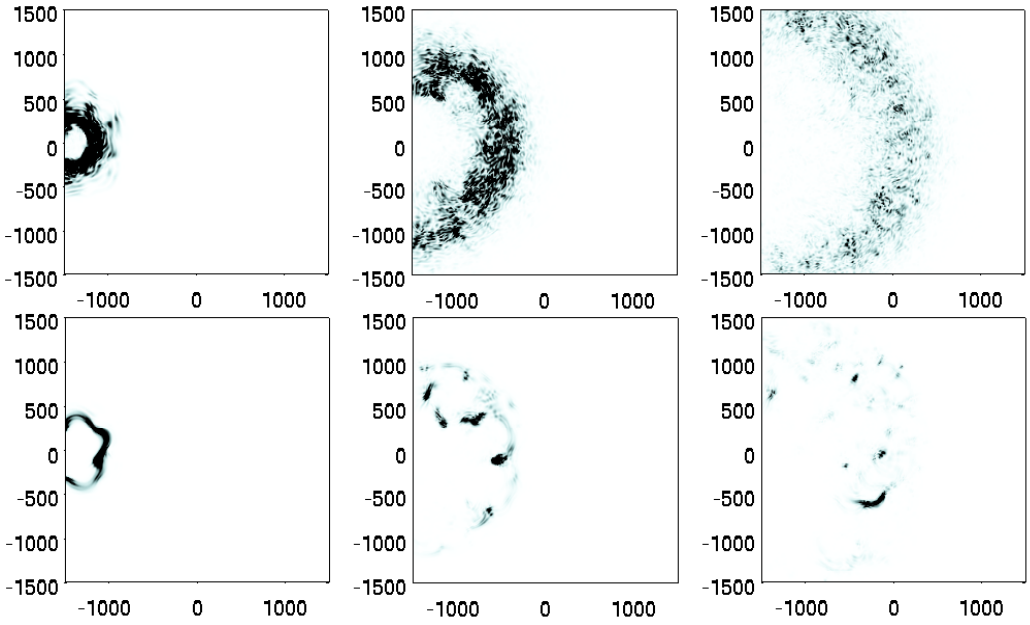

Figure 1.5 – *Temporal evolution (from left to right) of the velocity amplitude at the free surface of random half-spaces with the same isotropic average and strength of heterogeneities σ^2. The upper medium is locally anisotropic everywhere while the lower medium is locally isotropic everywhere. Taken from Ta et al. (2010).*

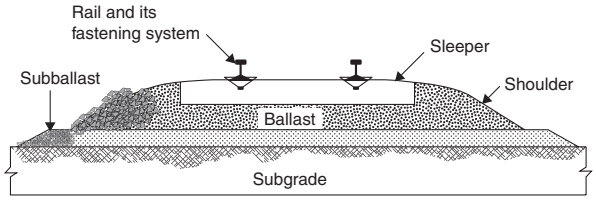

Figure 1.6 – *Typical section of a ballasted railway track. Taken from Indraratna et al. (2011)*

costly maintenance operations are organized. The modeling of the ballast aims at improving the understanding of the mechanical behavior of the track system and providing clues to mitigate the issues listed above (see for instance Heckl et al. (1996), Connolly et al. (2014) or Panunzio et al. (2016)). It represents a challenging task because the ballast exhibits various distincts behaviors (such as transition between fluid-like and solid-like behavior) depending on the applied stresses and strains. The important heterogeneity of the granular ballast is also challenging in dynamical observations because relative amplitudes of the coherent and coda parts of the signal are heavily dependent on the ratio $\epsilon = \lambda / \ell_c$, as illustrated in Fig. 1.8.

The relative displacements between two grains in the ballast are much larger in general than the strains within one grain. Models can then be constructed (Lim and McDowell 2005) where each grain of the ballast is a rigid body with a complex shape (Lu and McDowell 2007, Ahmed et al. 2015). At this local scale, the static variables are the contact forces $\mathbf{F}_\ell^k$ and moments $\mathbf{M}_\ell^k$ between grains k and ℓ and the kinematic variables are the rigid body movements of the grains, parameterized by the translation $\mathbf{u}_k$ and rotation $\boldsymbol{\theta}_k$ of grain k. They verify

$$\sum_\ell \mathbf{F}_\ell^k = m_k \ddot{\mathbf{u}}_k \quad \forall k, \quad \sum_\ell \mathbf{M}_\ell^k = \mathbf{I}_k \ddot{\boldsymbol{\theta}}_k \quad \forall k, \quad (\dot{\mathbf{u}}_k - \dot{\mathbf{u}}_\ell) \cdot \mathbf{n}_\ell^k \leq 0 \quad \forall k, \ell \tag{1.3}$$

where m_k and $\mathbf{I}_k$ are respectively the mass and inertia tensor of grain k and $\mathbf{n}_\ell^k$ is the normal exterior to grain k at the contact point with grain ℓ. These equations are complemented with friction laws that control the interaction of each grain with its neighbors. These models have given rise to various numerical implementations, among which the Discrete Element Method (DEM) (Cundall and Strack 1979) and the Non-Smooth Contact Dynamics method (NSCD) (Moreau 1989). In the DEM, the non-interpenetration condition at the interface between two grains is relaxed through a stiff non-linear repulsion law. This gives rise to an explicit scheme in time, which requires

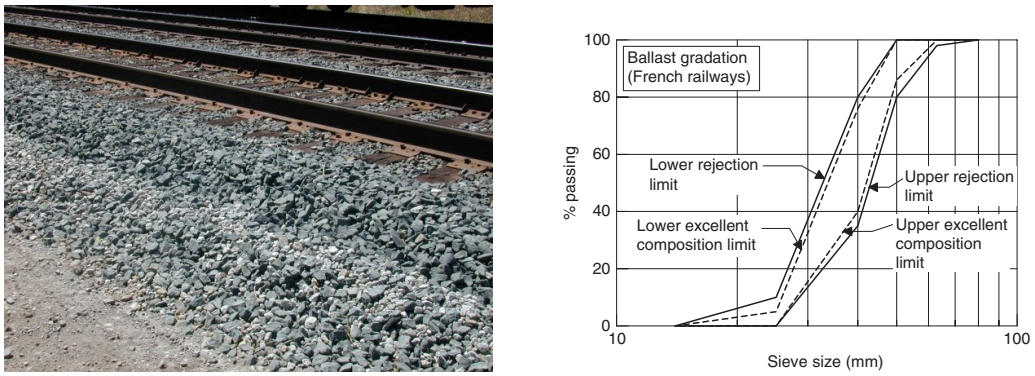

Figure 1.7 – *(Left) ballasted railway track in California*[1]*. (Right) French standard ballast gradations (taken from Indraratna et al. (2011)).*

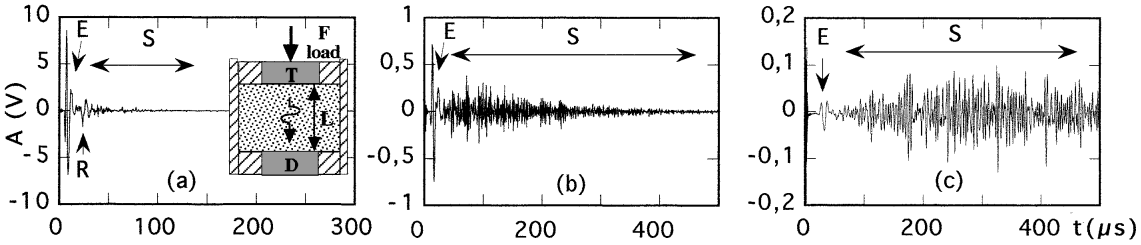

Figure 1.8 – *Ultrasonic signals measured by a 12-mm-diameter transducer in glass packings of different sizes under external normal stress $P = 0.75$ MPa at (a) $d = 0.2 - 0.3$ mm, (b) $d = 0.4 - 0.8$ mm and (c) $d = 1.5 \pm 0.15$ mm. E and R correspond, respectively, to the coherent ballistic pulse and its echo reflected from the bottom and top surfaces. S is associated with multiply scattered sound waves. The inset of (a) shows a schematic diagram of the apparatus: T and D are, respectively, the ultrasonic emitter and detector. Note the different time scale in (a). Taken from Jia et al. (1999).*

very small time steps and needs to handle the changes in the topology. The NSCD method can deal with multiple contacts and velocity changes within a single time step and reformulates the non-interpenetration condition as a quadratic optimization problem. It yields an implicit scheme, which remains stable for larger time steps, although the scalability of the parallel implementations of these models is not sufficient (Renouf et al. 2004, Thi Minh Phuong et al. 2011, Alart et al. 2012). The results obtained with these granular approaches are able to reproduce the solid to liquid transition and the inelastic deformations of the ballast (Radjai et al. 1996; 1998, Azéma et al. 2009) as well as the seemingly random patterns of contact forces (Liu et al. 1995, Bagi 2003) that can be observed experimentally at that scale (Drescher and de Josselin de Jong 1972). Because of the numerical issues mentioned above, however, these models cannot reproduce dynamical phenomena involving the passage of a train over a large portion of a track. Also, the requirement of inputing a precise geometry (Shin and Santamarina 2013) and initial position of the seemingly random assembly of grains is straining for most industrial applications, although large databases of digitized ballast grains have been created (Azéma et al. 2009).

An alternative approach consists in modeling the ballast as a continuous medium, using the equation (1.1), and considering the stress tensor $\sigma(\mathbf{x}, t)$ as the static variable and the displacement field $\mathbf{u}(\mathbf{x}, t)$ as the kinematical variable. To accommodate both solid and fluid behaviors, a viscoelastic constitutive relation can for instance be proposed:

$$\sigma = -\mathrm{p}\mathbf{I} + 2\mu\left(\epsilon - \frac{\mathrm{Tr}\epsilon}{3}\mathbf{I}\right) + \eta\dot{\epsilon}, \tag{1.4}$$

where p is the pressure[2], $\dot{\epsilon}$ is the strain rate and η is the (dynamic) viscosity. For incompressible materials, this relation is complemented by $\nabla \cdot \mathbf{u} = \mathrm{Tr}\epsilon = 0$, while we have $\mathrm{p} = -(\lambda + 2\mu/3)\mathrm{Tr}\epsilon$ for compressible materials. The stress tensor can be derived from the contact forces network (Weber 1966, Satake 1968, Bardet and Vardoulakis 2001, Moreau 2001, de Saxcé et al. 2004, Nguyen et al. 2012) and the strain tensor can be evaluated from the displacements of the

[1] taken from `http://www.zscale.org/`.

[2] To keep with the classical notations in mechanical engineering, tractions are assumed positive.

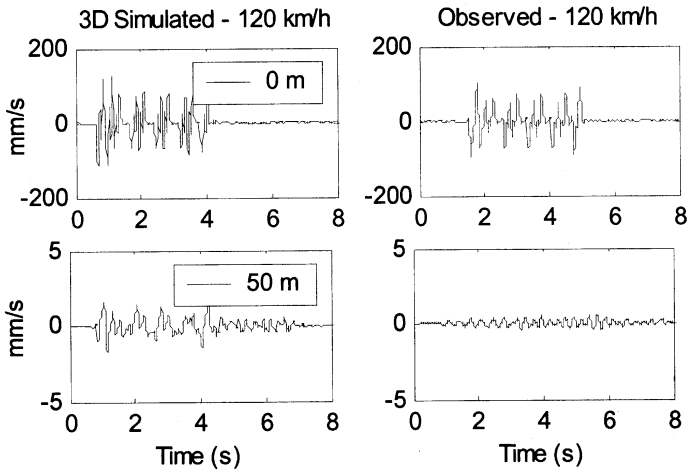

Figure 1.9 – *Comparison of 3D simulated vertical velocities with observations on and at 50 m from the track. Taken from Paolucci et al. (2003).*

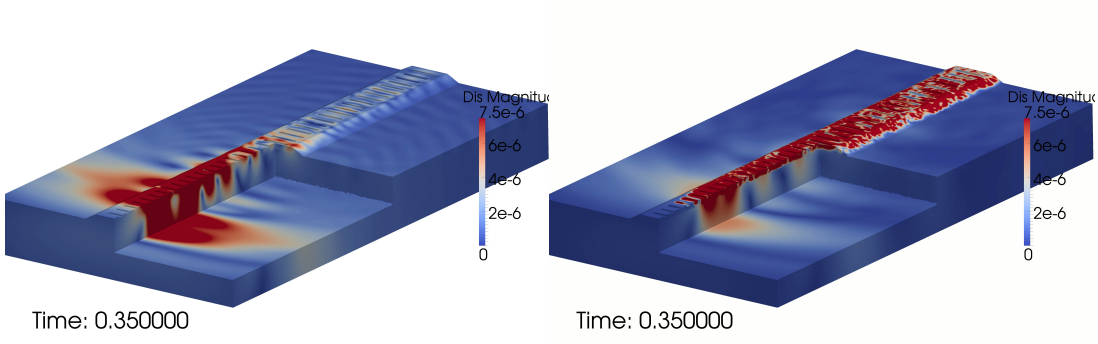

Figure 1.10 – *Localization in a ballasted railway track: comparison between the amplitude of the velocity field resulting from a moving load for a homogeneous (left) or heterogeneous (right) ballast layers. Taken from de Abreu Corrêa et al. (2016).*

grains (Tsuchikura and Satake 1998, Kuhn 1999, Cambou et al. 2000, Bagi 2006, Rothenburg and Kruyt 2009, Durán et al. 2010), but the relation between the parameters of the continuum and granular models is still a difficult question, except in some geometrically simplified settings. For instance, homogenization of random packings of spheres has been considered in Brandt (1955), Digby (1981), Walton (1987), Chang and Lun (1992), Chang et al. (1995), Jenkins et al. (2005), Agnolin and Roux (2008). Because they allow to simulate larger ballasted tracks as well as their surrounding environnement, these approaches have been preferred for dynamic analyses, where the influence of the passing train on the environment is evaluated (Paolucci et al. 2003, Lombaert et al. 2006). Unfortunately, large amplitude differences are found between the simulated and measured accelerations, in particular away from the track (see Figure 1.9).

To retain the capability of these continuum models to simulate wave fields over large distances while retaining some of the heterogeneity of the force network which is essential for the reproduction of its mechanical behavior, we recently introduced a heterogeneous continuum approach (see Fig. 1.10 and de Abreu Corrêa et al. (2016)). The Young's modulus is modeled as a random field whose statistical parameters are either identified from granular simulations or obtained from geometrical data such as the average grain size. The heterogeneities in the medium create an apparent damping that is compatible with the observations of Figure 1.9.

1.1.3 Damage in polycrystalline materials

Polycrystalline materials are random assemblies of crystalline grains. Within each grain, the orientation of the lattice is homogeneous, while pileups of dislocations (linear defects) at the grain boundaries induce large disorientations between neighboring grains (see Fig. 1.11). They include

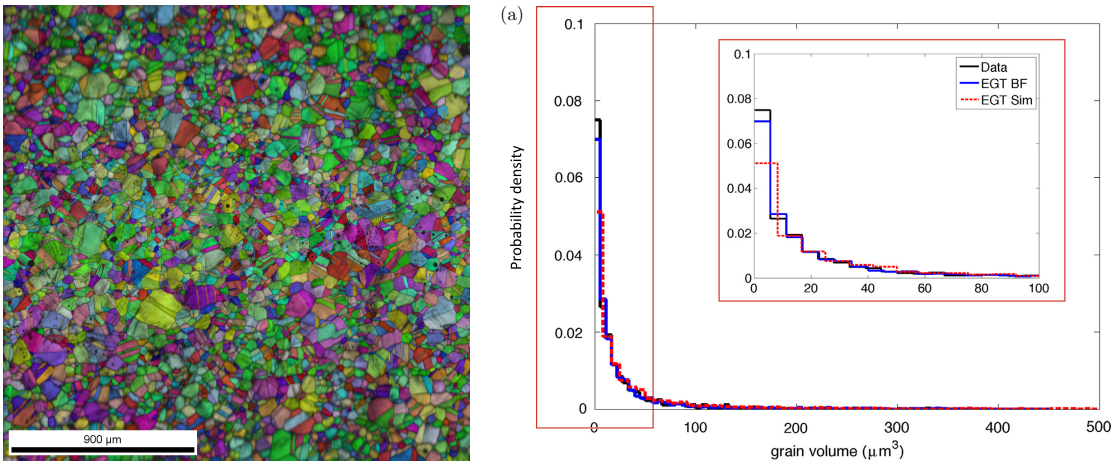

Figure 1.11 – *(Left) Electron BackScatter Diffraction image of an austenitic stainless steel 316L sample (2×2 mm²), where the color is related to the local orientation of the crystal lattice (adapted from Mu (2011)). (Right) Probability density function of the grain volume in a Nickel IN100 superalloy sample (black line), along with those obtained from two reconstructions of the same sample (taken from Teferra and Graham-Brady (2015)).*

most of the metals and many ceramics, so that they are found in almost all fields of engineering and industry, with systems undergoing a wide variety of loading conditions. Examples include motors designed to run millions of cycles under high thermal stress and nuclear plants confining walls undergoing cyclic irradiation and thermal loads. At the design stage, understanding the influence of the micro-scale structure on the behavior and damage of the macro-scale samples is fundamental (Hirsekorn 1990, Cuitiño and Ortiz 1993) to create new materials. In many industries, the choice of material is the key to innovation and competitiveness. Once in use, or during elaboration, non-destructive testing of polycrystalline materials with ultrasounds is very appealing to monitor the appearance of damage, and this requires to clarify the influence of texture and small-scale defects on the global features of the wave field at the macro-scale (Dubois et al. 1998).

Most phenomena of importance for damage take place within one grain or at the interface between two grains. At that scale, dislocations dynamics models (Hirth and Lothe 1982, Fivel and Forest 2004) can be used, where dislocations segments $\mathbf{d}\ell$ are followed individually while the crystal in which they evolve is treated as a continuum. The plastic deformation is the consequence of the collective displacements of enormous amounts of dislocations (the order of magnitude ranges from $10^{10} - 10^{16}$ m/m^3 in aluminum to 10^6 m/m^3 in silicon) under the external loads and the stresses they create by straining the crystal lattice. The Peach-Koehler force driving the motion of each dislocation segment is $(\sigma \cdot \mathbf{b}) \times \mathbf{d}\ell$, where $\mathbf{b}$ is the Burger vector, characteristic of the dislocation considered, and the stress σ includes the elastic field generated by all other dislocation segments in the crystal and the external load, as well as various (approximate) corrections for local curvature of the dislocation, presence of defects, interfaces and boundaries. The stress field induced by a single dislocation segment is computed analytically, assuming that the latter is a linear defect in an elastic continuum medium. The movement of individual dislocation segments is then evolved in time using material-dependent equations of motions. Efficient simulation codes are available (Devincre et al. 2011) that can routinely simulate a few percent of plastic strain in a single grain with several hundred dislocations (Vattré et al. 2014). Note that the consideration of transient loadings is not possible yet in these approaches.

At the inter-granular scale, the number of dislocations increases dramatically so that they cannot be followed individually anymore. It is then possible to introduce continuous fields of dislocation density $\rho_d^s(\mathbf{x})$ for each gliding plane s and to use them as internal variables in a non-linear constitutive model of continuum mechanics. Based on physical considerations regarding the displacement of actual dislocations, a hardening law can be introduced to follow the evolution of these dislocation densities (Evers et al. 2002, Cheong and Busso 2004, Fivel and Forest 2004, Ma et al. 2006). The plastic strain rate evolution is then given by:

$$\dot{\epsilon}^p = \sum_{s=1}^{N} \dot{\gamma}^s(\sigma, \rho_d^s) \hat{\mathbf{b}}^s \otimes_s \mathbf{n}^s \tag{1.5}$$

where $\hat{\mathbf{b}}^s$ is the normalized Burger vector for gliding plane s and $\mathbf{n}^s$ the normal to that plane. Combined with the resolved shear stresses $\tau^s = \mathbf{n}^s \cdot \sigma \cdot \hat{\mathbf{b}}^s$, this model can be used to describe the internal work in a classical Finite Element formulation. Phenomenological models exist (see for instance Cuitiño and Ortiz (1993) for a general review of computational approaches for continuum models of crystal plasticity), but the model described here is appealing because the link with the underlying physical phenomena is explicit, even though the dislocations are not followed individually. Numerically, these models can be solved efficiently for several hundreds of grains (Roters et al. 2011), although the number of internal variables limits somehow the possibilities. Also, creating meshed samples whose statistics are representative of real grains is an issue (see for instance Lochmann et al. (2006), Redenbach (2009), Teferra and Graham-Brady (2015)).

When interested in the non-destructive testing of polycrystalline samples or in the design of new materials, the scale to be considered is even larger. These crystal plasticity simulations are then out of reach, and upscaling techniques have to be considered. In statics, a large body of literature is dedicated to homogenization for polycrystalline materials (Hirsekorn 1990, Paroni 2000), either constructing bounds on homogenized coefficients (Chinh 2006) or computing these coefficients using numerical techniques (Bishop et al. 2015). Some researchers also concentrate on the construction of stochastic models at the meso-scale (Guilleminot et al. 2011, Lucas et al. 2015). In dynamics, early works concerning ultrasound probing techniques (with frequency in the order of ≈ 1 MHz) evaluated heuristically the influence of microstructure on the propagation of ultrasound (Mason and McSkimin 1947, Papadakis 1964; 1965, Murthy 2001). Later, models based on the Bourret approximation (Grigorev and Shemergor 1981), on second-order perturbation (Stanke and Kino 1984, Hirsekorn 1985), or on diffusion models (Sayers 1985, Guo et al. 1985, Weaver 1990a) were proposed for different frequency ranges. Interestingly, the diffusion models developed in the polycrystalline community are similar to those described earlier for geophysical media (see for instance the comparison in Turner (1998)).

1.2 Definition of multiscale problems

The three examples described in the previous section all have in common that there exist various models to represent the same physical phenomenon: (i) wave propagation, radiative transfer or diffusion for geophysics; (ii) granular methods or wave propagation in a continuum medium for ballasted railway tracks; and (iii) dislocation dynamics, crystal plasticity or diffusion for polycrystalline materials. Different models means here both different equations and different parameters, but also different unknown variables: displacement fields for wave equation and crystal plasticity, modal energy densities for radiative transfer equation and diffusion, and discrete displacements for granular methods and dislocation dynamics. We will call multiscale problems such problems that can be modeled in at least two different manners.

One of the two models has a richer kinematical description than the other, for example because parameters and solutions fluctuate more rapidly in space and time or because it includes internal variables. This model will be denoted micro-scale model. The model with the coarsest kinematical description will be called macro-scale model. The term mesoscale model can be used when three scales are available for the same multiscale problem. Alternatively, length or time scales can be used to differentiate between macro- and micro-scale models (as is proposed for instance in (E 2011, Fig. 1.5) or (Fivel and Forest 2004, Fig. 1)), but these definitions become ubiquitous in wave propagation problems as there are then three length scales (wave length λ, characteristic size of the heterogeneities ℓ_c and propagation length L) and time and space variables are coupled in a non-trivial manner. Different relative values for these three characteristic lengths yield different upscaling behaviors. The behaviors whose transition is at least partially understood theoretically are summarized in Fig. 1.12 (see also (Wu and Aki 1988b, Fig. 2)). Section 3 will describe the different regimes in detail.

The engineering problems of the previous section also have in common that at least one model of each involves a random material: random mechanical properties in geophysical media; random shapes and assembly of grains for the ballast; and random initial state of dislocation as well as random orientation and shape of the grains for polycrystalline materials. The choice of considering only stochastic applications is driven by personal scientific interest as well as the need to limit the scope of this document. The field of multiscale modeling for deterministic problems is well developed, and most techniques have actually been developed in that setting before their

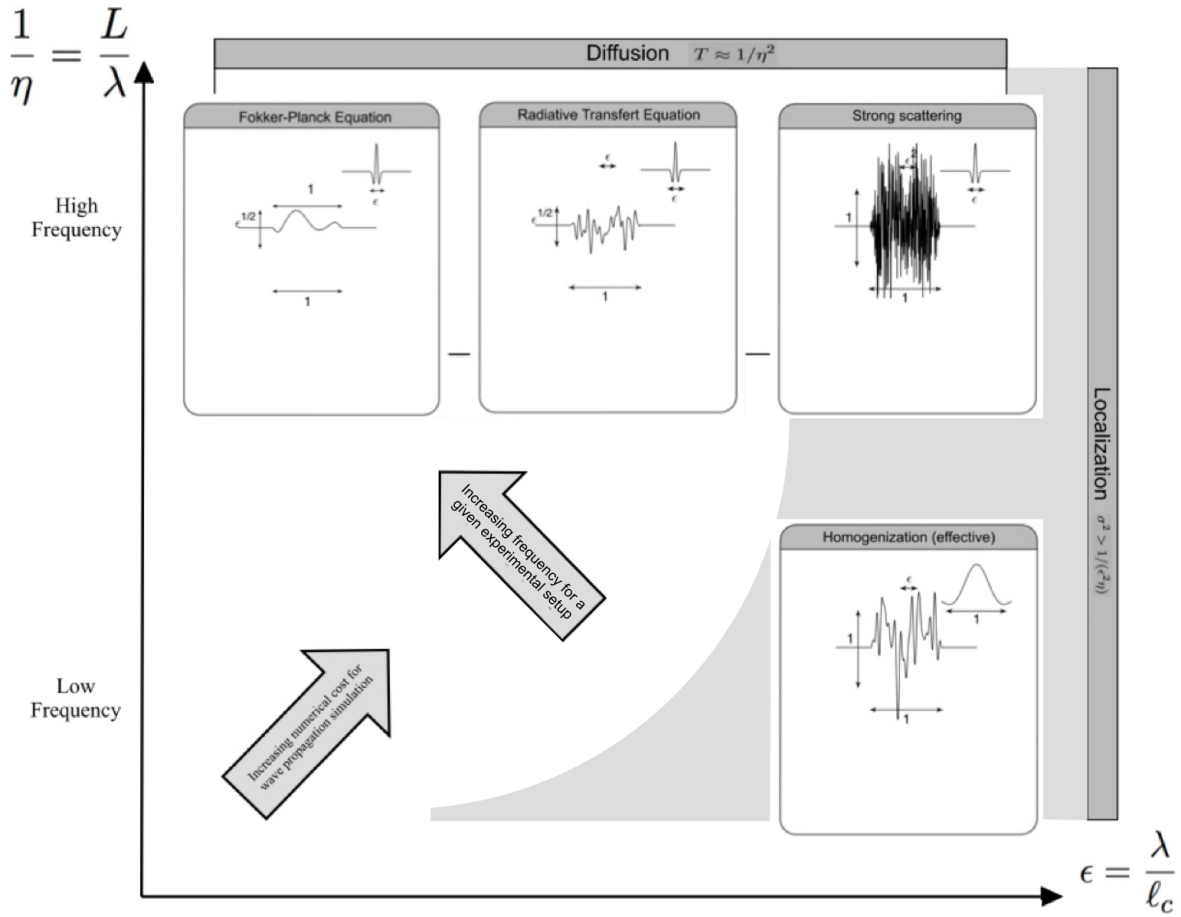

Figure 1.12 – *Classification of the different upscaling regimes by order of magnitude of the characteristic size ratios* $\epsilon = \lambda/\ell_c$ *and* $1/\eta = L/\lambda$.

stochastic counterpart. However, stochastic models are sufficiently specific and powerful tools to be worthy of a separate treatment. All references, descriptions, models and techniques will therefore be strongly biased towards the stochastic direction in this document, even though interesting deterministic counterparts might exist.

Historically, the different models of a multiscale problem are usually derived heuristically and independently. Based on experimental results at the appropriate scale, researchers introduce models and the corresponding parameters to explain and reproduce the observations. Only later are the two models paired up and their parameters related. For instance, temperature and the heat equation were used in engineering (and everyday life) long before molecular dynamics models were discovered, and the latter were derived from a different experimental information than temperature measurements at the macro-scale. Today, a full ladder of consistent models has been constructed, from quantum mechanics to continuum modeling of gases, through molecular dynamics and kinetic theory of gases (E 2011). Likewise, seismologists measured Q coefficients and wave velocities independently before the link between the wave equation and the diffusion equation was mathematically formulated. The derivation of the macro-scale equation and parameters based on the those of the micro-scale model is called upscaling (or homogenization). The inverse process is called downscaling. In the later case, however, it is often necessary to add information not contained in the macro-scale model itself.

One of the main interests of understanding in a mathematically precise way the transition from one model to the other gives insight into both models. Indeed, the link between the variables and parameters of the two models gives more physical understanding into what they represent. The process of changing scales also provides guidelines on the limits of each of the models. Homogenization has been widely investigated in statics (see the monographs Milton (2002) and Torquato (2001), respectively for deterministic and stochastic media, among many others), as well as in the dynamics case (see for example Chernov (1960), Ishimaru (1978), Rytov et al. (1989),

Table 1.1 – *Influence of boundary conditions, loading and quantities of interest on the choice of scale for modeling (assuming upscaling is actually possible). The grey area indicates the most interesting case in multiscale modeling.*

		quantity of interest	
		at micro-scale	at macro-scale
boundary conditions, mechanical parameters and loading	at micro-scale	micro-scale model	macro-scale or coupled model
	at macro-scale	macro-scale model with downscaling	macro-scale model

Sheng (2006), Fouque et al. (2007)). Different communities have been involved: engineers and material scientists interested in designing optimized composites and micro-structures (Ostoja-Starzewski 2007, Auriault et al. 2010, Hornung 2012), geophysicists confronted to the variability of the real world (Flatté et al. 1979, Sato et al. 2012), and mathematicians, exploring different notions of asymptotic analysis (Bensoussan et al. 1978, Dal Maso 1993, Tartar 2009). Recently, this field of research has gained new momentum, with the wide scientific and industrial interests for meta-materials. We will discuss in Section 3 different techniques and results, with a particular emphasis on upscaling of wave propagation in random media, and highlighting our own contributions to the field.

The use of one or another of the models available for a multiscale problem is highly dependent on the scale at which the parameters (including boundary conditions, mechanical parameters and loading) and quantities of interest are defined. Table 1.1 summarizes different possibilities. When parameters and quantities of interest live at the same scale, it is generally the scale that is chosen for the modeling. When the parameters are provided at the macro-scale while we are interested in a micro-scale quantity of interest, only the macro-scale model is available because not enough information is available to drive the micro-scale model. However, it is still possible to derive a macro-scale quantity of interest and perform downscaling, that is to say to locally introduce information to retrieve the quantity of interest at the micro-scale. The most interesting situation (from a numerical point of view) is when the parameters are provided at the micro-scale while we are interested in a macro-scale quantity of interest. In some cases, it might be possible to derive the macro-scale equivalent parameters and to simply use a full macro-scale model. In other cases, one might use a full micro-scale model to derive the micro-scale quantity of interest, before estimating the quantity of interest at the macro-scale. When the latter is too computationally expensive, one must use a coupled model, keeping both models on appropriate parts of the domain (Efendiev and Hou 2009, E 2011, Fish 2014). When considering such a coupled model, two situations arise, whether the (macro-scale) quantity of interest is sensitive to features of the micro-scale model everywhere or only from a limited area of the domain. In the latter case, the micro-scale is used only in that area. The scientific question behind coupling is then how to mathematically formulate the coupling at the interface between the macro-scale and micro-scale domains so that accurate solutions can be obtained numerically. In the former case, hypotheses of separation of scale are introduced to localize micro-scale patches everywhere and couple them to the macro-scale. The scientific question is then rather how to choose appropriate boundary conditions around the micro-scale patches for the macro-scale quantity of interest to be accurate. In both cases, the understanding of the upscaling process between the two models helps a lot in understanding the most appropriate way to couple the two models. Section 2 will review in details the existing techniques for coupling of multiscale models, with a particular emphasis on methods adapted to the coupling of stochastic models.

1.3 Robust multiscale numerical modeling

Multiscale analysis is an exercise in simplifying complex physical phenomena and parameterizations. As such, the question of error estimation is fundamental to determine when and where a micro-scale model can be replaced by its upscaled version. In the continuity of error estimation for deterministic problems (Babuška and Rheinboldt 1978a;b, Zienkiewicz and Zhu 1987, Ainsworth and Oden 2000, Ladevèze and Pelle 2005, Wiberg and Díez 2006), the numerical analysis for stochastic (mono-scale) problems has been widely discussed, either through *a pri-*

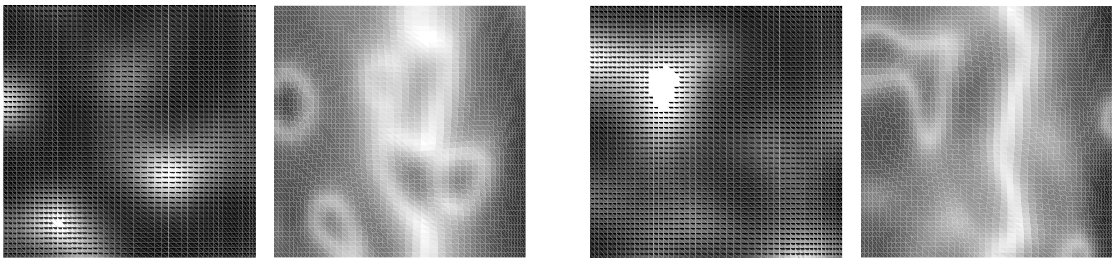

Figure 1.13 – *Two realizations of a material parameter field (first and third images from the left), and corresponding meshes with maps of the element sizes (second and fourth images from the left). White corresponds to higher material parameters values and larger element sizes.*

ori (Caflisch 1998, Babuška et al. 2010, Foo et al. 2008, Bespalov et al. 2012, Charrier 2012, Shi and Zhang 2012, Zhang and Gunzburger 2012), *a posteriori* (Deb et al. 2001, Mathelin and le Maître 2007, Chamoin et al. 2012), or goal-oriented estimates (Oden et al. 2005, Ladevèze and Florentin 2006, Matthies 2008, Butler et al. 2011, Florentin and Diez 2012). Specific error estimators have been designed for the Monte-Carlo method and the collocation method. As we will see in Section 3.1.3, some upscaling techniques allow for a clear derivation of *a priori* errors in various norms. Most of the multiscale coupling schemes have also been endowed with *a priori* error estimators (see for instance (E 2011, Section 6.7) as well as Section 2.2 of this document, or Givon and Kevrekidis (2008), Liu (2010) for multiscale problems with multiple time scales). *A posteriori* error estimation is less common for multiscale problems, in particular in the context of stochastic problems. In any case, a review of numerical analysis and error estimation goes beyond the scope of this document, and I will only list below my limited contributions to the field.

My first works in error estimation were performed during my post-doctoral studies at the Laboratori de Càlcul Numèric (Barcelona, Spain), in the context of deterministic Finite Element analyses (Cottereau et al. 2009; 2010b). More recently, we proposed (Cottereau and Díez 2015) an error estimation tool for Monte Carlo approximations of stochastic partial differential equations that allows to adapt *a priori* the mesh for each sample (see Fig. 1.13). During the Ph.D. studies of Cedric Zaccardi, that I co-advised with L. Chamoin and H. Ben Dhia, we proposed an error estimation tool (Zaccardi et al. 2013) for the stochastic-deterministic coupling scheme that will be described in Section 2.4. I am currently co-advising with B. Tie and D. Aubry the Ph.D. thesis of Wen Xu on error estimation and adaptivity for multiscale wave propagation problems.

Beyond error estimation, I have consistently tried to perform large scale and efficient numerical implementations of the algorithms and techniques that I developed (See Appendix A). This includes considering purely algorithmic aspects, such as introducing distributed-memory parallel implementations whenever possible, but also following particular development options: (i) using open source guidelines and licenses, (ii) ensuring the availability of the software, (iii) using version control and other development tools, and (iv) constructing test-cases and error estimation tools. Needless to say, these development options are cruelly time-consuming, but I believe they are necessary to reach the level of robustness that is needed for research.

1.4 Funding

Table 1.2 summarizes the funding that I received in the past years. Besides the CPU allocations provided by CINES, I should also acknowledge the help provided by the people at Mésocentre de Calcul de l'École Centrale, where most of the computations presented in this manuscript were performed.

Table 1.3 and 1.4 list the post-doctoral and Ph.D. students that I (co-)advised, or am currently (co-)advising, along with their funding. I thank them heartily for their involvement and passion. Note that I am the lead adviser for all the Ph.D. students co-advised with D. Clouteau, except for T. Okhulkova and A. Svay.

Table 1.2 – *List of funding projects and bodies, sorted by type and starting date.*

Acronym	Type	Funding body	dates	PI
BriScAr	Academic	Digiteo	2009-2012	R. Cottereau
TYCHE	Academic	ANR	2011-2013	C. Soize (MSME)
	Academic	F2M	2012-2013	E. Savin (ONERA)
	Academic	CAPES-COFECUB	2014-	R. Cottereau
SINAPS@	Academic	ANR	2014-	C. Berge (CEA)
CouESt	Academic	ANR	2015-	R. Cottereau
	Industrial	EDF R&D	2003-	D. Clouteau
	Industrial	SNCF R&D	2010-	R. Cottereau
	Industrial	INERIS	2010-2014	D. Clouteau
	Industrial	PetroBras	2012-2013	A. L. G. A. Coutinho
	Industrial	RATP	2014-	G. Puel
	Industrial	Tractebel	2014-	R. Cottereau
	CPU Allocation	CINES (Jade)	2010	R. Cottereau
	CPU Allocation	CINES (Occigen)	2015	R. Cottereau

Table 1.3 – *Advised post-doctoral students. Funding refers either to a project name (Table 1.2) or to a funding body.*

Name	Subject	Dates	Funding
T. Milanetto Schlittler	Numerical coupling of stochastic models of polycrystalline materials	2015-	CouESt
M. Taro	Coupling of wave propagation solvers for large-scale soil-structure interaction problems	2016-	SINAPS@

Table 1.4 – *Co-advised Ph.D. students. Funding refers either to a project name (Table 1.2) or to a funding body.*

Name	Title (tentative)	Dates	co-adviser(s)	Funding
C. Zaccardi	Stochastic-deterministic coupling in the Arlequin framework, and error estimations in quantity of interest	defended Jan. 21st, 2013	H. Ben Dhia & L. Chamoin	BriScAr
S. Khazaie	Influence of statistical parameters on elastic wave scattering: theoretical and numerical approaches	defended Feb. 23rd 2015	D. Clouteau	MENRT
T. Okhulkova	Integration of uncertainty and definition of critical thresholds in the procedure of CO_2 storage risk assessment	defended Dec. 15th 2015	D. Clouteau	INERIS (CIFRE)
A. Svay	Modeling of the spatial variability of seismic ground motions for soil-structure interaction applications	2013 –	F. Lopez-Caballero & D. Clouteau	EDF (CIFRE)
L. de Carvalho Paludo	Seismic wave propagation in heterogeneous non-linear media	2014 –	D. Clouteau	SINAPS@
W. Xu	Relevant numerical methods for meso-scale wave propagation in heterogeneous media	2014 –	B. Tie & D. Aubry	Chinese Science Council
A. Panunzio	Stochastic modeling for rail maintenance	2015 –	G. Puel	RATP (CIFRE)
L. de Abreu Corrêa	Non-linear stochastic model of a ballasted railway track	2015 –	D. Clouteau	SNCF
M. Hammami	Integrated methodologies for the dynamic analysis of concrete dams	2015 –	D. Clouteau	Tractebel (CIFRE)

Coupling of stochastic models 2

Let us consider a particular physical problem and assume that it can be studied through either one of two different models, denoted micro-scale and macro-scale models, and defined for simplicity through weak formulations[1]. For instance, a micro-scale solution $\mathbf{u}_m$ is defined through: find $\mathbf{u}_\mathrm{m} \in \mathcal{V}_\mathrm{m}$ such that

$$a_\mathrm{m}(\mathbf{u}_\mathrm{m}, \mathbf{v}; p_\mathrm{m}) = f_\mathrm{m}(\mathbf{v}; p_\mathrm{m}), \quad \forall \mathbf{v} \in \mathcal{V}_\mathrm{m}, \tag{2.1}$$

where the definition of the triplet (bilinear form a_m, linear form f_m, functional space $\mathcal{V}_\mathrm{m}$) constitutes the micro-scale model. The linear and bilinear forms depend on a set of micro-scale parameters p_m. In all the cases that we consider, the functional space can be separated with appropriate tensor structure in a deterministic functional space for the deterministic variables and a stochastic space. For instance, considering a (static) elastic problem defined on domain Ω with a (homogeneous) stiffness parameter modeled as a random variable, the functional space might be separated as $\mathcal{V}_\mathrm{m} = H^1(\Omega) \otimes L^2(\Theta, \mathbb{R})$, with $(\Theta, \mathcal{T}, \mathbb{P})$ a suitable probability space.

Likewise, and when available, a macro-scale solution $\mathbf{u}_\mathrm{M}$ is defined through: find $\mathbf{u}_\mathrm{M} \in \mathcal{V}_\mathrm{M}$ such that

$$a_\mathrm{M}(\mathbf{u}_\mathrm{M}, \mathbf{v}; p_\mathrm{M}) = f_\mathrm{M}(\mathbf{v}; p_\mathrm{M}), \quad \forall \mathbf{v} \in \mathcal{V}_\mathrm{M}. \tag{2.2}$$

By definition, the space $\mathcal{V}_\mathrm{M}$ is coarser than the space $\mathcal{V}_\mathrm{m}$ in the sense that the functions $\mathbf{v} \in \mathcal{V}_\mathrm{m}$ provide a richer kinematical description than the functions $\mathbf{v} \in \mathcal{V}_\mathrm{m}$. We assume that the micro-scale and macro-scale models are coherent in the sense that they represent the same physical phenomenon and predict the same behavior at the macro-scale (see Section 1.2).

As discussed in the introduction, a coupled model is constructed when a macro-scale quantity of interest cannot be properly evaluated based only on the macro-scale model. Two situations arise, depending whether the quantity of interest is sensitive to features of the micro-scale model everywhere or only a limited area is influential. In the former case (see the leftmost plot in Fig. 2.1), the micro-scale is needed everywhere so the only chance for numerical gain is through the introduction of some scale separation and localization of the micro-scale model on small patches. This situation will be considered in Section 2.1. When only a localized area needs to be treated with the micro-scale model, different numerical techniques can be used depending on the dimensionality of the modeling and coupling areas. For instance, point and surface details can be modeled with partition of unity techniques (see the second plot of Fig. 2.1 and Section 2.2). When the micro-scale model is supported on a volume, it is possible to couple the micro-scale and macro-scale models either through a surface or a volume (see the rightmost plots of Fig. 2.1 and Sections 2.3 and 2.4, respectively). We explore these different types of coupling one after the other in the different sections of this chapter.

As in the rest of this document, we focus mainly on stochastic models. However, thanks to the tensor structure mentioned above, extensions of deterministic coupling techniques to stochastic problems is often natural. In that case, the deterministic coupling technique will be presented for simplicity, and the extension to the stochastic case will only be mentioned briefly. More references about the coupling of deterministic models can be found in the review on the dynamics of structures coupled with elastic media (Clouteau et al. 2013), included in a special issue of the Journal of Sound and Vibration on advanced methods in structural dynamics (Clouteau and Cottereau 2013). More references about coupling of atomistic (or more generally non-local) to

[1] Note that we concentrate in this chapter on the coupling of the two models, assuming that both are given. Derivation of a macro-scale model from a given micro-scale model will be considered in Chapter 3.

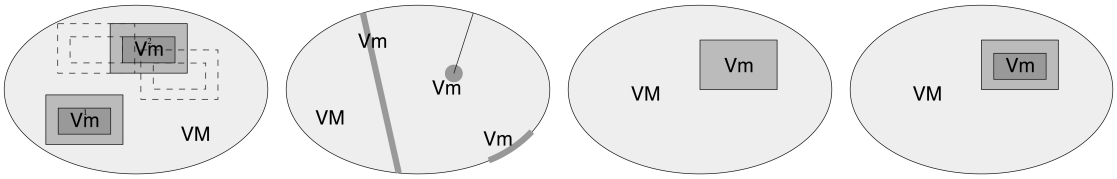

Figure 2.1 – *Different types of coupling between a micro-scale model (dark grey shade), supported on* $\mathrm{V_m}$*, and a macro-scale model (light gray shade), supported on* $\mathrm{V_M}$*: (from left to right) micro-scale model embedded everywhere; geometrically-supported details; interface coupling; volume coupling.*

continuum (local) models can be found in Curtin and Miller (2003). Other general reviews about coupled multi-scale problems include Brandt (2002), Geers et al. (2010) and (E 2011, Chapters 6-7). As earlier, I should remind that this document is presented in the format of a general review, although my personal contributions appear in blue. The latter are found in Section 2.3.2 on random models of boundary impedances, in Section 2.3.3 on the use of parameterized models for coupling, and in Section 2.4 on volume coupling.

2.1 Embedded micro-scale model

We first consider the case when the macro-scale quantity of interest is sensitive to features of the micro-scale model everywhere. In particular, this situation incorporates the case when the constitutive relation at the macro-scale lacks micro-scale mechanisms that would control its behavior. In that case, no macro-scale model is introduced and the techniques purely aim at reducing the numerical complexity by appropriate multi-grid treatments. The simulation of the full micro-scale model is therefore replaced by a (possibly large) sequence of smaller (in time and space) micro-scale models, such that the overall numerical cost is smaller. Existing techniques differ mainly by the definition of the patches over which the micro-scale simulations are performed. The first class of techniques (see Section 2.1.1) considers groups of elements of a coarse mesh as patches and includes the Generalized Finite Element Method (GFEM) of Babuška and Osborn (1983), the Residual Free Bubbles (RFB) of Brezzi and Russo (1994), the Variational Multiscale Method (VMS) of Hughes (1995) and the Multiscale Finite Element Method (MsFEM) of Hou and Wu (1997). These methods basically introduce for the micro-scale problem a coarse mesh and functional space $\mathcal{V}_\mathrm{M}$ and enrich the latter with functions solving the micro-scale equations on the patches with appropriate boundary conditions. The second class of techniques (see Section 2.1.2) includes the Quasi-Continuum (QC) method of Tadmor et al. (1996), the FE^2 method of Feyel (1999) and the Heterogeneous Multiscale Method (HMM) of E and Engquist (2003). These methods consider the same coarse mesh and functional space $\mathcal{V}_\mathrm{M}$, and additionally introduce a macro-scale functional, which is integrated by solving local micro-scale problems centered on the integration points. Discussion of these approaches with examples taken from the lower scales (quantum mechanics and molecular dynamics in particular) can be found in (E 2011, Chapter 6).

2.1.1 Element-based embedding (GFEM, RFB, VMS, MsFEM)

We first consider methods that introduce a coarse mesh and enrich the corresponding functional space $\mathcal{V}_\mathrm{M}$ with functions computed using the micro-scale model over patches of elements of that coarse mesh. Several methods (see Table 2.1 for a summary) share common features[2], that we discuss here following the framework developed for the VMS in Hughes (1995). The micro-scale functional space is decomposed into the orthogonal sum $\mathcal{V}_\mathrm{m} = \mathcal{V}_\mathrm{M} \oplus \mathcal{V}'$, where the coarse space $\mathcal{V}_\mathrm{M}$ typically includes FEM linear functions over the coarse mesh, and $\mathcal{V}'$ is a refined space chosen depending on the micro-scale problem at hand. Decomposing the solution $\mathbf{u}_\mathrm{m} = \mathbf{u}_\mathrm{M} + \mathbf{u}'$ accordingly, and testing Eq. (2.1) respectively with functions of the two spaces, the micro-scale problem is decomposed in: find $(\mathbf{u}_\mathrm{M}, \mathbf{u}') \in \mathcal{V}_\mathrm{M} \times \mathcal{V}'$ such that:

$$\begin{cases} a_\mathrm{m}(\mathbf{u}_\mathrm{M} + \mathbf{u}', \mathbf{v}; p_\mathrm{m}) = f_\mathrm{m}(\mathbf{v}; p_\mathrm{m}), & \forall \mathbf{v} \in \mathcal{V}_\mathrm{M} \\ a_\mathrm{m}(\mathbf{u}', \mathbf{v}; p_\mathrm{m}) = f_\mathrm{m}(\mathbf{v}; p_\mathrm{m}) - a_\mathrm{m}(\mathbf{u}_\mathrm{M}, \mathbf{v}; p_\mathrm{m}), & \forall \mathbf{v} \in \mathcal{V}' \end{cases} \tag{2.3}$$

[2]The emphasize is put here on these common features. Differences, that I personally consider more technical than fundamental, are discussed in Arbogast and Boyd (2006), Nolen et al. (2008) and Yu and Yue (2011).

The second equation is used to define the value of the micro-scale fluctuation as a function of the macro-scale solution $\mathbf{u}'(\mathbf{u}_\mathrm{M})$. The definition of the fluctuation is then incorporated in the first equation to define the macro-scale solution: find $\mathbf{u}_\mathrm{M} \in \mathcal{V}_\mathrm{M}$ such that:

$$a_\mathrm{m}(\mathbf{u}_\mathrm{M} + \mathbf{u}'(\mathbf{u}_\mathrm{M}), \mathbf{v}; p_\mathrm{m}) = f_\mathrm{m}(\mathbf{v}; p_\mathrm{m}), \quad \forall \mathbf{v} \in \mathcal{V}_\mathrm{M} \tag{2.4}$$

The key difficulty lies in the definition of the mapping between $\mathbf{u}'$ and $\mathbf{u}_\mathrm{M}$, which is *a priori* a problem of the same complexity as the original problem of Eq. (2.1). So the entire numerical gain lies in the localization of this large-scale problem into a large set of smaller problems. Note that, in general, $\mathbf{u}'$ fluctuates rapidly (at the micro-scale) so that integration of the terms $a_\mathrm{m}(\mathbf{u}'(\mathbf{u}_\mathrm{M}), \mathbf{v}; p_\mathrm{m})$ must be treated with care.

Table 2.1 – *Element-based multi-scale methods (K denotes an element of the coarse mesh with vertices $\mathbf{x}_i$ and $\mathbb{P}(K)^p$ represents a space of polynomial of order p over K)*

Name	Reference	Boundary conditions for the local problems
GFEM	(Babuška and Osborn 1983)	$\mathbf{v}_{\partial K} = \mathbf{0}$ (1D)
RFB	(Brezzi and Russo 1994)	$\mathbf{v}_{\partial K} = \mathbf{0}$
VMS	(Hughes 1995)	$\mathbf{v}_{\partial K} \in \mathbb{P}(K)^p$
MsFEM	(Hou and Wu 1997)	$\mathbf{v}_i(\mathbf{x}_j) = \delta_{ij}$ and $\partial_\perp(\sigma_{\partial K} \cdot \mathbf{n}_\perp) = 0$

The simplest proposal for such localization consists in choosing for $\mathcal{V}'$ a space of RFB (see Brezzi and Russo (1994) or Babuška and Osborn (1983) in 1D). These functions verify the second line of Eq. (2.3) with unit right hand side and homogeneous Dirichlet conditions at the boundary of the elements of the coarse mesh. For diffusion problems with a heterogeneous parameter fluctuating at scale ϵ, this RFB approximation yields error estimates $\|\mathbf{u}_\epsilon - (\mathbf{u}_\mathrm{M} + \mathbf{u}')\|_{H^1} \leq C(\epsilon + H + \sqrt{\epsilon/H})\|\mathbf{f}\|_{L^2}$, where C is a constant, H is the typical size of the coarse mesh, and $\mathbf{u}_\epsilon$ is the exact solution. As soon as $\epsilon \ll H$, this approximation is therefore controlled only by the size of the coarse elements. Otherwise, and in particular in the resonating case when $\epsilon \approx H$, the method may behave quite dramatically. The classical RFB can be complemented with edge- and vertex-bubble functions, that verify non-homogeneous (in general polynomial) Dirichlet conditions on the edges and the vertices, respectively, of the elements (Hughes et al. 1998). In the MsFEM (Hou and Wu 1997), mixed boundary conditions are considered for the element problems: boundary conditions corresponding to a projection along the edge of the equilibrium equation, and point-wise homogeneous Dirichlet conditions at the vertices of the elements (see Table 2.1). This yields functions that are oscillating along the edge of the element (although continuous from one element to the next) and error estimates (Hou et al. 1999) of the form $\|\mathbf{u}_\epsilon - (\mathbf{u}_\mathrm{M} + \mathbf{u}')\|_{H^1} \leq C(H\|\mathbf{f}\|_{L^2} + \sqrt{\epsilon/H})$.

In a series of papers, Zabaras and co-authors extended the VMS to various problems with stochastic parameters (advection diffusion and incompressible Navier-Stokes (Velamur Asokan and Zabaras 2005) and diffusion (Ganapathysubramanian and Zabaras 2007)) by enforcing almost sure homogeneous boundary conditions at the boundary of the elements for the computation of the local problems. Although the multi-scale approach is the same in all papers, different numerical techniques are discussed for the solution of the stochastic equations: either Stochastic Finite Elements (Velamur Asokan and Zabaras 2006) or collocation based techniques (Ganapathysubramanian and Zabaras 2007). Xu (2007) proposed an extension to stochastic problems where, as in Velamur Asokan and Zabaras (2006), the boundary conditions for the local problems are enforced almost surely. Finally, it is also possible to use homogeneous Neumann boundary conditions (see Gao et al. (2015), for instance, where harmonic analysis of wave propagation in anisotropic heterogeneous media is considered). These conditions do not imply that the computed micro-scale functions are continuous at the macro-scale, so the Partition of Unity Method (PUM, see Section 2.2 for details) is used to retrieve the continuity of the basis functions.

In all these methods, the influence of the boundary conditions can be minimized by computing the functions of $\mathcal{V}'$ over larger domains than the simple elements that are later used on. This approach is called oversampling (Nolen et al. 2008, Gao et al. 2015). Model reduction is also often used to reduce the computational burden of the local problems (see for instance Efendiev et al. (2013)), which becomes particularly important for stochastic problems (Ganapathysubramanian and Zabaras 2009).

2.1.2 Quadrature-based embedding (HMM, FE^2, QC)

The second class of methods starts from slightly more information than the previous, as the functional form of the macro-scale model (Eq. (2.2)) is assumed to be known, although the values of the parameters p_M are unknown. The integrals appearing in the weak formulation are evaluated using some Gaussian quadrature, as shown here for the left-hand side:

$$a_{\mathrm{M}}(\mathbf{u}_{\mathrm{M}}, \mathbf{v}; p_{\mathrm{M}}) = \int_{\Omega} a_{\mathrm{M}}^{\mathrm{intgd}}(\mathbf{u}_{\mathrm{M}}, \mathbf{v}; p_{\mathrm{M}}) d\mathbf{x} \approx \sum_{g=1}^{N_g} \omega_g a_{\mathrm{M}}^{\mathrm{intgd}}(\mathbf{u}_{\mathrm{M}}(\mathbf{x}_g), \mathbf{v}(\mathbf{x}_g); p_{\mathrm{M}}) \tag{2.5}$$

where the $\{\omega_g\}_{1\leq g\leq N_g}$ and $\{\mathbf{x}_g\}_{1\leq g\leq N_g}$ are the N_g Gauss weights and points and $a_{\mathrm{M}}^{\mathrm{intgd}}(\cdot,\cdot;\cdot)$ denotes the integrand of the bilinear form $a_{\mathrm{M}}(\cdot,\cdot;\cdot)$. Unfortunately, when the parameters p_{M} are not explicitly known, these integrands cannot be evaluated.

The general idea of the HMM (E and Engquist 2003) consists in evaluating these point-wise quantities through the solution of a micro-scale problem over a patch $\Omega_{\mathbf{x}_g}$ centered on position $\mathbf{x}_g$ and with chosen boundary conditions:

$$a_{\mathrm{M}}(\mathbf{u}_{\mathrm{M}}, \mathbf{v}; p_{\mathrm{M}}) \approx \sum_{g=1}^{N_g} \omega_g a_{\mathrm{M}}^{\mathrm{intgd}}(\mathbf{u}_{\mathrm{M}}(\mathbf{u}_{\mathrm{m}}[\Omega_{\mathbf{x}_g}; p_{\mathrm{m}}])), \mathbf{v}(\mathbf{x}_g); \cancel{p_{\mathrm{M}}}) \tag{2.6}$$

For instance, for a diffusion problem with a heterogeneous parameter fluctuating at scale ϵ, one might evaluate the fluxes appearing in the integrand through the solution of a micro-scale problem with Dirichlet boundary conditions inherited from the value of the macro-scale functions $\mathbf{v} \in \mathcal{V}_{\mathrm{M}}$ in the vicinity of $\mathbf{x}_g$ (linear if linear Finite Elements are used for the solution of the macro-scale problem). Although the knowledge of the functional form of the macro-scale model $a_{\mathrm{M}}^{\mathrm{intgd}}(\cdot,\cdot;\cdot)$ is required, this approach bypasses the need to evaluate the parameters of the macro-scale model. For the multi-scale diffusion problem, error estimates of the form $\|\mathbf{u}_\epsilon - \mathbf{u}_{\mathrm{HMM}}\|_{H^1} \leq C(H + \epsilon/h + h)$ can be obtained (E et al. 2005), where H is the size of the macro-scale elements, and h is the size of the patch around $\mathbf{x}_g$. Specific *a priori* error estimators for the random diffusion problem are described in E et al. (2005) and *a posteriori* error estimators are discussed in Abdulle and Nonnenmacher (2009). It is possible to extend the HMM to the wave equation (Engquist et al. 2011). Long-time behavior, where diffusive effects appear (see Section 3.3.4), are considered in Engquist et al. (2012) and Abdulle et al. (2014). Error estimation is considered in Abdulle et al. (2014) and Arjmand and Runborg (2014).

As the HMM aims at being general in formulation, it includes various earlier methods. Among those, the FE^2 method (Feyel 1999, Feyel and Chaboche 2000) was mainly applied in a Finite Element Context for mechanical problems, and the QC method (Tadmor et al. 1996) was mainly used for continuum-discrete formulations. The HMM also includes the many instances of computational homogenization, that go back at least to Renard and Marmonier (1987) and are still in wide use today (see for instance Babuška et al. (2014) where three-scales computational homogenization is applied to the low-frequency wave equation with random parameters). For this latter class, *a priori* error estimates are discussed in Guedes and Kikuchi (1990) and Babuška et al. (2014).

The main differences between the quadrature-based methods and the element-based methods lie in: (i) the information required to use the methods, and (ii) the patches over which the micro-scale problems are localized. Indeed, the element-based methods do not need any information on the macro-scale model, since everything is solved at the micro-scale model, while the quadrature-based methods require at least the knowledge on the functional form of the macro-scale model (compare the functionals appearing in Eq. (2.3) and (2.6)). Concerning the patches, those of the element-based methods are constrained to follow the coarse mesh because they are used to define conformal basis functions for the weak formulation. In the quadrature-based methods, the patches can be chosen with more freedom. In particular, they do not necessarily cover the entire domain when their size is smaller than the distance between quadrature points. This last difference is reflected in the error estimates introduced above: they have a similar structure, but with a separate parameter for the micro-scale size in the quadrature-based methods. On the other hand, many features of the two methods are similar. In particular, the main approximation comes through the introduction of chosen boundary conditions, and over-sampling can be used to reduce the impact of this choice.

2.2 Geometrically-supported details (PUM, XFEM)

We now consider the case when the macro-scale quantity of interest is only sensitive to features of the micro-scale model within a limited portion of the full domain. Before moving to more general situations in the next sections, we address here specifically the situation when the sub-domain where the macro-scale model is not sufficient has a lower dimensionality than the full domain (second plot from the left in Fig. 2.1). For example, it might be necessary to introduce a micro-scale model close to the tip of a fracture within a globally macro-scale continuum model. Likewise, it might be interesting to introduce a specific micro-scale model along the edge of a dislocation within a linear model of dislocation dynamics or a boundary layer behavior in a continuum mechanics model. It is interesting to address separately the situation when the micro-scale support has lower dimensionality than the macro-scale support because the corresponding gradients, which are often used in classical coupling schemes, might be difficult to evaluate in general or be numerically unstable.

The partition of unity method (PUM, proposed by Melenk and Babuška (1996)) allows to enrich locally the macro-scale functional space $\mathcal{V}_M$ of Eq. (2.2) with functions known to solve the micro-scale problem (2.1) in the vicinity of the geometrical detail by using a partition of unity. Such a partition is a set of smooth non-negative functions $P = \{P_i(\mathbf{x}), 1 \leq i \leq N_P\}$ with $\text{supp}P_i(\mathbf{x}) = \Omega_i$ and $\sum_{i=1}^{N_P} P_i(\mathbf{x}) = 1$, for all $\mathbf{x} \in \Omega$, and defined over a set of overlapping patches Ω_i covering the domain ($\cup_i \Omega_i = \Omega$). For instance the hat functions of the linear FEM form a partition of unity over the patches of elements that are in contact with a node (sometimes called "stars", see Cottereau et al. (2009)). Considering functions $\psi(\mathbf{x})$ that have good approximation properties for the micro-scale problem but are defined only locally or are non-conformal globally, the PUM consists in using the set of approximation functions $\psi P = \{\psi(\mathbf{x})P_i(\mathbf{x}), \text{supp}\psi \cap \Omega_i \neq \emptyset\}$. This set inherits the approximation property of $\psi(\mathbf{x})$ and the conformal character and the smoothness of the partition of unity functions. Note that these approximating functions are usually not polynomial over the coarse-scale elements so that iterative quadrature schemes or sub-integration must be set up.

When the micro-scale approximating functions $\psi(\mathbf{x})$ are discontinuous along a line or surface, the PUM is usually called eXtended Finite Element Method (XFEM, see for instance Moës et al. (1999) for discontinuities in the function itself and Chessa and Belytschko (2003) or Cottereau et al. (2010c) for discontinuities in the derivative). This approach has been used[3] to model random interfaces and boundaries (Ghanem and Brzakala 1996, Nouy and Clément 2010). The differences between the approaches stand in the discretization of the interface, the random variables being the coefficients of the XFEM discretization of the interface, or the coefficients of its Karhunen-Loève expansion. Alternative (and similar) techniques include a stochastic version of the fictitious domain approach (Canuto and Kozubek 2007), embedding the domain in a larger one and enforcing weakly the boundary condition through Lagrange multipliers, and the construction of a (random) mapping from the random domain onto a deterministic domain, which modifies (through the Jacobian) the weak formulation (Xiu and Tartakovsky 2006).

2.3 Interface coupling

Still in the case when the macro-scale quantity of interest is only sensitive to features of the micro-scale model within a limited portion of the full domain, we now consider the non-overlapping case (third plot from the left in Fig. 2.1). The full domain Ω is separated into two non-overlapping subdomains Ω_M and Ω_m, supporting respectively the macro-scale and micro-scale models, and the interface between the two models is the surface $\overline{\partial\Omega}_M \cap \overline{\partial\Omega}_m$. This is the field of classical non-overlapping domain decomposition techniques, that we present in Section 2.3.1, with a special focus on their applications to stochastic problems. We also discuss two more specific cases, that are of special interest in practical applications and allow for more particular treatments. In Section 2.3.2, when the support of the quantity of interest if included in the micro-scale domain, the macro-scale model can be condensed on the interface and modeled as a boundary impedance operator. In Section 2.3.3, when both the micro- and macro-scale models are parameterized

[3]Note that, as observed in Díez et al. (2012; 2013), XFEM modeling of two-phase diffusion improves the approximation of the displacement field, but not that of the gradient at the interface.

instances of the same model, coupling can be performed simply by considering a single model with heterogeneous parameters.

2.3.1 Non-overlapping domain decomposition methods

Domain decomposition techniques have been developed in the context of the numerical approximation of partial differential equations over large-scale clusters of computers (Dolean et al. 2015). In their non-overlapping versions, the operators exchanging information about the solutions are supported over surfaces. They can be described based on the following coupled formulation[4]: find $(\mathbf{u}_\mathrm{M}, \mathbf{u}_\mathrm{m}, \phi) \in \mathcal{V}_\mathrm{M} \times \mathcal{V}_\mathrm{m} \times \mathcal{V}_c$ such that

$$\begin{cases} a_\mathrm{M}(\mathbf{u}_\mathrm{M}, \mathbf{v}; p_\mathrm{M}) + C(\phi, \Pi_\mathrm{M}(\mathbf{v})) = f_\mathrm{M}(\mathbf{v}; p_\mathrm{M}), & \forall \mathbf{v} \in \mathcal{V}_\mathrm{M} \\ a_\mathrm{m}(\mathbf{u}_\mathrm{m}, \mathbf{v}; p_\mathrm{m}) - C(\phi, \Pi_\mathrm{m}(\mathbf{v})) = f_\mathrm{m}(\mathbf{v}; p_\mathrm{m}), & \forall \mathbf{v} \in \mathcal{V}_\mathrm{m} \\ C(\mathbf{v}, \Pi_\mathrm{M}(\mathbf{u}_\mathrm{M}) - \Pi_\mathrm{m}(\mathbf{u}_\mathrm{m})) = 0, & \forall \mathbf{v} \in \mathcal{V}_c \end{cases}, \tag{2.7}$$

where C is a coupling operator supported on the interface Γ, designed to select in what sense the equality of the two solutions is weakly enforced, and the projection operators Π_M and Π_m restrict the functions to their trace on Γ and are also necessary to compare different physical quantities, such as for instance when discrete and continuum models are coupled. Domain decomposition methods can be differentiated based on the kind of iterative scheme selected for the solution of Eq. (2.7), for instance enforcing strongly the last line of Eq. (2.7) to obtain a scheme posed directly in terms of the displacement at the interface $\mathbf{u}_{\mathrm{M}|\Gamma} = \mathbf{u}_{\mathrm{m}|\Gamma}$, or actually computing the Lagrange multiplier ϕ as an intermediary step (Farhat and Roux 1991). Examples of applications of similar techniques include the coupling of the spectral element method with a modal solution through regularized Dirichlet-to-Neumann operators in time for elastic wave propagation in global Earth models (Capdeville et al. 2003) and the application (although with little scalability) to granular assemblies solved through implicit schemes (Alart et al. 2012). Note that so-called ghost forces (Curtin and Miller 2003) arise when long-range models (such as particle models) are coupled to local ones (such as classical continuum models). These issues are related to a loss of equilibrium depending on the position of the interface, and have to be treated with care.

Concerning stochastic models, Chevreuil et al. (2013) proposed a domain decomposition method with $C(\mathbf{u}, \mathbf{v}) = \mathbb{E}\left[\int_\Gamma \mathbf{u}\mathbf{v}dx\right]$ and selected the coupling space $\mathcal{V}_c$ as the space of square integrable functions defined on the probabilistic space with values in $\mathcal{H}^{-1/2}(\Gamma)$. This work assumes that the sources of uncertainty are localized within each subdomain, and tensor approximations of the (stochastic) functional spaces (following Nouy (2009)) are then constructed locally on each subdomain:

$$\mathbf{u}_i = \sum_k \alpha^{i,k} \psi^{i,k}_\mathbf{x}(\mathbf{x}) \psi^{i,k}_\mathrm{m}(\theta_\mathrm{m}) \psi^{i,k}_\mathrm{M}(\theta_\mathrm{M}), \quad i \in \{\mathrm{m}, \mathrm{M}\}, \tag{2.8}$$

although both sets of sources of randomness θ_M and θ_m are used in the construction of the tensor bases in each of the two subdomains. Another version of the same formulation is proposed in Hadigol et al. (2014), with slightly different tensor approximations and algorithmic details. A hierarchical approach can also be chosen (Arnst et al. 2014) where a separate representation is constructed in each subdomain based only on the local source of randomness, and the coefficients of that representation are then made to depend on the random germs of the other domain

$$\mathbf{u}_i = \sum_k \alpha^{i,k}(\theta_{\sim i}) \psi^{i,k}_\mathbf{x}(\mathbf{x}) \psi^{i,k}_i(\theta_i), \quad i \in \{\mathrm{m}, \mathrm{M}\}, \quad \sim i \in \{\mathrm{M}, \mathrm{m}\}, \tag{2.9}$$

during the solution of the coupled problem. Depending on the particular cases at hand, it is not clear which of the two approaches yields the largest reduction in global numerical complexity.

2.3.2 Random models of boundary impedances

In many fields of application, as civil engineering or aeronautics, engineers have to design structures that are in contact with unbounded domains (see Fig. 2.2). In these applications, only the structure is really of interest for the engineers, and the exterior domain is important only through

[4] This formulation is the same for volume coupling in Section 2.4, with the coupling operator C supported on a surface instead of a volume.

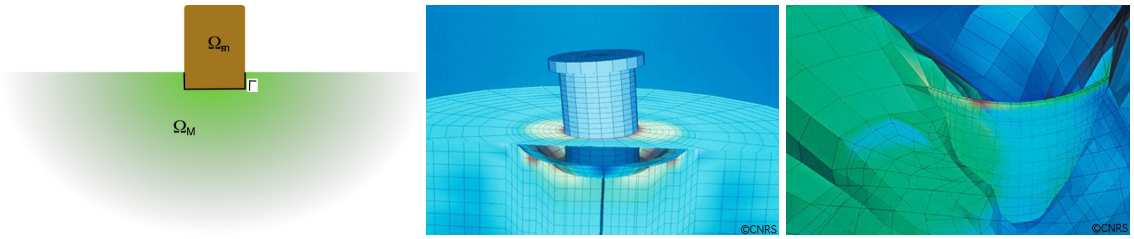

Figure 2.2 – *Coupling of a bounded structure of interest Ω_m to an unbounded exterior domain Ω_M through a boundary Γ (left) and two applications: seismic design of a nuclear reactor building (center) and a dam (right). The center and right figures are taken from the manual of Boundary Element software MISS.*

its Steklov-Poincaré operator, also called equivalent stiffness or boundary impedance in elastodynamics, or Schur complement in a discretized setting. As the spatial support of the operator a_M is unbounded, while that of the Steklov-Poincaré operator is Γ, it appears interesting to perform the random modeling directly in terms of the latter. This was done in a series of papers (Cottereau et al. 2005; 2006; 2007a) with applications in earthquake (Cottereau et al. 2007b) and railway engineering (Ropars and Desceliers 2015).

The construction follows the nonparametric approach, originally introduced in structural vibration problems for the modeling of matrices of mass, damping and stiffness (Soize 2000; 2001). The maximum entropy principle (Shannon 1948, Jaynes 1957) is used to construct a random model of a so-called "hidden variables models" (Chabas and Soize 1987) of the impedance, which is essentially a rational approximation (in terms of the frequency) of the impedance operator. The structure of the hidden variables model and the use of the Maximum Entropy principle ensure that the random boundary impedance is almost surely symmetric, stable, and corresponds to a causal function in the time domain. The random model is constructed based on a mean impedance operator and a set of dispersion parameters that can be identified from experiments (Soize 2005, Arnst and Ghanem 2008).

The essential building block that allows to construct an adequate rational approximation of the operator is a two steps process: (i) a matrix-valued rational approximation (with common denominator) is identified using any appropriate optimization technique, and (ii) three matrices M, D and K, similar to mass, damping and stiffness matrices, are identified such that the Schur complement of $S(\omega) = -\omega^2 M + j\omega D + K$ is the boundary impedance matrix:

$$Z(\omega) \approx \frac{N(\omega)}{d(\omega)} = S_\Gamma(\omega) - S_c(\omega) S_h(\omega)^{-1} S_c(\omega)^T, \tag{2.10}$$

where $S_i(\omega) = -\omega^2 M_i + j\omega D_i + K_i$ for $i \in \{\Gamma, c, h\}$, Γ refers to the boundary diagonal block, h to the interior diagonal block, and c to the coupling part of the matrices. This rational approximation has been later used to construct approximate formulas for the dynamic stiffness of pile groups (Taherzadeh et al. 2009) but could potentially also allow to construct efficient preconditioners for more classical domain decomposition methods (Dolean et al. 2015), or derive local approximations of boundary operators for absorbing boundary conditions (Magoulès and Harari 2006).

The method described in this section is called non-parametric in the sense that it is not related to the construction (or identification) of the random model of any mechanical parameter (such as the Lamé coefficients). The latter would require a solver of the type presented in Section 2.3.1. It is sometimes acknowledged that non-parametric approaches have the possibility of representing both parametric uncertainties (on specific mechanical variables and parameters) and modeling errors (arising from the choice of an inappropriate model), while parametric approaches can only account for parametric uncertainties. In Cottereau et al. (2008), we constructed a parametric model of the impedance matrix for which the modeling error was expected to be important for some elements and negligible for others. It was then possible to identify the dispersion parameters of the nonparametric model from the parametric model, using only the latter elements.

2.3.3 Parameterized models

Another particular case of interest is that of parameterized models, in which both micro-scale and macro-scale models are represented by the same partial differential equations, with the only difference standing in the value of the parameters. For instance, the (quasi-static) Stokes equation for the velocity $\mathbf{v}(\mathbf{x})$ and pressure $p(\mathbf{x})$ in domain Ω reads: find $(\mathbf{v}, p) \in [\mathcal{H}^1_0(\Omega)]^d \times \mathcal{L}^2(\Omega)/\mathbb{R}$ such that:

$$\begin{cases} -\nabla \cdot (\nu \nabla_s \mathbf{v}) + \nabla p = \rho \mathbf{g} \\ \nabla \cdot \mathbf{v} = 0 \end{cases} \tag{2.11}$$

with appropriate boundary conditions. In these equations, ν is the viscosity of the fluid, ρ its density and $\mathbf{g}$ is the gravitational acceleration vector. Stokes equations are used to model the flow of a fluid in which advective forces are small compared with viscous forces (low Reynolds number). Darcy's law is an alternative for the modeling of filtration of an incompressible fluid through a porous medium[5], which states: find $(\mathbf{v}, p) \in [\mathcal{H}^1(\Omega)]^d \times \mathcal{L}^2(\Omega)/\mathbb{R}$ such that:

$$\begin{cases} \nu \mathbf{M}_0 \mathbf{v} + \nabla p = \rho \mathbf{g} \\ \nabla \cdot \mathbf{v} = 0 \end{cases} \tag{2.12}$$

with appropriate boundary conditions. Both these models are parameterized versions of the Brinkman equation, which states: find $(\mathbf{v}, p) \in [\mathcal{H}^1_0(\Omega)]^d \times \mathcal{L}^2(\Omega)/\mathbb{R}$ such that:

$$\begin{cases} -\nabla \cdot (\nu \nabla_s \mathbf{v}) + \frac{\nu}{\sigma^2} \mathbf{M}_0 \mathbf{v} + \nabla p = \rho \mathbf{g} \\ \nabla \cdot \mathbf{v} = 0 \end{cases} \tag{2.13}$$

with appropriate boundary conditions. Indeed, when choosing ν finite and $\nu/\sigma^2 \approx 0$, the Stokes equation is retrieved, and when choosing $\nu \approx 0$ and ν/σ^2 finite, the Darcy equation is obtained[6]. Note that considering the coupling of parameterized models in particular implies that the unknowns to be solved on both sides of the interface are the same.

Coupling between two instances of a parameterized model can be performed by simply using any method designed for equations with heterogeneous parameters. For instance, in Cottereau and Díez (2011), the XFEM is used to solve the Darcy-Stokes coupling problem, with an application to the erosion of a fluid-saturated sand around the foot of a pier (see Fig. 2.3). Note that, in the context of penalization of fictitious domain methods, the coupling of a Stokes flow with a Darcy's law (with a Neumann boundary condition on the pressure) can be seen (Angot et al. 1999) as an $\mathcal{L}^2$ penalization of the Stokes flow, while the coupling with a Brinkman equation can be seen as an $\mathcal{H}^1$ penalization. Although this approach seems to be efficient for a large class of coupled problems, I am not aware of any example of application to stochastic models in the literature.

2.4 Volume coupling

Still interested in situations when the macro-scale quantity of interest is only sensitive to features of the micro-scale model within a limited portion of the full domain, we finally consider the overlapping case (rightmost plot in Fig. 2.1). This time, the subdomains Ω_M and Ω_m overlap and the interface between the two models is the volume $\Omega_\mathrm{M} \cap \Omega_\mathrm{m}$. In this section, we introduce the Arlequin framework (Ben Dhia 1998, Ben Dhia and Rateau 2001; 2005, Ben Dhia 2008), for

[5] Note that it is usually introduced in terms of the specific discharge $\mathbf{q} = \Phi \mathbf{v}$, the piezometric head $h = z + p/\rho|\mathbf{g}|$ and the permeability $\mathbf{K} = \rho|\mathbf{g}|\Phi \mathbf{M}_0^{-1}/\nu$, where Φ is the volumetric porosity (Darcy 1856).

[6] Interestingly, asymptotic analysis shows that a 3D Stokes flow within a medium with periodic inclusions (with homogeneous Dirichlet boundary conditions at the solid-fluid interfaces) is well described by: (i) a Brinkman model if the size ϵ of the periodicity cell and the size a_ϵ of the obstacles both tend to zero, such that the ratio $\sigma^2_\epsilon = \epsilon^3/a_\epsilon$ tends to a constant value $0 < \sigma^2 < +\infty$ (Allaire 1991a); and (ii) a Darcy equation if the rate of convergence of the size of the matrix a_ϵ is larger asymptotically ($\sigma = 0$) (Allaire 1991b). More precisely, the rescaled solution $(\mathbf{v}_\epsilon/\sigma^2_\epsilon, p_\epsilon)$ of Stokes equation on the periodic problems with cell size ϵ can be shown to converge to the solution of the Darcy problem. The scaling of $\mathbf{v}_\epsilon$ by σ^2_ϵ should be understood in the sense that, for a small enough ϵ, the Stokes problem for $\mathbf{v}_\epsilon$ really gives the same solution as Darcy's law with a coefficient $\nu \mathbf{M}_0/\sigma^2_\epsilon$. In that context, the linear term in $\mathbf{v}$ in the balance of momentum represents a homogenized drag force of the obstacles on the fluid, and the tensor $\mathbf{M}_0$ only depends on the shape of the matrix in the periodicity cell.

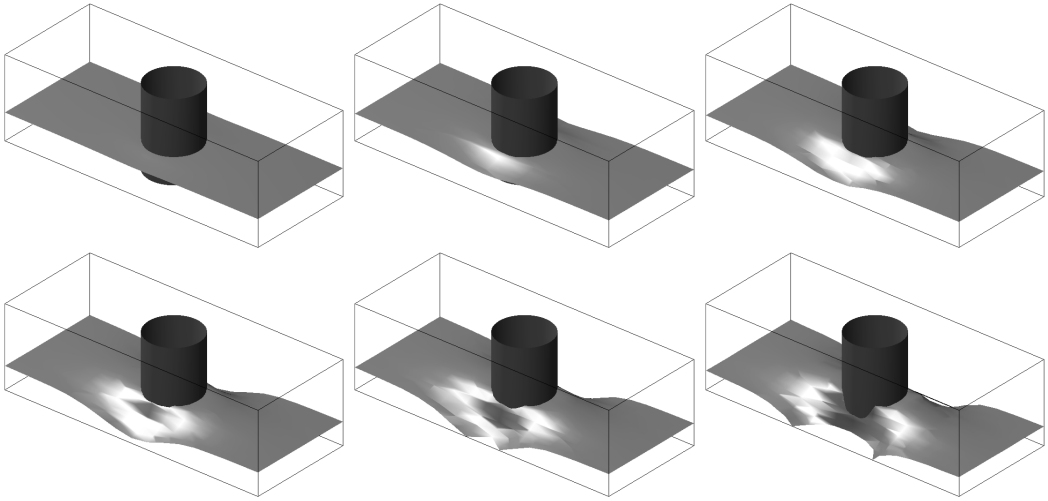

Figure 2.3 – *Evolution (from left to right and up to down) of the fluid-sand interface at the foot of a pier. The pier is represented by the dark cylinder, while the greyish surface is the interface between the fluid (above) and the fluid-saturated sans (below). Taken from Cottereau and Díez (2011).*

which extensions were proposed both for the stochastic-deterministic case (Cottereau et al. 2010a; 2011) and the stochastic-stochastic case (see Chamoin et al. (2008) and Le Guennec et al. (2014)). Other (deterministic) applications of the Arlequin method include the coupling of granular and continuum models (Gavoille et al. 2007, Wellmann and Wriggers 2012), and of heterogeneous wave propagation solvers (Gavoille et al. 2007, Marchais et al. 2012, Ghanem et al. 2013, Ben Dhia and Abben 2015). Similar approaches include the bridging domain method, where a $\mathcal{L}^2$ coupling operator is considered (Belytschko and Xiao 2003, Xiao and Belytschko 2004), and the work of Degond and Jin (2005), which enforces the coupling equation strongly.

In the Arlequin framework, the coupling problem reads: find $(\mathbf{u}_\mathrm{M}, \mathbf{u}_\mathrm{m}, \phi) \in \mathcal{V}_\mathrm{M} \times \mathcal{V}_\mathrm{m} \times \mathcal{V}_c$ such that

$$\begin{cases} a^\alpha_\mathrm{M}(\mathbf{u}_\mathrm{M}, \mathbf{v}; p_\mathrm{M}) + C(\phi, \Pi_\mathrm{M}(\mathbf{v})) = f^\beta_\mathrm{M}(\mathbf{v}; p_\mathrm{M}), & \forall \mathbf{v} \in \mathcal{V}_\mathrm{M} \\ a^\alpha_\mathrm{m}(\mathbf{u}_\mathrm{m}, \mathbf{v}; p_\mathrm{m}) - C(\phi, \Pi_\mathrm{m}(\mathbf{v})) = f^\beta_\mathrm{m}(\mathbf{v}; p_\mathrm{m}), & \forall \mathbf{v} \in \mathcal{V}_\mathrm{m} \\ C(\mathbf{v}, \Pi_\mathrm{M}(\mathbf{u}_\mathrm{M}) - \Pi_\mathrm{m}(\mathbf{u}_\mathrm{m})) = 0, & \forall \mathbf{v} \in \mathcal{V}_c \end{cases}, \tag{2.14}$$

where the forms a^α_M and f^β_M, on the one hand, and a^α_m and f^β_m, on the other hand, are the forms appearing in the classical weak formulations for each model, weighted by functions that partition the energy between the two available models. More specifically, for a stochastic diffusion model (with random diffusion parameter $\mathbf{k}_\mathrm{m}(\mathbf{x})$) coupled to a homogenized diffusion model (with effective diffusion parameter K_M), these forms are:

$$a^\alpha_\mathrm{M}(\mathbf{u}, \mathbf{v}) = \int_{\Omega_\mathrm{M}} \alpha_\mathrm{M}(\mathbf{x}) K_\mathrm{M} \nabla \mathbf{u} \cdot \nabla \mathbf{v} \, d\mathbf{x}, \quad a^\alpha_\mathrm{m}(\mathbf{u}, \mathbf{v}) = \mathbb{E}\left[\int_{\Omega_\mathrm{m}} \alpha_\mathrm{m}(\mathbf{x}) \mathbf{k}_\mathrm{m}(\mathbf{x}) \, \nabla \mathbf{u} \cdot \nabla \mathbf{v} \, d\mathbf{x} \right], \tag{2.15}$$

with similar partitioning for the loading terms (possibly with different functions $\beta_\mathrm{M}(\mathbf{x})$ and $\beta_\mathrm{m}(\mathbf{x})$). These weight functions allow to split appropriately the total energy among the two models. For instance, they verify (see Fig. 2.4 for an illustration in 1D) $\alpha_\mathrm{m}(\mathbf{x}) + \alpha_\mathrm{M}(\mathbf{x}) = 1$ wherever they are both defined and $\alpha_\mathrm{m}(\mathbf{x}) = 1$ or $\alpha_\mathrm{M}(\mathbf{x}) = 1$ wherever only one of the two is defined. Further, they allow to put more emphasis on the micro-scale model where it is defined and not coupled to the macro-scale model. The coupling operator C is taken as the stochastic extension of the $\mathcal{H}^1(\Omega_c)$ scalar product: $C(\mathbf{u}, \mathbf{v}) = \mathbb{E}\left[\int_{\Omega_c} (\mathbf{u} \cdot \mathbf{v} + \ell^2 \nabla \mathbf{u} : \nabla \mathbf{v}) \, d\mathbf{x} \right]$, where the constant length ℓ is introduced to weight relatively the L^2 and H^1 parts of the scalar product (see Ben Dhia (2008) for a discussion on the robustness of the method with respect to the choice of ℓ). The support of the coupling operator C and the introduction of the weighting functions are the main difference between Eq. (2.7) for interface coupling and Eq. (2.14) for volume coupling.

For a coupled scalar diffusion problem with homogeneous Dirichlet conditions on $\partial\Omega_\mathrm{M}$ (Cottereau et al. 2011), the functional spaces are $\mathcal{V}_\mathrm{M} = \mathcal{H}^1_0(\Omega_\mathrm{M})$, $\mathcal{V}_\mathrm{m} = \mathcal{L}^2(\Theta, \mathcal{H}^1(\Omega_\mathrm{m}))$ (assuming that Ω_m is strictly embedded in Ω), and

$$\mathcal{V}_c = \mathcal{H}^1(\Omega_c) \oplus \mathcal{L}^2(\Theta, \mathbb{R}) = \left\{ \psi(\mathbf{x}) + \theta \mathbb{I}_c(\mathbf{x}) | \psi \in \mathcal{H}^1(\Omega_c), \theta \in \mathcal{L}^2(\Theta, \mathbb{R}) \right\}. \tag{2.16}$$

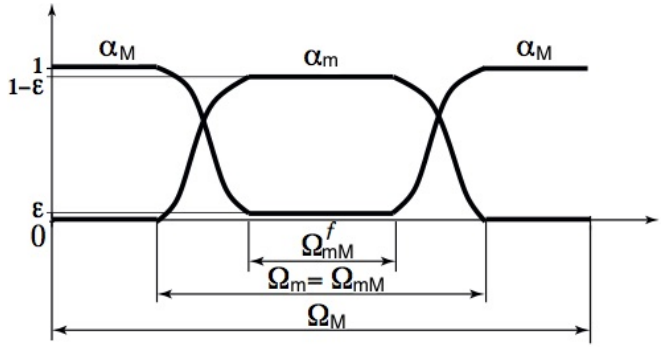

Figure 2.4 – *Example of α_m and α_M functions in a 1D setting. The ϵ represents a small value, typically $\epsilon = 0.01$ in numerical implementations. Modified from Néron et al. (2015).*

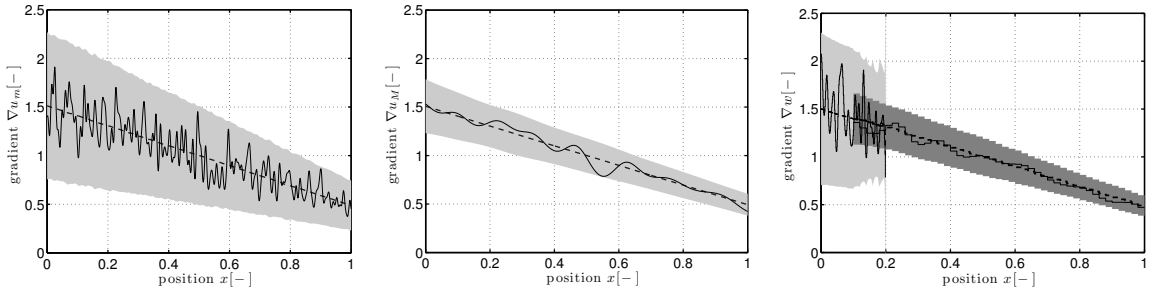

Figure 2.5 – *Gradient of a 1D micro-scale mono-model solution (left), of the macro-scale mono-model solution (center), and of the coupled model (right), with $\Omega_c = [0.1, 0.2]$: average (dashed lines), 90%-confidence interval (grey shades) and one realization (solid lines). Taken from Le Guennec et al. (2014).*

In the scalar case, the indicator function $\mathbb{I}(\mathbf{x})$ is such that $\mathbb{I}_c(\mathbf{x} \in \Omega_c) = 1$ and $\mathbb{I}_c(\mathbf{x} \notin \Omega_c) = 0$. Hence the mediator space $\mathcal{V}_c$ can be seen as composed of functions with a spatially-varying ensemble average and perfectly spatially-correlated randomness. The fluctuations in space of the random part actually follow the generator of the kernel of the acoustic operator. For the vector case, the function $\mathbb{I}(\mathbf{x})$ would include all the rigid body motions, so that the mediator space would be the superposition of a space-fluctuating average and of six rigid-body movements with random coefficients. In the case we are considering here, the projectors Π_M and Π_m can be simply taken as identity and left aside. As in the case of surface coupling, they are necessary when the unknown fields of the two models are defined on different spaces, for instance when considering the coupling of a random elastic continuum model with a deterministic beam model (Cottereau 2013b). Here, thanks to the specific structure of the space $\mathcal{V}_c$, the last equality of the system (2.14) can be written equivalently, $\forall \psi \in \mathcal{H}^1(\Omega_c)$ and $\forall \theta \in \mathcal{L}^2(\Theta, \mathbb{R})$,

$$C(\Psi, \mathbf{u}_M - \mathbf{u}_m) = C(\mathbb{E}[\Psi], \mathbf{u}_M - \mathbb{E}[\mathbf{u}_m]) - \mathbb{E}\left[\theta \int_{\Omega_c} (\mathbf{u}_m - \mathbb{E}[\mathbf{u}_m])\, d\mathbf{x}\right] = 0. \tag{2.17}$$

Therefore, this condition imposes that the (ensemble) average of the micro-scale solution $\mathbb{E}[\mathbf{u}_m]$ should follow the macro-scale solution $\mathbf{u}_M$ almost surely in space, and that the variability of the space-averaged random variable $\int_{\Omega_c} (\mathbf{u}_m - \mathbb{E}[\mathbf{u}_m]) d\mathbf{x}$ should vanish almost surely. In Chamoin et al. (2008), a larger coupling space was considered $\mathcal{V}_c = \mathcal{L}^2(\Theta, \mathcal{H}^1(\Omega_c))$, similar to that used by Chevreuil et al. (2013) in interface coupling (although supported over Ω_c). This choice imposes much stronger conditions on the continuity of the micro-scale and macro-scale solutions than what is obtained with the choice of Eq. (2.16). In the case when two stochastic models are coupled, as done in Le Guennec et al. (2014), it is clear that the point-wise variances of the two models should not be equal (compare the two leftmost plots in Fig. 2.5, corresponding to mono-model solutions). Hence, this property should not be enforced erroneously (see the rightmost plot of Fig. 2.5) by the coupling scheme using Eq. (2.16).

The stability of the coupled problem (2.14) for the random diffusion problem was proven in Cottereau et al. (2011). Numerical approximation of the solutions can be performed either with Monte Carlo sampling of the random space or by a spectral approach. An *a posteriori*

error estimation method is proposed in Zaccardi et al. (2013), that includes separation of error sources due to meshes, number of Monte Carlo samples, and size of the micro-scale model patch. Finally, an iterative non-intrusive (in the sense that already-existing model-dependent and model-optimized numerical schemes and software can be re-used) approach is described in Néron et al. (2015).

One of the major interests of considering volume coupling with respect to interface coupling is that a numerical patch of a micro-scale model can be imprinted on a pre-existing macro-scale model by simply modifying the parameters of that pre-existing model. In particular, the mesh, which is one of the most time-consuming task in the modeling of industrial problems, may remain unmodified. One of the drawbacks is the need to solve systems with potentially higher number of degrees of freedom since both the micro-scale and macro-scale models are discretized in the coupling area (although this remains marginal if the patch size is much smaller than the model size). Another drawback comes from the requirement to integrate micro-scale functions on macro-scale meshes, due to the integration of mixed operators defined on both micro-scale and macro-scale functional spaces (see the functions appearing in the coupling operator of Eq. (2.14)). As with the embedded methods of Section 2.1, this requires to devote special attention to the quadratures used to integrate the integrals of the weak formulations. Note that the introduction of volume coupling does not relieve the issue of ghost forces, which must still be treated with care (Chamoin et al. 2010, Wellmann and Wriggers 2012).

Stochastic upscaling 3

In this chapter, we concentrate on the upscaling of micro-scale models, defined by the triplet (bilinear form a_m, linear form f_m, functional space $\mathcal{V}_\mathrm{m}$) in Eq. (2.1), and the derivation of the corresponding macro-scale models, defined by the triplet (a_M, f_M, $\mathcal{V}_\mathrm{M}$) in Eq. (2.2). The macro-scale model can be called either homogenized, upscaled or effective model. In the simplest case, the functional form of the equations and loads is conserved through upscaling, with only a modification of the parameters. In more complicated situations, as was already seen with the derivation of Brinkman and Darcy models from Stokes model in footnote 6 of Sec. 2.3.3, the functional form of a_M is also different from that of a_m.

The most obvious interest of such upscaling process lies in general in a strong reduction of number of degrees of freedom. This is for instance clear when removing the small-scale fluctuations of the parameter of a diffusion problem, which usually allows to coarsen dramatically the mesh, and potentially leads to enormous savings of computational power. It may also provide interesting insights into the physical understanding of the system under study. For instance, following the phase of every little wriggle of a high frequency wave propagating in a heterogeneous medium might hide a general diffusion pattern of the energy. This is particularly important when designing new materials and structures (so-called meta-materials), optimized to present specific macro-scale behaviors. Finally and optimally, the upscaling process should also set clear bounds to each specific upscaled behavior. This is unfortunately not always possible, and one is often left with bounds defined as asymptotic limits.

We focus more specifically in this chapter on the wave equation in random media (for the micro-scale model), with a wide range of upscaled behaviors that were summarized in Fig. 1.12. The different situations are controlled by the relative ratios of the wave length λ, correlation length of the heterogeneities ℓ_c and propagation length L, as well as by the amplitude of the fluctuations of the heterogeneities σ^2. We separate these regimes in two classes[1]: low-frequency homogenization for $\eta = \lambda/L \approx 1$ (that we describe in Section 3.2), and high-frequency homogenization for $\eta \ll 1$ (that we consider in Section 3.3). We discuss localization separately in Section 3.4, and begin the chapter with a general discussion on upscaling techniques (Section 3.1). General books and reviews about upscaling in random media include Chernov (1960), Ishimaru (1978), Rytov et al. (1989) and van Rossum and Nieuwenhuizen (1999) with more emphasis on electromagnetics, Torquato (2001) for composite materials and Sato et al. (2012) for geophysics. My personal contributions are found in Section 3.2.1 with the development of a novel numerical homogenization technique in statics, in Section 3.3.3 with theoretical and numerical contributions to the radiative transfer equation in anisotropic elastic media, and in Section 3.4 with the numerical observation of localization in ballasted railway tracks.

3.1 Upscaling techniques

This section introduces some upscaling techniques for the wave equation in random media. We concentrate here on the techniques themselves and describe the upscaled regimes they allow to obtain in the following sections. For particular regimes (in particular in the low frequency and for weak heterogeneities), the same result can be obtained with different techniques. In other cases, the same technique with different parameters can yield different regimes. For instance, multiscale

[1] Another customary classification relies rather on ℓ_c/λ: Rayleigh regime for low values $\ell_c/\lambda \ll 1$, Rayleigh-Gans regime for mid-values $\ell_c/\lambda \approx 1$, and stochastic regime for higher values $\ell_c/\lambda \gg 1$.

expansion (Section 3.1.3) allows to derive both the low-frequency effective wave equation and the radiative transfer equation in a higher frequency range.

3.1.1 Single scattering approximation (Born and Rytov approximations)

One of the simplest upscaling technique consists in the single scattering approximation. In that context, the primary waves (solution of the equation with homogeneous mechanical properties) are assumed unmodified during their propagation through the inhomogeneous region, and contribute to the scattered field by a single reflection on the inhomogeneities. The constitutive tensor is written $\mathbb{C}(\mathbf{x}) = \mathbb{C}_0 + \sigma\mathbb{C}_1(\mathbf{x})$, with a small standard deviation $\sigma \ll 1$, and the density is assumed homogeneous for simplicity[2]. The solution field is then expanded in terms of σ: $\mathbf{u}(\mathbf{x},t) = \mathbf{u}_0(\mathbf{x},t) + \sigma\mathbf{u}_1(\mathbf{x},t) + \sigma^2\mathbf{u}_2(\mathbf{x},t) + o(\sigma^2)$. Introducing this expansion in the wave equation (1.1), we obtain a series of problems:

$$\begin{cases} \rho_0\ddot{\mathbf{u}}_0(\mathbf{x},t) - \nabla\cdot(\mathbb{C}_0 : \nabla\otimes\mathbf{u}_0(\mathbf{x},t)) &= \mathbf{f}(\mathbf{x},t) \\ \rho_0\ddot{\mathbf{u}}_1(\mathbf{x},t) - \nabla\cdot(\mathbb{C}_0 : \nabla\otimes\mathbf{u}_1(\mathbf{x},t)) &= \nabla\cdot(\mathbb{C}_1(\mathbf{x}) : \nabla\otimes\mathbf{u}_0(\mathbf{x},t)) \,, \\ \dots \end{cases} \tag{3.1}$$

that can be solved sequentially. The solution of the first equation represents the incident field in a homogeneous medium, while the solution of the second equation is the singly-scattered field on the heterogeneities. The solution at first order $\mathbf{u}_{\text{Born}} = \mathbf{u}_0 + \sigma\mathbf{u}_1$, obtained with only the first two equations is called the Born approximation (Sato et al. 2012, Chapter 4). Statistics on the intensity $\mathbb{E}\left[\mathbf{u}_{\text{Born}}\otimes\mathbf{u}_{\text{Born}}\right]$ and an equivalent attenuation can then be estimated by simple calculus (Shapiro and Kneib 1993). Scattering cross-sections can also be obtained by considering the specific case of a plane wave incident on the heterogeneity (Sato 1984).

The Rytov approximation (Ishimaru 1978, Chapter 6) is a slightly different occurence of the single scattering approximation, where the phase of the solution is expanded rather than the amplitude: $\mathbf{u}(\mathbf{x},t) \approx \mathbf{u}_0(\mathbf{x},t)\exp(\sigma\psi_1(\mathbf{x},t) + \sigma^2\psi_2(\mathbf{x},t) + \dots)$. Introducing this expansion in the wave equation (1.1), and after some algebraic manipulations, we obtain

$$\begin{cases} \rho_0\ddot{\mathbf{u}}_0(\mathbf{x},t) - \nabla\cdot(\mathbb{C}_0 : \nabla\otimes\mathbf{u}_0(\mathbf{x},t)) &= \mathbf{f}(\mathbf{x},t) \\ \rho_0(\ddot{\mathbf{u}_0\psi_1}) - \nabla\cdot(\mathbb{C}_0 : \nabla\otimes(\mathbf{u}_0\psi_1)) &= \nabla\cdot(\mathbb{C}_1(\mathbf{x}) : \nabla\otimes\mathbf{u}_0(\mathbf{x},t)) \,. \\ \dots \end{cases} \tag{3.2}$$

The Rytov approximation is obtained by considering the first order solution $\mathbf{u}_{\text{Rytov}} = \mathbf{u}_0(\mathbf{x},t)\exp(\sigma\psi_1(\mathbf{x},t))$. Observing that the term $\mathbf{u}_0\psi_1$ in the Rytov approximation is equal to the term $\mathbf{u}_1$ in the Born approximation (compare the second lines of Eq. (3.1) and Eq. (3.2)), and expanding the exponential in powers of $\sigma \ll 1$, we see that $\mathbf{u}_{\text{Rytov}} = \mathbf{u}_{\text{Born}} + \sigma^2\psi_1^2\mathbf{u}_0/2 + o(\sigma^2)$. The two approximations therefore only coincide up to the first order in σ. There has been some debate (Keller 1969, Oristaglio 1985, Woodward 1989, Cairns and Wolf 1990) over which of the two approximations was better, and the consensus seems to be that the Born approximation describes the reflected energy better while the Rytov approximation performs better in the description of the transmitted energy.

These two approximations have been widely used in geophysics (Sato 1984, Shapiro and Kneib 1993, Sato et al. 2012) and the modeling of ultrasounds in polycrystalline materials (Li and Rokhlin 2015), either directly or through approximations of scattering cross-sections. Interestingly, we have used the Born approximation to derive an efficient error indicator for mesh adaptivity in the context of Monte Carlo solutions of stochastic partial differential equations (Cottereau and Díez 2015) . Although very appealing for their simplicity, these approaches are rather limited. Indeed, there is a hidden assumption that $\lambda/L \approx 1$ and $\ell_c/L \approx 1$, since they are not considered influential in the asymptotic expansions. Other authors have proposed to use the Born approximation directly, with no formal derivation from the full wave equation, but checking its validity *a posteriori* through conservation of energy. However, the mathematical foundation of such approach appears debatable.

[2] Considering a heterogeneous density yields an obvious extension of the results presented here, as long as the density fluctuations are also very small: $\rho(\mathbf{x}) = \rho_0 + \sigma_\rho\rho_1(\mathbf{x})$, with $\sigma_\rho \ll 1$.

3.1.2 Mean field approximation (Dyson and Bethe-Salpeter equations)

The mean field approximation technique (see Karal and Keller (1964), Frisch (1966), Willis (1997), Sheng (2006, Chapter 3) or Sato et al. (2012, Chapter 7), and (Stanke and Kino 1984) for the consideration of anisotropic media) is a different upscaling technique, based on the Lippmann-Schwinger formalism. The integral form of the wave equation (1.1) is considered:

$$\mathbf{u}(\mathbf{x},t) = \mathbf{u}_0(\mathbf{x},t) - \sigma \int_0^T \int_\Omega \mathbf{G}_0(\mathbf{x},t;\mathbf{y},s)\nabla\cdot(\mathbb{C}_1(\mathbf{y}) : \nabla\otimes\mathbf{u}(\mathbf{y},s))d\mathbf{y}ds \tag{3.3}$$

where $\mathbf{G}_0(\mathbf{x},t;\mathbf{y},s)$ is the homogeneous Green's function, that is to say the solution of the wave equation with chosen homogeneous properties $\mathbb{C}_0$ and unit impulse load $\delta(s)\delta(\mathbf{y})$ at $\mathbf{y}$ and s, and $\mathbf{u}_0(\mathbf{x},t)$ is the solution of the homogeneous wave equation for loading $\mathbf{f}$, that is to say $\mathbf{u}_0(\mathbf{x},t) = \int_0^T \int_\Omega \mathbf{G}_0(\mathbf{x},t;\mathbf{y},s)\rho(\mathbf{y})\mathbf{f}(\mathbf{y},s)d\mathbf{y}ds$. This equation can be rewritten, using obvious operator notations:

$$\mathbf{u} = \mathbf{u}_0 - \mathcal{G}_0\Lambda_\sigma\mathbf{u}. \tag{3.4}$$

This equation is exact whatever the choice of homogeneous tensor $\mathbb{C}_0$, and does not require any assumption on the order of magnitude of σ. Replacing the true solution $\mathbf{u}$ in the right hand side of Eq. (3.4) by the solution $\mathbf{u}_0$ would yield the Born approximation seen in the previous section, and be valid only for $\sigma \ll 1$. The mean field approximation technique does not perform such simplification, but rather looks for an approximation only of the average of the solution $\mathbf{u}$ or of higher moments of that solution. In the sense that it looks for equation of upscaled quantities of interest, it is more of an upscaling technique than the single scattering approximation, that was trying to approximate the full solution.

Using Feynman diagrams or the regularization method (Frisch 1966), one obtains the Dyson equation (Dyson 1949a;b), that drives the coherent wave:

$$\mathbb{E}[\mathbf{u}] = \mathbf{u}_0 + \mathcal{G}_0\mathcal{M}\mathbb{E}[\mathbf{u}], \tag{3.5}$$

where the operator $\mathcal{M}$ is called the mass operator[3] or self-energy. Although this formulation is appealing for its simplicity, the operator $\mathcal{M}$ is defined (see for instance (Frisch 1966, Eq. (9-20))) as a formal expansion involving moments and cross-correlations of various orders of the random operator Λ_σ. The series does not contain obvious secular terms (although no formal proof is available), but a necessary condition for its convergence is that $\sigma\ell_c^2 \ll \lambda^2$. A slightly different formulation is given in Willis (1997; 2012) that incorporates a dependency on the average strain and the average velocity accounts for any kind of fluctuations of both constitutive tensor and density, and possible nonlinearities at the micro-scale. Using similar ideas as Dyson, the equation driving the behavior of the intensity, the so-called Bethe-Salpeter equation (Salpeter and Bethe 1951), can also be derived:

$$\mathbb{E}[\mathbf{u}\otimes\mathbf{u}] = \mathbb{E}[\mathbf{u}]\otimes\mathbb{E}[\mathbf{u}] + (\mathcal{G}_0\otimes\mathcal{G}_0)\Gamma\mathbb{E}[\mathbf{u}\otimes\mathbf{u}]. \tag{3.6}$$

Γ is sometimes called the intensity operator, and is likewise defined as a formal infinite sum (see for instance (Frisch 1966, Eq. (9-21)) for the precise definition).

When the mass operator is known exactly, the Dyson equation can be solved through a Fourier transformation. Otherwise, the operator must be approximated by the first terms of its sum. Truncation at the first order leads to the Bourret approximation of the Dyson equation (Bourret 1962) and the so-called ladder approximation for the Bethe-Salpeter equation (See Lombaert and Clouteau (2006) for an example in the field of seismic engineering). When the mass operator is independent of the wave number $\mathbf{k}$, for instance with point-like scatterers or with finite-volume scatterers with $\ell_c/\lambda \ll 1$, the Coherent Potential Approximation and Spectral Function Approach (Sheng 2006) provide self-consistent techniques[4] to identify upscaled coefficient of the wave equation by seeking those that yield no average scattering. For sparse ($\sigma^2 \ll 1$) distributions of small ($\ell_c \ll \lambda$) scatterers, the Foldy (or Foldy-Lax) approximation simplifies the mass operator by considering all second-order scatterings except those involving self-interaction on the same scatterers.

[3] This name comes from the quantum physics community (see Sheng (2006) for instance) and does not have any relation with a mechanical mass.

[4] However, they do not provide any *a priori* proof of existence.

3.1.3 Multiple scale analysis

Multiple scale techniques try to control potential secular terms in the previous expansions by introducing additional independent scale variables in the formulation. The dependency on the scale variable (for instance, space $\mathbf{x}$ in the example below) in the micro-scale operator and variables is separated into a slow scale $\mathbf{x}$ and a fast scale $\mathbf{x}/\eta$, with $\eta \ll 1$, which are then considered as independent. Convergence analysis of the sequence of solution parameterized by η allows, when it exists, to derive the equation driving the behavior of the slow part of the solution (see Papanicolaou and Varadhan (1981) for details in a stochastic setting). The parameters of that equation (the homogenized coefficients) are also obtained in the convergence process.

Considering the wave equation (1.1), we therefore introduce a small parameter $\eta \ll 1$ and assume that the parameters $\rho(\mathbf{x}/\eta)$ and $\mathbb{C}(\mathbf{x}/\eta)$ fluctuate at the fast scale $\mathbf{x}/\eta$ while the loading $\mathbf{f}(\mathbf{x}, t)$ fluctuates at the slow scale $\mathbf{x}$ (which corresponds to assuming $\ell_c \ll \lambda \approx L$). The solution $\mathbf{u}(\mathbf{x}, \mathbf{x}/\eta, t)$ then fluctuates at both scale $\mathbf{x}$ and $\mathbf{x}/\eta$. Removing the dependency on time t for simplicity, the wave equation reads:

$$\rho\left(\frac{\mathbf{x}}{\eta}\right)\ddot{\mathbf{u}}\left(\mathbf{x}, \frac{\mathbf{x}}{\eta}\right) - \nabla\cdot\mathbb{C}\left(\frac{\mathbf{x}}{\eta}\right) : \nabla\otimes_s \mathbf{u}\left(\mathbf{x}, \frac{\mathbf{x}}{\eta}\right) = \mathbf{f}(\mathbf{x}) \tag{3.7}$$

Assuming independence of the two variables $\mathbf{x}$ and $\mathbf{y} = \mathbf{x}/\eta$, the derivation operator is written $\nabla = \eta^{-1}\nabla_{\mathbf{y}} + \nabla_{\mathbf{x}}$, and the expansion of the solution in powers of η: $\mathbf{u}(\mathbf{x}, \mathbf{y}) = \mathbf{u}_0(\mathbf{x}, \mathbf{y}) + \eta\mathbf{u}_1(\mathbf{x}, \mathbf{y}) + \eta^2\mathbf{u}_2(\mathbf{x}, \mathbf{y}) + ...$, yields a series of equations:

$$\begin{cases} \nabla_{\mathbf{y}}\cdot\mathbb{C} : \nabla_{\mathbf{y}}\otimes_s \mathbf{u}_0 &= \mathbf{0} \\ \nabla_{\mathbf{y}}\cdot\mathbb{C} : \nabla_{\mathbf{y}}\otimes_s \mathbf{u}_1 &= -\nabla_{\mathbf{y}}\cdot\mathbb{C} : \nabla_{\mathbf{x}}\otimes_s \mathbf{u}_0 - \nabla_{\mathbf{x}}\cdot\mathbb{C} : \nabla_{\mathbf{y}}\otimes_s \mathbf{u}_0 \\ \nabla_{\mathbf{y}}\cdot\mathbb{C} : \nabla_{\mathbf{y}}\otimes_s \mathbf{u}_2 &= \mathbf{f} - \rho\ddot{\mathbf{u}}_0 - \nabla_{\mathbf{y}}\cdot\mathbb{C} : \nabla_{\mathbf{x}}\otimes_s \mathbf{u}_1 - \nabla_{\mathbf{x}}\cdot\mathbb{C} : (\nabla_{\mathbf{x}}\otimes_s \mathbf{u}_0 + \nabla_{\mathbf{y}}\otimes_s \mathbf{u}_1) \end{cases} . \tag{3.8}$$

The first equation indicates that the macroscale solution $\mathbf{u}_0$ does not depend on the microscale variable $\mathbf{y}$. Hence, $\nabla_{\mathbf{x}}\cdot\mathbb{C} : \nabla_{\mathbf{y}}\otimes_s \mathbf{u}_0(\mathbf{x}, \mathbf{y}) = \mathbf{0}$ in the second equation, and the corrector $\mathbf{u}_1$ is linearly related to $\nabla_{\mathbf{x}}\otimes_s \mathbf{u}_0$ through a proportionality (third-order) tensor $\mathbf{W}(\mathbf{y})$ that can be explicitly constructed: $\mathbf{u}_1 = \nabla_{\mathbf{x}}\otimes_s \mathbf{u}_0 : \mathbf{W} = \sum_{ij}\partial_{\mathbf{x}_i}\mathbf{u}_{0,j}\mathbf{W}_{ij}$. Finally the third equation admits a solution only if a certain solvability condition is satisfied, and this condition yields the equation driving the upscaled solution $\mathbf{u}_0(\mathbf{x})$. In the periodic case, this condition (the Fredholm alternative) is simply that the integral of the right hand side over the periodic cell should vanish. In the stochastic case, the solvability condition requires hypotheses of stationarity, ergodicity and uniform ellipticity of tensor $\mathbb{C}$ (see for instance Papanicolaou and Varadhan (1981)). In the rapidly fluctuating case ($\ell_c \ll \lambda$) we have considered here, the upscaled equation is then the following wave equation:

$$\rho^*\ddot{\mathbf{u}}_0(\mathbf{x}) - \nabla_{\mathbf{x}}\cdot\mathbb{C}^* : \nabla_{\mathbf{x}}\otimes_s \mathbf{u}_0(\mathbf{x}) = \rho_0\mathbf{f}(\mathbf{x}) \tag{3.9}$$

where the homogenized density is simply $\rho^* = \mathbb{E}\left[\rho(\mathbf{y})\right]$ and the fourth-order homogenized tensor $\mathbb{C}^*$ is given by

$$\mathbb{C}^*_{ijk\ell} = \mathbb{E}\left[(\mathbf{e}_i\otimes\mathbf{e}_j + \nabla_{\mathbf{y}}\otimes_s \mathbf{W}_{ij}) : \mathbb{C}(\mathbf{y}) : (\mathbf{e}_k\otimes\mathbf{e}_\ell + \nabla_{\mathbf{y}}\otimes_s \mathbf{W}_{k\ell})\right], \tag{3.10}$$

where the $\{\mathbf{e}_i\}_{1\le i\le d}$ are the unit vectors of $\mathbb{R}^d$.

The so-called corrector tensor $\mathbf{W}(\mathbf{y})$ is only implicitly defined, so its actual evaluation may be computationally demanding. In the simplest case when the properties $\mathbb{C}$ are periodic, its computation involves the solution of a partial differential equation supported only on the periodic cell. When considering a random model of properties, the corrector problem is supported on the full domain Ω. For properties fluctuating at both scales $\mathbb{C}(\mathbf{x}, \mathbf{x}/\eta)$, a corrector problem should be set around each position $\mathbf{x}$. In all cases, once computed, the corrector tensor can be used to improve the solution $\mathbf{u}_0$, fluctuating only at the slow scale, with the first order term $\eta\mathbf{u}_1$, which fluctuates on the rapid scale: $\mathbf{u}^*(\mathbf{x}, \mathbf{x}/\eta) = \mathbf{u}_0(\mathbf{x}) + \eta\nabla_{\mathbf{x}}\otimes_s \mathbf{u}_0(\mathbf{x}) : \mathbf{W}(\mathbf{x}, \mathbf{x}/\eta)$. In the static case, the displacement field $\mathbf{u}^*(\mathbf{x})$ converges (as a function of η) in $\mathcal{H}^1(\Omega)$ norm to the solution $\mathbf{u}(\mathbf{x})$ of Eq. (3.7), while $\mathbf{u}_0(\mathbf{x})$ converges only in $\mathcal{L}^2(\Omega)$ norm.

In the example given here, we obtain a homogenized partial differential equation that has the same form as the initial one. Only the parameters have been homogenized. However, this is not always the case. In particular, applying this technique on the transport equation for the Wigner transform of $\mathbf{u}$ yields a radiative transfer equation (see Section 3.3.3). Note also that the

implicit assumption that the amplitude of fluctuations of $\mathbb{C}$ is of order $\sigma \approx 1$ can be challenged depending on the example at hand. For instance, it is necessary to consider $\sigma \approx \sqrt{\lambda/L} \ll 1$ to obtain the radiative transfer equation. Finally, similar scale decomposition can be performed with the time variable, yielding homogenization in time (Guenounni and Aubry 1986, Devulder et al. 2010, Fish et al. 2012).

Rigorous mathematical justification of the asymptotic expansion above can be performed in various manners. For instance, in the energy method (see Tartar (2009) for a general exposition and Kozlov (1980), Yurinskii (1980) and Papanicolaou and Varadhan (1981) for the stochastic setting), convergence (in η) is proven for the product of the solution field $\mathbf{u}(\mathbf{x}, \mathbf{x}/\eta)$ with the parameter field $\mathbb{C}(\mathbf{x}/\eta)$, both weakly converging, by using a weak formulation with a specifically designed set of functions oscillating at rate η. These functions are the elements of the corrector tensor $\mathbf{W}(\mathbf{y})$. Other frameworks can be considered for the convergence analysis, potentially with relaxed hypotheses (periodicity, ergodicity, linearity) on the parameters. For instance, Γ-convergence relates to the convergence of sequences of integral functionals (see Dal Maso (1993) for the stochastic setting) while G- (or H-) convergence studies the convergence of elliptic operators (see Zhikov et al. (1979) for the stochastic setting). More specific results in random settings include Sab (1992) (for linear and non-linear elasticity) and Bourgeat et al. (1994) (two-scale convergence in the mean).

3.1.4 Other approaches

Although emphasis was set on three particular techniques above, many other methods exist for more specialized cases. For critical phenomena (such as localization, see Section 3.4), it is sometimes possible to study the upscaling process through renormalization group analysis. In that approach, a family of operators is constructed, which possesses the structure of a group under the chosen upscaling operations. Fixed points then provide insights on the critical behavior (see E (2011, Section 2.6) or Sepehrinia et al. (2008)). Matched asymptotic techniques apply to problems with boundary or internal layers, including shocks. Asymptotic solutions are sought separately in the bulk and on the boundary, and later reconstructed by postulating continuity at some small distance for the boundary (see (E 2011, Section 2.1) for more details). Finally, Fouque et al. (2007) present detailed analytical results in the upscaling of wave propagation in 1D random media in a wide range of ratios of λ, ℓ_c and L using advanced random processes tools. Theses results can be extended to 3D media, but only for mono-dimensional randomness, such as in randomly layered soils or layered composite materials.

In this chapter (and entire document), we concentrate on the upscaling of stochastic problems. We will therefore leave aside discussions related to upscaling of waves in periodic media, using Bloch waves in particular (Bensoussan et al. 1978, Chapter 14). This includes the interesting literature on upscaling in the non-separated regime ($\lambda \approx \ell_c$), where Craster et al. (2010) and Boutin et al. (2012) propose to seek the solution as the slow modulation of a rapidly-fluctuating eigenmode of the periodic cell. Finally, we will also leave aside upscaling techniques that are essentially numerical, such as wavelet-based numerical homogenization (Brewster and Beylkin 1995, Dorobantu and Engquist 1998, Engquist and Runborg 2001). These techniques do not yield homogenized equation but rather allow to compute the solution of a micro-scale problem in an efficient manner by the condensation of the discretized operators. More techniques of numerical homogenization were already discussed in Section 2.1.2.

3.2 Upscaling in the low-frequency range ($\eta \approx 1$)

We now turn to results obtained in particular regimes. We start with the low-frequency regime, where $\eta = \lambda/L \approx 1$, either in statics ($\lambda, L \to \infty$) or dynamics ($\lambda$ and L finite). These two regimes have been the most widely studied because both the micro-scale and upscaled equations are wave propagation equations. We then move on to regimes where the correlation length is larger with respect to the wavelength.

3.2.1 (Static) homogenization ($\epsilon = \infty$, $\sigma^2 \approx 1$)

In statics, the developments of Section 3.1.3 apply, just removing the inertial term. Hence, starting from an elliptic equation as Eq. (3.7) without the inertial term, one obtains Eq. (3.9), also without the inertial term. The definition of the upscaled constitutive tensor is given in Eq. (3.10). The theoretical question of finding the upscaled equation being solved, the only issue stands in the computation of the upscaled tensor $\mathbb{C}^*$. Besides some particular cases for which analytical (layered random media in particular) or specific numerical solutions are available (see for instance Blanc et al. (2007) and Le Bris (2010) in a random quasi-periodic setting), this computational problem is often expensive. Indeed, the prediction of the effective tensor involves the solution of a corrector problem which is *a priori* posed on a domain of infinite size. In order to approximate the effective tensor through numerical simulations, the domain therefore has to be truncated at some finite distance and boundary conditions to be introduced. It has been proven (Sab 1992, Bourgeat and Piatnitski 2004) that, whatever the choice of boundary conditions, the limit of the estimated tensor was indeed the effective tensor. However, convergence with respect to the size of the domain may be very slow. Alternatively, it is also possible (see Sab (1992), Kanit et al. (2003)) to use a smaller domain and perform averages over several realizations of the random medium. Several authors[5] have followed this path (see for instance Povirk (1995), Gusev (1997), Roberts and Garboczi (2000) or Zeman and Šejnoha (2001)), even implementing schemes to accelerate convergence (through angular averaging in Meille and Garboczi (2001) among others, or through the use of antithetic variables in Costaouec et al. (2011)). Even though these schemes converge (in terms of the random dimension) for finite size-domains, they do so to biased values. And these biases only vanish when the size of the domain becomes very large (with respect to the correlation length).

In Cottereau (2013;b; 2014), we introduced a numerical strategy to compute the homogenized tensor of a random medium. It allows to extend the size of the domain in a cost-effective manner and to play simultaneously with the size of the domain and the discretization along the random dimension (number of Monte Carlo samples) to yield the effective tensor. This is achieved through the coupling of the random microstructure with a homogenized macrostructure, the characteristics of which are updated iteratively using a self-consistent approach (see Fig. 3.1). Using this coupled approach, the size of the complex microstructure is limited, while the boundary conditions are pushed away and their influence limited through the tentative homogenized medium. In the 2D scalar case with a continuously fluctuating parameter following a log-normal first-order marginal density, where the homogenized tensor does not depend on the correlation structure or other high-order moments of the parameter field, it was shown that boundary effects completely disappeared (see Fig. 3.2). The main feature of the coupling strategy is that it really couples the random microstructure with the deterministic homogenized model, and not each (deterministic) realization of the random medium with a homogenized model, in a fully independent manner. Hence, the ergodicity of the random medium is used in full to accelerate convergence and minimize the bias introduced by the finite size of the domain. The idea of coupling the microstructure to a homogenized medium to limit the influence of the boundary conditions was already developed in Héraud et al. (1998) and Haddadi et al. (2003), but with three major differences: (1) the microstructure is here random, while it was deterministic (and heterogeneous) in the previous papers, (2) the coupling is here made over a volume rather than along a surface, and (3) the approach is coupled to an iterative scheme in order to identify the value of the effective tensor, while it was previously only used to perform direct computations, for a given value of the homogenized tensor. Note also that Cancès et al. (2015) use a similar embedding to derive efficient approximation technique for the corrector problem for a particular type of binary microstructure.

Leaving aside the approximation of the corrector problem, it is also possible to rewrite the upscaled tensor definition in Eq. (3.10) as a minimization problem and to derive bounds for that tensor. Many different bounds have been derived, usually with a trade-off between generality (application to a wide range of microstructure and incorporation of more or less precise information on the micro-structure) and accuracy (distance between lower and upper bounds). The books of Torquato (2001) and Milton (2002) review a large set of these bounds.

[5]Note that, to the best of my knowledge, the very effective FFT method of Moulinec and Suquet (1998) has not been extended yet to stochastic homogenization, although an obvious Monte Carlo extension could be considered.

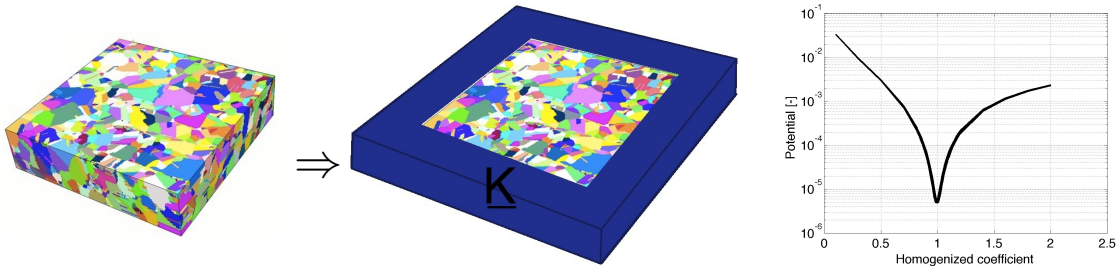

Figure 3.1 – *Principle of the homogenization method in Cottereau (2013): the microstructure (left) is surrounded by a homogenized medium (center), and an optimization scheme finds the homogenized coefficient by minimizing the elastic energy (right). The rightmost plot is taken from Cottereau (2013) and the polycrystalline image from Schwartz (2011).*

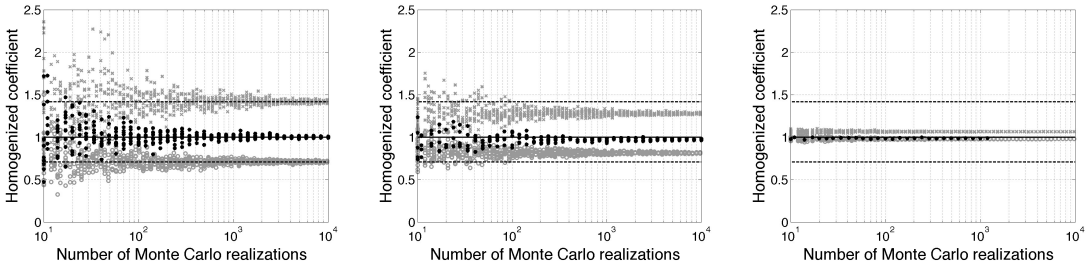

Figure 3.2 – *Convergence of the Arlequin estimate (black pluses) for different sizes of the computing box: (left) $\ell_c/L = 10$, (center) $\ell_c/L = 1$, and (right) $\ell_c/L = 0.1$) as a function of the numbers of Monte Carlo trials, and comparison with the coefficients obtained for Dirichlet (light grey crosses) and Neumann (light grey circles) boundary conditions. The dashed and solid lines indicate respectively the values of the arithmetic and harmonic averages. Taken from Cottereau (2013).*

3.2.2 Dynamic homogenization ($\epsilon \gg 1$, $\sigma^2 \approx 1$)

In the 1950s, a series of papers discussed the upscaling of wave propagation equations in layered media (see Postma (1955) among others). This research was rooted in actual seismic measurements showing anisotropy of the propagated wave field (Uhrig and van Melle 1955), and aimed at revealing the origin of anisotropy in geophysical materials (Backus 1962). Interest in this field was later renewed with the appearance of layered composite materials (see Willis (1997) or Milton (2002), among many others). These papers proved that a horizontally-layered medium with locally isotropic behavior can be upscaled as a homogeneous transversely isotropic medium, provided that $\lambda \gg \ell_c$, where ℓ_c corresponds to the layer thickness. Although applicable to full 3D problems, the formalism in these original papers was simplified by the consideration only of mono-dimensional heterogeneity (that is to say layering along a fixed direction with fluctuations in the thicknesses and/or properties in each layer) and alignment with the principal directions. Most of these early results were not explicitly considering random media, although periodicity was not necessarily a required argument, and replaced with a loose definition of statistical homogeneity.

As discussed in Section 3.2.1, for general fluctuations (not limited to layered media), upscaling of a wave equation in the low-frequency ($\lambda \approx L$) and rapidly fluctuating ($\lambda \gg \ell_c$) regime yields also a wave equation, with homogenized coefficients. The homogenized density is simply the arithmetic average of the micro-scale density. The homogenized elastic tensor $\mathbb{C}$ is defined in Eq. (3.10), as in statics. These results can be obtained using the asymptotic expansion technique, as in Section 3.1.3, or equivalently using the mean-field approximation (Frisch 1967, Chapter 17a), or advanced techniques based on stochastic processes in layered media (Fouque et al. 2007, Chapter 4). This regime of low-frequency homogenization has been known for a long time, and was considered anew with the numerical experiments in Capdeville and Marigo (2007) and Capdeville et al. (2010). The explicit recognition that the upscaling results remain correct when the constitutive tensor fluctuates at both the rapid $\epsilon\mathbf{x}$ and slow $\mathbf{x}$ scales allowed to compute partially upscaled density and constitutive tensor in a non-periodic case. Indeed, the results presented in Section 3.1.3 extend naturally to that case, although Eq. (3.10) must be approximated around each local position $\mathbf{x}$ using a spatial filter and extension operator, practically solving each time a different corrector problem. It is a computationally intensive approach, although the corrector

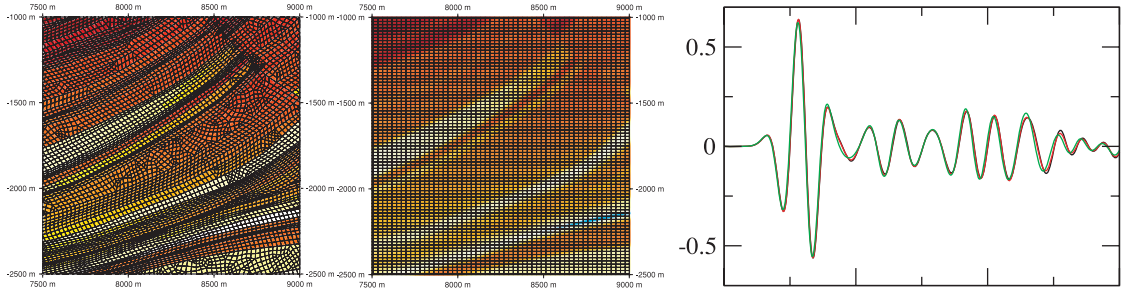

Figure 3.3 – *Seismic wave propagation in 2D Marmousi models: with all layers accurately meshed (left mesh and green line in the rightmost plot), or with an upscaled model, continuously fluctuating and anisotropic everywhere (center mesh and red line in the rightmost plot). Taken from Capdeville et al. (2010).*

problems are formulated in statics. The properties of the upscaled medium fluctuate in space (at the slow scale $\mathbf{x}$) and are everywhere anisotropic, even though the original medium was locally isotropic everywhere. Capdeville et al. (2010) solved the classical Marmousi benchmark problem (see Fig. 3.3) either directly, with layers much smaller than the wave length, or with an upscaled model. In the expected frequency range, the results of the two simulations are remarkably similar[6].

3.2.3 Non-separated homogenization ($\epsilon \approx 1$, $\sigma^2 \approx 1$ or $\sigma^2 \gg 1$)

When the wavelength decreases, relative to the correlation length, separation of scales cannot be assumed anymore[7]. This lack of separation of scales induces non-locality of the constitutive relations for the ensemble-averaged stress field (Willis 1997; 2012), and simple classical upscaled models cannot be formulated in general. We discuss in this section particular situations when partial upscaling can still be obtained. Note that the developments presented here were developed only in periodic media, but they are expected to apply to random media in a rather straightforward fashion.

A first case, already hinted at in the previous section, consists at upscaling only the high-frequency part of the mechanical properties. This consists in separating the mechanical properties into a slowly-fluctuating part (for instance $\mathbb{C}^s$) and a rapidly-fluctuating part ($\mathbb{C}^f$) through a well chosen filter $\mathcal{F}^{\epsilon_0}$:

$$\mathbb{C}^s(\mathbf{x}) = \mathcal{F}^{\epsilon_0}(\mathbb{C}), \quad \mathbb{C}^f(\mathbf{x}, \epsilon\mathbf{x}) = (\mathbf{I} - \mathcal{F}^{\epsilon_0})(\mathbb{C}). \tag{3.11}$$

The filter is parameterized by $\epsilon_0 = \lambda/\ell_c^0$, with ℓ_c^0 the typical size of the smallest fluctuations that should be homogenized. Essentially, the rapidly-fluctuating properties $\mathbb{C}^f$ are then homogenized, while the slowly-fluctuating part $\mathbb{C}^s$ is left untouched. The choice of filter $\mathcal{F}^{\epsilon_0}$ and length scale ϵ_0 can be done at will, but separation of scales is required for homogenization to take place, so that the wavelength should be large in the sense that $\ell_c^0 \ll \lambda$. The optimal choice of filter in terms of separation of frequencies would be a Heaviside low-pass filter in the wavenumber domain, but it would imply an infinite support in the space domain, so smoother filters are advocated. See Capdeville et al. (2013), Yvonnet and Bonnet (2014) or Capdeville and Cance (2015) for a general discussion on the choice of filters and Laptev (2009) for a discussion on the related question of the extension of $\mathbb{C}^f$ into a periodic function in $\epsilon\mathbf{x}$, in the case of periodic homogenization.

To try and actually address the non-separated case, Boutin and Auriault (1993) extended the asymptotic developments of Section 3.1.3 further than the second order in $1/\epsilon$ and analyzed the corrections induced by the higher order terms on a plane wave crossing the heterogeneous domain. The higher-order terms verify for $i \geq 2$:

$$\nabla_{\mathbf{y}} \cdot \mathbb{C} : \nabla_{\mathbf{y}} \otimes_s \mathbf{u}_{i+1} = -\nabla_{\mathbf{y}} \cdot \mathbb{C} : \nabla_{\mathbf{x}} \otimes_s \mathbf{u}_i - \nabla_{\mathbf{x}} \cdot \mathbb{C} : (\nabla_{\mathbf{x}} \otimes_s \mathbf{u}_{i-1} + \nabla_{\mathbf{y}} \otimes_s \mathbf{u}_i) \tag{3.12}$$

[6] Interestingly, one of the original motivation of this work was to simplify the meshing problem, which is difficult when very small layers must be meshed with hexahedra. With the smooth model obtained after the upscaling process, a structured mesh becomes sufficient, with a substantial decrease of the number of degrees of freedom (compare the two meshes of Fig. 3.3).

[7] As the upscaling results are only asymptotic, the ratio $\epsilon = \lambda/\ell_c$ for which upscaling cannot be applied anymore is not defined precisely. Some authors (see Helbig (1984) for instance) have tried to be more specific about these limits using numerical simulations, but the results are necessarily heavily dependent on the particular example at hand.

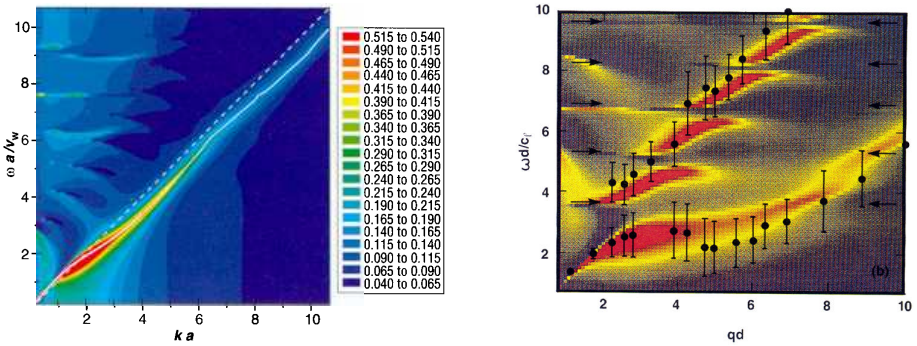

Figure 3.4 – *Normalized dispersion curves for: (left plot) a water tank filled with glass beads (white solid line) and water (white dashed line), and (right plot) a colloidal suspension of solid spheres (comparison of the model, in colors, with experimental measurements, in black dots). Taken from Page et al. (1996) and Jing et al. (1991), respectively.*

The elasticity equations are transformed with non-local elasticity and non-local mass, the latter induced by a fluctuating density, which is not considered in the equations above. The successive corrections are seen respectively as modifications of the polarization, dispersion of the wave velocity, and attenuation of the wave. This last effect in particular is seen as interesting because it is readily observable in experimental measurements. Although these equations are expected to apply for lower ratios $\lambda/\ell_c \approx 1$ than classical homogenization, they are still based on asymptotic expansion, and hence valid only for relatively large λ/ℓ_c.

A last interesting situation should be considered, called co-dynamics by Auriault and Boutin (2012). It corresponds to the case when, in a bi-phasic material, one of the constituents is in the classical low-frequency homogenization regime $\lambda_1 \gg \ell_c^1$, while a resonating regime $\lambda_2 \approx \ell_c^2$ is reached for the other one. This discrepancy can be due either to a large difference in the geometry, through a large discrepancy of ℓ_c^1 and ℓ_c^2, or in the local wave velocities, that induce a large discrepancy of λ_1 and λ_2. The effects of the micro-scale may be dramatic when local resonances in the cell are indeed reached. Examples that can be treated with this approach include the modification of a seismic signal by its passage through a city (Boutin et al. 2014), pressure waves through a periodic array of acoustic cavities connected to the matrix through very small ducts (Boutin 2013), bending and extension waves with very different wave velocity within a reticulated array (Chesnais et al. 2012) or the appearance of a second pressure wave above a certain frequency in poro-elastic materials (Auriault et al. 2010, Chapter 14). Using an extension of the mean-field approximation technique, the strangely low group velocity of acoustic waves in water tank filled with glass beads (Page et al. 1996) and the appearance of two acoustic modes in colloidal suspensions of solid spheres (Jing et al. 1991; 1992) were likewise explained (see Fig. 3.4). Note that there are relations between this regime and the localization regime (see Section 3.4), and their respective limits are debated.

3.2.4 Parabolic equation (Markov approximation, $\epsilon \ll 1$, $\sigma^2 \approx \epsilon$)

Finally, when the correlation length increases even more ($\lambda \ll \ell_c$), scattering occurs mainly in the forward direction. It then becomes possible to use the parabolic approximation. It was originally developed for optical waves and acoustic waves (see (Tappert 1977) for a review of applications in heterogeneous deterministic media and Klyatskin and Tatarskii (1970) for early consideration of random media). It considers slowly varying and weakly heterogeneous media ($\sigma^2 \approx \epsilon \ll 1$) and additionally introduces a small scattering angle assumption. The latter implies that the wave field amplitude is smoother along the propagation direction than perpendicular to it, and that backscattering is neglected. The parabolic approximation explains rather well the broadening with distance of the envelopes of the first wave arrivals (see Figure 3.5 for example). It cannot however be used to describe the coda as its validity decreases with time and distance, when the small scattering angle approximation becomes erroneous. This approximation has been widely used in geophysics and the exploration industry, in the context of classical migration analysis[8].

[8] In the context of deterministic media, it has also been used to derive absorbing boundary conditions (Bamberger et al. 1988a), building on the fact that backscattered wave are are neglected in this approximation.

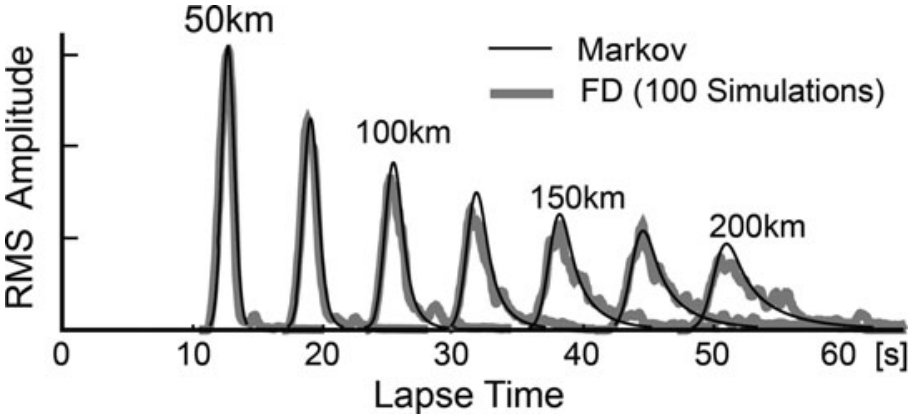

Figure 3.5 – *Comparison of Finite Difference envelopes (gray curves, based on the wave equation) and Markov envelopes (solid curves, based on the parabolic approximation) in 2-D random media characterized by a Gaussian autocorrelation with 5% fluctuations and velocity 4 km/s for the cylindrical radiation of a 2 Hz Ricker wavelet from a point source. Taken from Fehler et al. (2000), with a copyright from the Seismological Society of America.*

Following Hudson (1980), the behavior of a quasi-plane wave $\mathbf{u} = \tilde{\mathbf{u}}(\mathbf{x}, \mathbf{k}, \omega) \exp i(\mathbf{k} \cdot \mathbf{x} - \omega t)$is studied. The wave propagates along a constant direction $\hat{\mathbf{k}}$, and the weak heterogeneity hypothesis implies $|\mathbf{k}|^2 = (\omega/c_P)^2 + \mathrm{O}(\epsilon^2)$. The small scattering angle approximation is written as[9] $|\partial_k \tilde{u}_i|/|\nabla_\perp \tilde{u}_i| = \mathrm{O}(\epsilon)$ for any component $\tilde{u}_i$ of $\tilde{\mathbf{u}}$. Using the asymptotic approximation in Eq. (1.1) with homogeneous right hand side, and with these scalings, one obtains at the lowest order a parabolic equation for the longitudinal component of the displacement amplitude $\tilde{u}_{\mathbf{k}} = \tilde{\mathbf{u}}_0 \cdot \hat{\mathbf{k}}$:

$$2i|\mathbf{k}|\partial_k \tilde{u}_{\mathbf{k}} + \Delta_\perp \tilde{u}_{\mathbf{k}} + g(\mathbf{k}, \lambda, \mu)\tilde{u}_{\mathbf{k}} = 0. \tag{3.13}$$

where $g(\mathbf{k}, \lambda, \mu)$ is a complicated (and explicit) function of the mechanical parameters and the wave vector, and dependent on the mechanical heterogeneities. The transverse components $\tilde{\mathbf{u}}_\perp = \tilde{\mathbf{u}}_0 - \tilde{u}_{\mathbf{k}}\hat{\mathbf{k}}$ can then be retrieved through $i|\mathbf{k}|(\lambda + \mu)\tilde{\mathbf{u}}_\perp = \nabla_\perp(\lambda \tilde{u}_{\mathbf{k}}) + \mu \nabla_\perp \tilde{u}_{\mathbf{k}}$. Being scalar and parabolic, Eq. (3.13) is relatively simple to approximate numerically. Other approaches with similar hypotheses but posed in term of P and S potentials (Landers and Claerbout 1972, McCoy 1977) allow to consider conversions between P and S waves. A comparison of the different approaches is presented in Wales and McCoy (1983). A simpler approach, considering only S waves, is presented in Sato (1989), and extended in Fehler et al. (2000) and Saito et al. (2002) to spherical waves. Higher orders in ϵ can also be considered to go further away from the small scattering angle hypothesis (see Bamberger et al. (1988b) or Samuelides (1998) for instance).

In the case of a random medium, the average displacement field is modeled by Eq. (3.13) and additional approximations are introduced to treat the correlated terms. In random media, this setting is often denoted as Markov approximation (Rytov et al. 1989), based on the local approximation of the last term, which allows to write the gradient of the field as a function only of the local position, as with Markov processes. Using additional assumptions, Sato et al. (2012) proposed the following analytical solution:

$$\mathbb{E}\left[\tilde{u}_{\mathbf{k}}\right] = \tilde{u}_0 \exp\left(-|\mathbf{k}|^2 \ell_c \sigma^2 x_{\mathbf{k}}\right). \tag{3.14}$$

The coherent signal therefore decays exponentially along the propagation path. It vanishes over a so-called localization length $\ell_{\mathrm{loc}} = 1/(|\mathbf{k}|^2 \ell_c \sigma^2)$, which decreases with increasing correlation length, strength of the heterogeneities and frequency. It is also possible to derive an equation for the intensity $\mathbb{E}\left[u_{\mathbf{k}} u_{\mathbf{k}}^*\right]$ as a function of time, which is the mean square envelope of the signals plotted in Fig. 3.5. Many authors (see Saito et al. (2003), Korn and Sato (2005), Sato and Fehler (2007) among others, see also (Sato et al. 2012, Section 9.2.4) for a review) have presented comparisons of such mean-square envelopes and wave propagation results (usually computed with the Finite Difference Method) in the appropriate frequency range. This allows to explore cases that are further away from the theory, such as with a free surface (Emoto et al. 2010) or non-isotropic

[9] The operators $\partial_k = \hat{\mathbf{k}} \cdot \nabla$ and $\nabla_\perp = \nabla - \hat{\mathbf{k}}\partial_k$ represent space derivations along the propagation direction and perpendicular to it.

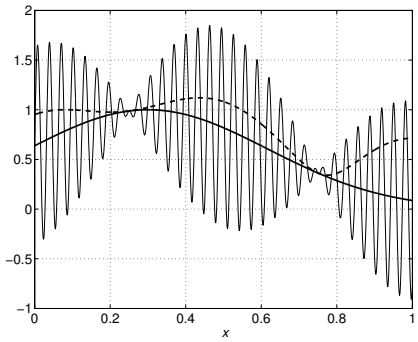

Figure 3.6 – *The energy limit of a strongly oscillating sequence: the oscillating function $u_\eta(x)$ (thin line), the mean function $\underline{u}(x)$ (thick line), and the square-root limit $\sqrt{\underline{u}(x)^2 + a(x)^2/2}$ (thick dashed line). Taken from Baydoun et al. (2014), after Savin (2013).*

media (Sato et al. 2012, section 9.3.7). Note that, although interesting from a modeling point of view, the interest of this upscaling regime in terms of predictive power is limited. Indeed, its range of validity is within the predictive range of direct computational solution of the wave equation.

3.3 Upscaling in the high-frequency range ($\eta \ll 1$)

In the previous section, we have analyzed the low-frequency situation, in which the propagation distance is not large with respect to the wavelength. Even with relatively large fluctuations of the mechanical properties, the overall scattering remained limited and the coherent part of the displacement field was the appropriate quantity of interest. When longer propagation paths are considered ($L \gg \lambda$), this scattering builds up and the coherent energy is not predominant anymore. The phase of the displacement field is then heavily dependent on the particular realization of the random medium, while the energy density (quadratic observable) often remains statistically stable. Section 3.3.1 introduces the Wigner measure, which is the appropriate mathematical tool to describe that energy density. It is then shown in the subsequent sections that it verifies a transport equation (Section 3.3.2), a radiative transfer equation (Section 3.3.3) or a diffusion equation (Section 3.3.4), depending on the regime considered.

3.3.1 Energy density and Wigner measure

To motivate the interest of quadratic observables for high frequency waves in heterogeneous media, let us consider the following displacement field (taken from Savin (2013), see Fig. 3.6) $u_\eta(x) = \underline{u}(x) + a(x)\sin(x/\eta)$. It oscillates rapidly at scale ($\eta \ll 1$) with an amplitude $a(x)$ about its slowly fluctuating average $\underline{u}(x)$. Although it does not converge strongly when $\eta \to 0$, its square still converges weakly. Indeed, for any continuous function ϕ with compact support on $\mathbb{R}$, we have $\lim_{\eta\to 0} \int_{\mathbb{R}} \phi(x)(u_\eta(x))^2 dx = \int_{\mathbb{R}} \phi(x)((\underline{u}(x))^2 + (a(x))^2)/2 dx$, so that the "energy" associated with $u_\eta(x)$ admits a limit given by $\underline{u}(x)^2 + a(x)^2/2$. Note that the limit still retains information on the amplitude of the small-scale features while the small-scale fluctuations themselves have vanished. Hence, this quadratic quantity is more amenable to simulation and experimental investigation than $u_\eta(x)$. Note also that these quadratic observables are classical in science, as they are at play when replacing quantum waves, which are spatially varying fields solutions of the Schrödinger equation, by classical mechanics, described by position and momentum in phase space.

In elastodynamics, the most obvious energy quantities are the high-frequency strain energy $\mathcal{V}_\eta(t) := \int_\Omega \mathbb{C}\epsilon_\eta : \epsilon_\eta \, d\mathbf{x}/2$ and kinetic energy $\mathcal{T}_\eta(t) := \int_\Omega \rho |\partial_t \mathbf{u}_\eta|^2 \, d\mathbf{x}/2$. Without dissipation, the total energy $\mathcal{V}_\eta(t) + \mathcal{T}_\eta(t)$ is of course conserved in time ($\partial_t(\mathcal{V}_\eta + \mathcal{T}_\eta) = 0$), but more localized quantities, such as $(\mathbb{C}\epsilon_\eta : \epsilon_\eta)$ and $\rho|\partial_t \mathbf{u}_\eta|^2$, would be interesting to describe more accurately the state of the system. Unfortunately, these quantities do not verify obvious closed-form equations. The Wigner measure was shown to be the appropriate tool, providing for a localized description of energy (see below Eq. (3.17) and (3.18)) while at the same time following a closed-form equa-

tion (see next sections for different examples). More details can be found in Gérard et al. (1997), Martinez (2002) and Bal et al. (2010).

For a given vector field $\mathbf{u}_\eta$, the Wigner measure $\mathbf{W}[\mathbf{u}_\eta]$ is constructed as the weak limit of the Wigner transform $\mathbf{W}_\eta[\mathbf{u}_\eta, \mathbf{u}_\eta] \rightharpoonup_{\eta\to 0} \mathbf{W}[\mathbf{u}_\eta]$. This transform is defined by

$$\mathbf{W}_\eta[\mathbf{u},\mathbf{v}](\mathbf{x},\mathbf{k}) = \frac{1}{(2\pi)^3}\int_{\mathbb{R}^3} \mathbf{e}^{i\mathbf{k}\cdot\mathbf{y}}\mathbf{u}\left(\mathbf{x}-\frac{\eta}{2}\mathbf{y}\right)\otimes\mathbf{v}\left(\mathbf{x}-\frac{\eta}{2}\mathbf{y}\right)^* d\mathbf{y}\,. \tag{3.15}$$

For instance, the Wigner measure of a strongly converging (in $L^2(\mathbb{R}^3)$) $\mathbf{u}_\eta(\mathbf{x})$ is $|\mathbf{u}(\mathbf{x})|^2\delta(\mathbf{k})$. The Wigner measure of $\eta^{-d/2}\mathbf{u}(\mathbf{x}/\eta)$ (for a compactly supported $\mathbf{u}(\mathbf{x})$) is $(2\pi)^{-d}|\tilde{\mathbf{u}}(\mathbf{k})|^2\delta(\mathbf{x})$, where $\tilde{\mathbf{u}}(\mathbf{k})$ is the Fourier transform of $\mathbf{u}(\mathbf{x})$. The Wigner measure of $A(\mathbf{x})\exp(iS(\mathbf{x})/\eta)$ with smooth amplitude and phase functions is $W(\mathbf{x},\mathbf{k}) = |A(\mathbf{x})|^2\delta(\mathbf{k}-\nabla S(\mathbf{x}))$.

The Wigner measure is a sort of localized energy density, resolved in wavenumber. Indeed, it is such that for any matrix observable ϕ with smooth and compactly supported coefficients:

$$\lim_{\eta\to 0}(\phi(\mathbf{x},\eta\mathbf{D})\mathbf{u}_\eta,\mathbf{u}_\eta)_{L^2} = \mathrm{Tr}\int_{\mathbb{R}^3\times\mathbb{R}^3}\phi(\mathbf{x},\mathbf{k})\mathbf{W}[\mathbf{u}_\eta](d\mathbf{x},d\mathbf{k})\,. \tag{3.16}$$

where $\mathbf{D}$ denotes the space derivative operator and $\varphi(\mathbf{x},\mathbf{k})$ is the symbol of $\phi(\mathbf{x},\mathbf{y})$. In particular, for elastodynamics applications, the high-frequency strain energy may be estimated with $\phi(\mathbf{x},\mathbf{k}) \equiv \rho(\mathbf{x})\mathbf{\Gamma}(\mathbf{x},\mathbf{k})$:

$$\lim_{\eta\to 0}\mathcal{V}_\eta(t) = \frac{1}{2}\int_{\Omega\times\mathbb{R}^3}\rho(\mathbf{x})\mathbf{\Gamma}(\mathbf{x},\mathbf{k}) : \mathbf{W}[\mathbf{u}_\eta(\mathbf{x},t)](d\mathbf{x},d\mathbf{k})\,, \tag{3.17}$$

where $\mathbf{\Gamma}(\mathbf{x},\mathbf{k})$ is the Christhoffel tensor of the medium. Similarly, the kinetic energy is estimated with $\phi(\mathbf{x},\mathbf{k}) \equiv \rho(\mathbf{x})\mathbf{D}_t^2\mathbf{I}$:

$$\lim_{\eta\to 0}\mathcal{T}_\eta(t) = \frac{1}{2}\int_{\Omega\times\mathbb{R}^3}\rho(\mathbf{x})\mathrm{Tr}\mathbf{W}[\eta\partial_t\mathbf{u}_\eta(\mathbf{x},t)](d\mathbf{x},d\mathbf{k})\,. \tag{3.18}$$

Note however that the Wigner measure is only informative at the chosen scale η because it cannot capture oscillations at any other scale. If the fluctuations of $\mathbf{u}_\eta$ are faster than the scale of the Wigner transform, the Wigner transform vanishes in the limit, while if they are slower, the Wigner limit is the same as if there were no fluctuations at all.

3.3.2 Fokker-Planck equations ($\epsilon \ll 1$, $\sigma^2 \approx \eta \ll 1$)

Now equipped with this measure of the energy associated with the displacement field $\mathbf{u}_\eta(\mathbf{x},t)$, it is possible to derive[10] transport equations associated to the propagation of high frequency waves in a medium with slowly fluctuating material properties ($\ell_c \gg \lambda$). Rescaling the time and space variables in the wave equation (1.1) by η, a series of equations for the Wigner measure $\mathbf{W}[\mathbf{u}_\eta]$ are obtained using multiscale analysis in η (Section 3.1.3). The leading order term yields dispersion equations, fluctuating slowly in space with the mechanical properties. The Wigner measure is then projected along the eigenmodes of the Christoffel tensor, introducing the specific intensities $\mathbf{a}_\alpha(t,\mathbf{x},\mathbf{k})$:

$$\mathbf{W}(t,\omega,\mathbf{x},\mathbf{k}) = \sum_{\alpha=1}^{\mathrm{R}}\mathbf{p}_\alpha(\mathbf{x},\mathbf{k})\mathbf{a}_\alpha(t,\mathbf{x},\mathbf{k})\mathbf{p}_\alpha^*(\mathbf{x},\mathbf{k})\delta\left(\omega^2-\omega_\alpha^2(\mathbf{x},\mathbf{k})\right)\,, \tag{3.19}$$

where the $\mathbf{p}_\alpha(\mathbf{x},\mathbf{k})$ and $\omega_\alpha^2(\mathbf{x},\mathbf{k})$ are respectively the eigenvectors and eigenvalues of the slowly fluctuating Christoffel tensor $\mathbf{\Gamma}(\mathbf{x},\mathbf{k}) = \sum_{\alpha=1}^3\omega_\alpha^2(\mathbf{x},\mathbf{k})\mathbf{p}_\alpha(\mathbf{x},\mathbf{k})\mathbf{p}_\alpha^*(\mathbf{x},\mathbf{k})$, and R is the number of different eigenvalues. When the eigenvalue ω_α is simple (as with the P mode in an isotropic medium), the eigenmode $\mathbf{p}_\alpha$ is a vector and the specific intensity $\mathbf{a}_\alpha$ is a scalar. Otherwise (as with the S modes for an isotropic medium), both the eigenmode and the specific intensity are matrices. If all eigenvalues are simple, R = 3. Otherwise, $R < 3$.

[10] See for instance (Ryzhik et al. 1996, Section 3) for the derivation for acoustics, electromagnetic and elastodynamics, in terms of first-order hyperbolic systems or Bal (2005) or (Savin 2010, Appendix A) for a direct derivation in terms of second-order hyperbolic systems.

The next order terms of the equation for the Wigner measure yield Liouville equations for the specific intensities:

$$\partial_t \mathbf{a}_\alpha(t,\mathbf{x},\mathbf{k}) + \{\omega_\alpha(\mathbf{x},\mathbf{k}), \mathbf{a}_\alpha(t,\mathbf{x},\mathbf{k})\} + [\mathbf{N}_\alpha(\mathbf{x},\mathbf{k}), \mathbf{a}_\alpha(t,\mathbf{x},\mathbf{k})] = \mathbf{0}\,. \tag{3.20}$$

Here, the Lie bracket is such that $[\mathbf{A},\mathbf{B}] = \mathbf{AB} - \mathbf{BA}$ and the Poisson bracket is such that $\{\mathbf{A},\mathbf{B}\} = \nabla_\mathbf{k}\mathbf{A}\cdot\nabla_\mathbf{x}\mathbf{B} - \nabla_\mathbf{x}\mathbf{A}\cdot\nabla_\mathbf{k}\mathbf{B}$. The matrices $\mathbf{N}_\alpha(\mathbf{x},\mathbf{k})$ are skew-symmetric and vanish when the eigenvalue ω_α is simple. Note that the equations for different specific intensities are uncoupled although the various polarizations of multiple eigenvalues are coupled through the matrices $\mathbf{N}_\alpha(\mathbf{x},\mathbf{k})$. These matrices describe the rotation of the polarization vector with the slow fluctuations of the medium, and can hence be removed by an appropriate choice of basis for the projection of the Wigner measure. Note, finally, that the coupling terms also vanish when writing the equations in terms of the total energy of each mode $\bar{\mathbf{a}}_\alpha = \mathrm{Tr}(\mathbf{a}_\alpha)$:

$$\partial_t \bar{\mathbf{a}}_\alpha(t,\mathbf{x},\mathbf{k}) + \{\omega_\alpha(\mathbf{x},\mathbf{k}), \bar{\mathbf{a}}_\alpha(t,\mathbf{x},\mathbf{k})\} = 0\,. \tag{3.21}$$

Let us consider the exemple where, although heterogeneous, the medium is everywhere isotropic. Then, the Wigner measure is projected along a simple P-mode, with $\omega_P(\mathbf{x},\mathbf{k}) = c_P(\mathbf{x})|\mathbf{k}|$ and $\mathbf{p}_P = \hat{\mathbf{k}}$, and a double S-mode, with $\omega_S(\mathbf{x},\mathbf{k}) = c_S(\mathbf{x})|\mathbf{k}|$ and $\mathbf{p}_S$ is any vector perpendicular to $\hat{\mathbf{k}}$. The Liouville equations for the two modes (considering only the modes propagating towards the "positive" direction) are then:

$$\begin{cases} \partial_t \mathbf{a}_P + c_P(\mathbf{x})\hat{\mathbf{k}}\cdot\nabla_\mathbf{x}\mathbf{a}_P - |\mathbf{k}|\nabla_\mathbf{x}c_P\cdot\nabla_\mathbf{k}\mathbf{a}_P &= 0 \\ \partial_t \bar{\mathbf{a}}_S + c_S(\mathbf{x})\hat{\mathbf{k}}\cdot\nabla_\mathbf{x}\bar{\mathbf{a}}_S - |\mathbf{k}|\nabla_\mathbf{x}c_S\cdot\nabla_\mathbf{k}\bar{\mathbf{a}}_S &= 0 \end{cases} \tag{3.22}$$

These Liouville equations generalize the classical ray method (Červený 2005, Červený et al. 2007). It consists in decomposing a wave in wave packets or elementary waves and choosing an *a priori* ansatz for each of them in the form $\mathbf{u} = \tilde{\mathbf{u}}\exp(iS(\mathbf{x})/\eta)$. The phase $S(\mathbf{x})$ is then shown to verify an eikonal equation, while the amplitude $\tilde{\mathbf{u}}$ verifies a transport equation with fluctuating coefficients depending on the phase.

We now consider a random medium with weak heterogeneities, of amplitude $\sigma \approx \sqrt{\eta}$, and still slowly fluctuating ($\lambda \ll \ell_c$). The average of the solution of the previous equation can be shown (Bal et al. 2003) to converge to the solution of a Fokker-Planck equation. For the P-mode considered above, and assuming for simplicity of exposition that the background P-velocity $\overline{c_P}$ is homogeneous and that the correlation structure $\mathrm{R}_{c_P}(|\mathbf{x}|)$ is isotropic, that Fokker-Planck equation reads:

$$\partial_t \mathbb{E}\left[\mathbf{a}_P\right] + \overline{c_P}\hat{\mathbf{k}}\cdot\nabla_\mathbf{x}\mathbb{E}\left[\mathbf{a}_P\right] - \nabla_\mathbf{k}\cdot(\mathbf{d}(\mathbf{k})\nabla_\mathbf{k}\mathbb{E}\left[\mathbf{a}_P\right]) = 0\,, \tag{3.23}$$

where the diffusion matrix is $\mathbf{d}(\mathbf{k}) = d_0|\mathbf{k}|^2(\mathbf{I} - \hat{\mathbf{k}}\otimes\hat{\mathbf{k}})/\overline{c_P}$ where $d_0 = \int_{\mathbb{R}^+}\mathrm{R}'_{c_P}(\ell)d\ell/\ell$.

3.3.3 Radiative Transfer Equations ($\epsilon \approx 1$, $\sigma^2 \approx \eta \ll 1$)

We now consider random heterogeneities of the mechanical properties with the same amplitude $\sigma \approx \sqrt{\eta}$, but this time with faster oscillations $\ell_c \approx \lambda$. A similar multiple scale expansion in the variable η is performed. The leading order term provides a dispersion equation that motivates the projection of the Wigner measure $\mathbf{W}(t,\omega,\mathbf{x},\mathbf{k})$ along the eigenmodes of the Christoffel tensor and introduce the specific intensities $\mathbf{a}_\alpha(t,\mathbf{x},\mathbf{k})$. Note however that the eigenmodes and eigenvalues considered here are those of the background medium $\mathbb{C}_0(\mathbf{x})$. They may fluctutate in space, but only at a slow pace (spatial period much larger than the wavelength).

After averaging, the higher order terms of the equation for the Wigner measure yield the radiative transfer equations for the ensemble-averaged specific intensities:

$$\begin{aligned} \partial_t \mathbb{E}\left[\mathbf{a}_\alpha(t,\mathbf{x},\mathbf{k})\right] + \{\omega_\alpha(\mathbf{x},\mathbf{k}), \mathbb{E}\left[\mathbf{a}_\alpha(t,\mathbf{x},\mathbf{k})\right]\} + [\mathbf{N}_\alpha(\mathbf{x},\mathbf{k}), \mathbb{E}\left[\mathbf{a}_\alpha(t,\mathbf{x},\mathbf{k})\right]] = \\ \sum_{\beta=1}^{\mathrm{R}} \int_{\mathbb{R}^3} \sigma_{\alpha\beta}(\mathbf{x},\mathbf{k},\mathbf{q})\left[\mathbb{E}\left[\mathbf{a}_\beta(t,\mathbf{x},\mathbf{q})\right]\right]\delta(\omega_\beta(\mathbf{x},\mathbf{q}) - \omega_\alpha(\mathbf{x},\mathbf{k}))\frac{d\mathbf{q}}{(2\pi)^3} \\ - \Sigma_\alpha(\mathbf{x},\mathbf{k})\mathbb{E}\left[\mathbf{a}_\alpha(t,\mathbf{x},\mathbf{k})\right] - \mathbb{E}\left[\mathbf{a}_\alpha(t,\mathbf{x},\mathbf{k})\right]\Sigma^*_\alpha(\mathbf{x},\mathbf{k})\,. \end{aligned} \tag{3.24}$$

The differential scattering cross sections $\sigma_{\alpha\beta}(\mathbf{x},\mathbf{k},\mathbf{q})$ and total scattering cross sections $\Sigma_\alpha(\mathbf{x},\mathbf{k})$ are constructed explicitly as functions of the power spectrum $\mathrm{S}_\mathbb{C}(\mathbf{k})$ of the mechanical parameters of

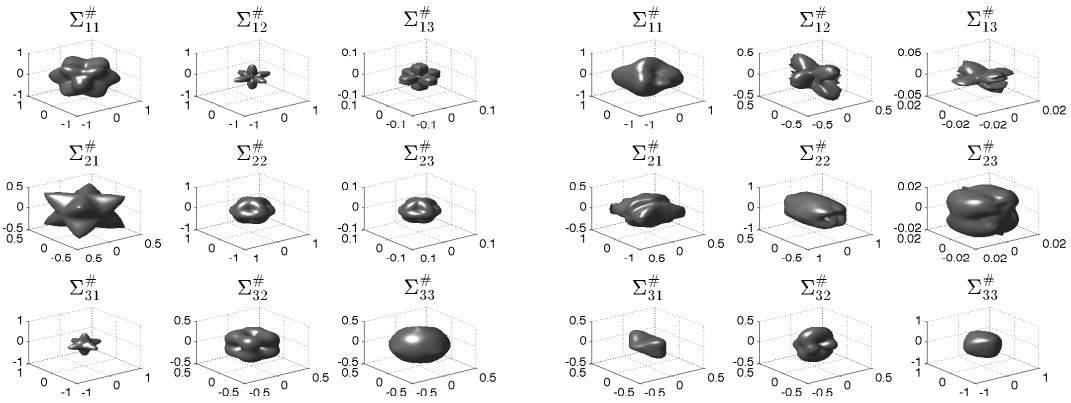

Figure 3.7 – *Normalized total scattering cross-sections for single crystal nickel (cubic anisotropy, left figure) and celestite ($SrSO_4$, orthotrope, right figure). Taken from Baydoun et al. (2014).*

the wave equation (see Baydoun et al. (2014) for the formulas). Note that the Radiative Transfer Equation and the Liouville equations (3.21) only differ through the right-hand side, where the heterogeneities couple the energies carried by different modes of propagation. While the different specific intensities were not interacting in the Liouville equation (although different polarizations of the same mode were indeed coupled), the interactions of the wave with the medium is much stronger in Radiative Transfer due to the proximity of the wavelength and the correlation length. The Radiative Transfer Equations (3.24) above generalize Eqs. (4.32) of Ryzhik et al. (1996) to arbitrary anisotropy of the elastic medium, in that the differential and total scattering cross-sections we have derived embed all possible cases of elastic constitutive models. Examples of specific scattering cross sections for different classical anisotropies can be found in Baydoun et al. (2014) (see Fig. 3.7 for single crystal nickel and celestite). The influence of the correlation function on the differential and total scattering cross sections is described in detail in Khazaie et al. (2016a) in the elastic case (with isotropic background).

The Radiative Transfer Equations have been derived using multiple scale expansion (see for instance Ryzhik et al. (1996) or Baydoun et al. (2014)) and the Bethe-Salpeter equation (see Rytov et al. (1989), Weaver (1990a) or Margerin (2006)). Some analytical solutions are described in Wu (1985), Zeng (1991), Sato (1993) and Paasschens (1997) for particular cases. The elastic applications of this theory are mainly found in geophysics (see Shang and Gao (1988), Wu and Aki (1988a), Zheng et al. (1991), Sato (1994), Gusev and Abubakirov (1996), among many other) for the generation of synthetic seismogram envelopes and for the non-intrusive testing of polycrystalline materials with ultrasounds (Weaver 1990a, Turner and Weaver 1994).

3.3.4 Diffusion regime ($\epsilon \ll 1$ or $\epsilon \approx 1$, $\sigma^2 \approx \eta \ll 1$, late times)

In the previous two sections, both the time and space variables were rescaled by η for the asymptotic analysis. Essentially, this linearity between space and time meant that we were trying to observe the high-frequency behavior in the vicinity of the main pulse. In this section, we try to understand what happens in the late coda of the signal, where the time variable is much larger than the first-arrival of the waves. This behavior is obtained by asymptotic analysis starting either from the Fokker-Planck equation (Section 3.3.2, with $\epsilon \ll 1$) or from the Radiative Transfer Equation (Section 3.3.3, with $\epsilon \approx 1$), and considering a scaling of space with η and time with η^2. Note that a diffusion model can also be retrieved from the wave equation in the white noise regime, where $\epsilon \gg 1$, $\eta \ll 1$ and the heterogeneities are strong $\sigma^2 \approx 1$. It will not be discussed here because its mathematical analysis is restricted to layered media.

With the chosen rescaling in time and space, the solutions of the Fokker-Planck equation can be shown (Bal et al. 2010) to converge to those of a diffusion equation:

$$\partial_t \mathbb{E}\left[\mathbf{a}_P(t,\mathbf{x},\mathbf{k})\right] - \nabla_{\mathbf{x}} \cdot \left(\mathbf{D}(|\mathbf{k}|)\nabla_{\mathbf{x}} \mathbb{E}\left[\mathbf{a}_P(t,\mathbf{x},\mathbf{k})\right]\right) = 0\,, \tag{3.25}$$

where the diffusion matrix is $\mathbf{D}(|\mathbf{k}|) = \int_{\mathbb{S}^{d-1}} \hat{\mathbf{k}} \otimes \chi(\mathbf{k}) dS(\hat{\mathbf{k}}) / |\mathbb{S}^{d-1}|$, $\mathbb{S}^{d-1}$ is the unit sphere in d dimensions, $|\mathbb{S}^{d-1}|$ its surface area, and the correctors $\chi(\mathbf{k})$ are the mean-zero solutions of the equation $\nabla_{\mathbf{k}} \cdot (\mathbf{d}(\mathbf{k})\nabla_{\mathbf{k}}\chi) = -\mathbf{k}$. Note that, after integration, the diffusion matrix still depends

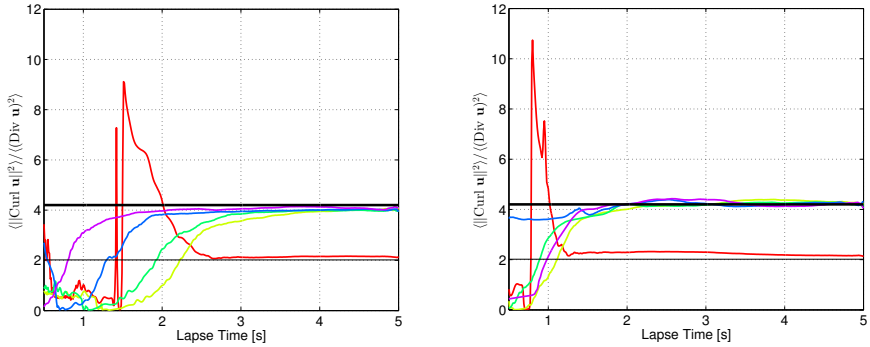

Figure 3.8 – *Temporal evolution of the ratio of S-wave energy to P-wave energy averaged over slices of a half-space at different depths. The red curve corresponds to the surface, while the others are computed at 250 m intervals (the wavelength is $\lambda \approx 100$ m). The black thick and thin lines correspond to the theoretical equipartition ratios for the full space and half space, respectively. Left and right plots correspond respectively to the low-pass white noise and exponential correlation models. Taken from Khazaie et al. (2016).*

on the norm of the wavenumber $|\mathbf{k}|$, since the integration was only performed on the different possible directions $\hat{\mathbf{k}}$. Through $\mathbf{d}$, defined in Eq. (3.23), the diffusion matrix $\mathbf{D}(|\mathbf{k}|)$ depends on the covariance of the slowly-fluctuating random properties of the medium.

Starting from the Radiative Transfer Equation (see Ryzhik et al. (1996) for the multiscale analysis and Weaver (1990a) for the Bethe-Salpeter formalism), we observe that the energy is scattered equally among all modes (equipartition state), that the S waves are depolarized, and that the energy densities are independent of the direction of the wave vector (isotropic). In particular, for an isotropic background (where the energy densities are separated into P and S modes), this means that

$$\mathbb{E}\left[\mathbf{a}_P(t,\mathbf{x},\mathbf{k})\right] = \phi(t,\mathbf{x},|\mathbf{k}|), \quad \mathbb{E}\left[\mathbf{a}_S(t,\mathbf{x},\mathbf{k})\right] = \phi(t,\mathbf{x},|\mathbf{k}|/K)\mathbf{I}, \tag{3.26}$$

where the scalar potential ϕ follows a diffusion equation:

$$\frac{\partial \phi}{\partial t} = \nabla \cdot (\mathbf{D}(|\mathbf{k}|)\nabla\phi)\,, \tag{3.27}$$

where the diffusion parameter $\mathbf{D}(|\mathbf{k}|)$ can be computed explicitly as a function of the power spectrum of the rapidly fluctuating random fields of Lamé parameters and density (Ryzhik et al. 1996, Eq. (5.46)). Note that in this regime of rapidly-fluctuating parameters, the interaction between the energy modes is much stronger than in the regime considered above, so that the diffusion equation obtained is the same for both modes, while two independent diffusion equations were obtained in the previous case.

One essential property of the diffusion regime is the equipartition of energies. In the case of an elastic full space, it means that the ratio of energy of the P waves $\mathcal{E}_P$ to the energy of the S waves $\mathcal{E}_S$ stabilizes around a value that is independent of the detail of the microstructure. This value actually depends only on the wave velocity ratio (in 3D):

$$\frac{\mathcal{E}_S}{\mathcal{E}_P} = 2\left(\frac{c_P}{c_S}\right)^3. \tag{3.28}$$

Equipartition has been observed experimentally many times (Shapiro et al. 2000, Hennino et al. 2001, Galluzzo et al. 2015). Numerically, it has been observed both for full space and half spaces, where the Rayleigh mode must be considered, so that Eq. (3.28) is modified (see Figure 3.8, taken from Khazaie et al. (2016)). Note however that the numerical observation of equipartition for elastic spaces is not trivial because it requires the simulation over very large dimensions. Hence it has been necessary to develop efficient wave propagation solvers (see Section A.3) and random field generation schemes (see Section A.2) to perform these simulations. Note also that the equipartition property is not specific to the diffusion regime, which additionally requires that the energy depend only on $|\mathbf{k}|$.

The diffusion regime has been used in experiments far before its relation with the wave equation was understood. Indeed, the exponential decrease of the envelope of the coda waves was early on identified to be a characteristic of the material rather than of the source, and to be well

reproduced by the solution of a diffusion equation. Diffusion models were used to model the results of observations made in geophysical media (Aki and Chouet 1975, Turner 1998), polycrystalline materials (Guo et al. 1985, Weaver 1990a, Turner and Weaver 1994), concrete (Anugonda et al. 2001) or granular media (Jia et al. 1999, Weaver and Sachse 1995, Tournat and Gusev 2009). Norris (2008) discusses anisotropic diffusion in elastic solids and characterizes the directional diffusion of energy for different type of anisotropy at the upper scale. Anisotropy was shown numerically to have a dramatic effect on the long-time patterns (see Fig. 1.5, taken from Ta et al. (2010;b)).

Finally, the Statistical Energy Analysis (SEA, Hodges and Woodhouse (1986), Lyon and DeJong (1995)), widely used in the vibration engineering community, is related to these diffusion models (Savin 2013). The main difference is that the diffusion models we consider are continuous, while a structure is viewed in the SEA as a discrete set of coupled sub-systems. Mean total and kinetic energies for each mode are entered in a balance equation, with assumptions on the flows of energy between two sub-systems. In the rare cases when the SEA is mathematically justified, it relies on strong hypotheses of equipartition of energy among the modes and incoherence of the different modal contributions.

3.4 Localization

In 1977, Philipp Anderson was granted the Nobel prize (with Nevill Mott and John van Fleck) for his explanation of a critical phenomenon in electron diffusion: the metal-insulator transition (Anderson 1958). He modeled it by observing that, above a certain concentration of scattering defects in a crystal, electrons do not simply diffuse less effectively, they become bound to a subregion of the crystal. This phenomenon became known as strong localization, or Anderson localization. It is characterized by an exponential decay in space of the wave intensity away from the source, and is stationary in time (in the absence of damping). As all critical phenomena, dimension plays a crucial role, with low-dimensional systems being more prone to localization.

After this observation in quantum physics, localization was recognized also for classical waves, from light transmission to room acoustics (Anderson 1985, Lagendijk et al. 2009, Sheng 2006). Localization of ultrasounds in a heterogeneous plate is reported for instance in Lobkis and Weaver (2008) (see also Weaver (1990b)). It is seen as a gap, stationary in time, between the energy levels close and away from the source (see the center plot of Figure 3.9, where the exponential decay is due to material damping). The authors also report (rightmost plot) that localization takes place only at relatively low wavelengths λ. Localization also plays an important role for many structural engineering systems, such as rotor blades, pipelines or large space structures. Often, it appears in the form of small deviations from periodicity that drastically modify the dynamical behavior of the system. It was very widely studied for mistuning of rotor blades in particular (see Feiner and Griffin (2004) for instance). More recently, a large community gathers around the developments of dynamic meta-materials, that mimic negative mass of a system through internal resonance (see for instance the work of Fang et al. (2006), Yang et al. (2008), Liu et al. (2011), Zheludev and Kivshar (2012), Chesnais et al. (2012), Boutin (2013)) Finally, while most experimental observations have been made on 1D or 2D systems (beams and plates among them, but also for Rayleigh waves (Garber et al. 2000), or along seismic faults (Igel et al. 2002, Hillers et al. 2014)), which are more prone to localization, Hu et al. (2008) have also reported recently the observation of localization of ultrasounds in a 3D granular system.

Besides Anderson localization, experiments report another type of spatial focusing of the energy: coherent backscattering, also called weak localization. It is seen as a doubling of the intensity within a wavelength of the source compared to the rest of the medium. The physical explanation of weak localization is that, when waves propagate in a random medium over long distances (larger than the mean free path ℓ^*) and undergo multiple diffractions, wave packets arrive at a given point uncorrelated in general. However, if the arrival point is the source itself (in which case the wave path is a closed loop), there are always two wave packets that arrive correlated: those who have followed opposite paths along the loop. Hence, intensity builds on the interaction of these wave packets and is the double of the general intensity. Experimental observation of weak localization include that of Larose et al. (2004) for Rayleigh waves in a volcano in France (see Figure 3.10). As expected, the doubling of the intensity takes place over a wavelength around the source. Also, localization is observed to settle in only after a characteristic time,

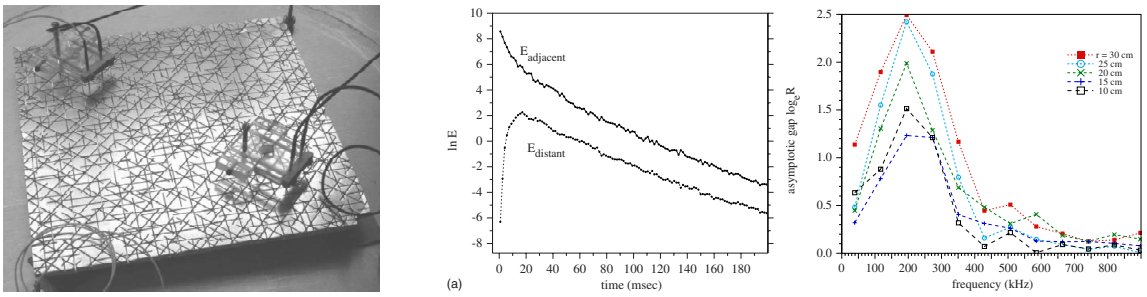

Figure 3.9 – *Anderson localization of ultrasounds in a plate: experimental setup (left), energy as a function of time for at two different distances from the source (center) and as a function of the excitation frequency (right). Taken from Lobkis and Weaver (2008).*

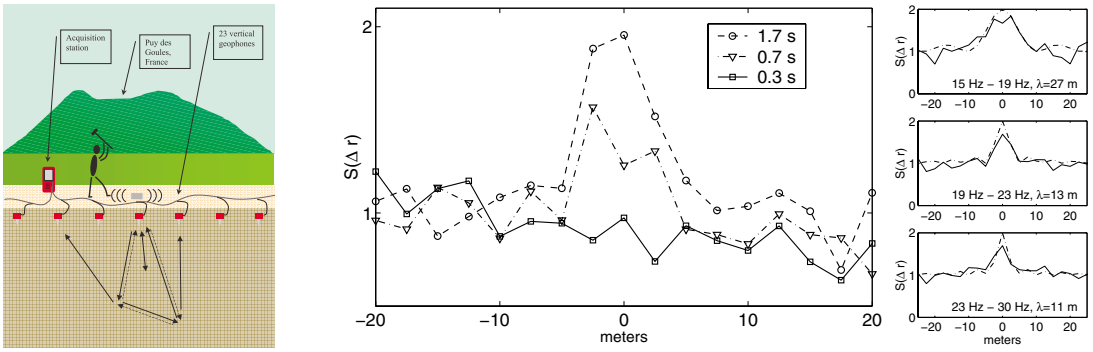

Figure 3.10 – *Weak localization of seismic waves: experimental setup (left), energy as a function of distance from the source at different times (center) and different frequencies (right). On the rightmost plot, the dashed-dotted lines are based on the theory by Trégourès and van Tiggelen (2002). Taken from Larose et al. (2004).*

necessary for the waves to go into multiple scattering mode (see the center plot of Figure 3.10). At shorter times, the height of the peak can be evaluated using specific approximations (see for example (Sheng 2006, Chapter 6) or Trégourès and van Tiggelen (2002)).

Although the physics of localization are rather well understood and it has been observed in many experiments, there is still today no general theory deriving localization from the wave equation. Some elements of theory have been derived in the self-consistent framework (Vollhardt and Wölfle 1980) and using scaling theory (Abrahams et al. 1979, MacKinnon and Kramer 1983), or by deriving a position-dependent diffusion in a bounded medium (Cherroret and Skipetrov 2008). Interesting insights can be found in the ideas of Filoche and Mayboroda (2012), who derive frequency-dependent boundaries for the localized modes that explain the transition from localized to extended state. Ioffe and Regel (1960) derived a criterion for localization based on the comparison of wavelength and mean free path: $2\pi\ell^* \approx \lambda$. However, an extensive theory exists only in 1D, with the works of Scott (1985) and Pierre (1990) for chains of springs, Li and Wang (2006) for an elastic beam, and the very complete mathematical analysis of Fouque et al. (2007) both for weakly and strongly scattering media. The theory is valid for $\lambda, \ell_c \ll L$ and $\ell_c^2 \ll \lambda^2/\sigma^2$ and proposes a localization length proportional to $\ell_c^2/(\lambda\sigma^2)$. The influence of anisotropy on localization phenomena is obviously neither well understood.

In a recent work with Ph.D. student Lucio de Abreu Corrêa (de Abreu Corrêa et al. 2016;a), and in the framework of a project with SNCF, we observed localization in numerical simulations of the passage of a train over a ballast layer. The two images in Figure 1.10 correspond to simulations of the same numerical model, except for the material properties of the ballasted layer, which are homogeneous in the left image and heterogeneous in the right image. It is clear from Figure 1.10, where the colors indicate the magnitude of the displacement field, that localization takes place within the ballast. As the energy remains trapped close to the source, the effect of localization on structures can be easily mistaken for that of damping. Indeed, very high (Rayleigh) damping ratios are used in the railway industry to reproduce the experimental observations far from the track. This numerical observation is also consistent with the observation that, in recent years, with the increased velocity of the trains, ballast has undergone faster degradation than

foreseen. The dispersion curves present slow waves similar to those observed in localization in granular media (Jing et al. 1991, Page et al. 1996, Mouraille and Luding 2008).

Perspectives 4

I described in this document both my contributions and a general review on the research in the fields of coupling and upscaling of elastostatics and elastodynamics models in random media. I list below a few directions of research I intend to explore in the next coming years. Contrarily to the rest of the document, this part is very personal and does not pretend to present an exhaustive list of unsolved problems in the field.

Homogenization at boundaries through numerical coupling techniques. While classical homogenization is only defined for unbounded domains (or, equivalently, infinitely small fluctuations of the mechanical parameters), all real problems come with boundaries. Considering the homogenization of a model with boundaries requires in principle setting an altogether different problem, where the sample includes a boundary whose geometrical size is taken to the limit with the microstructure. Several authors considered periodic and non-periodic free surfaces in statics and dynamics (see for instance Capdeville and Marigo (2013), and references therein), while Huang and Maradudin (1987), for example, considered random gratings. The appearance of boundary layers in fluids is a consequence of the homogeneous Dirichlet condition at a rigid boundary (E 2011, Section 2.1). For a Navier-Stokes flow around inclusions with homogeneous Dirichlet boundary conditions, Allaire (1991a) derived the Darcy equation. For a different relative convergence rate of the geometrical size of the cell and the inclusion, Allaire (1991b) derived the Brinkmann equation. Although many cases have been treated in the literature, there are still many cases where upscaling of boundary conditions is difficult, at least analytically. For the Radiative Transfer Equation in particular, deriving the boundary or interface conditions from those of the wave equation is a complicated problem, mainly because of the appearance of guided waves along the interface (see for instance Savin (2013) and references therein). However, the behavior at the boundary is often crucial for industrial applications. It might be appealing therefore to introduce numerical coupling techniques as a general alternative to the derivation of homogenization boundary conditions. The bulk of the domain could be upscaled while the vicinity of the boundary would be modeled at the micro-scale.

Homogenization of non-linear problems and modeling of apparent damping. The multiple-scale analysis described in Section 3.1.3 is constructive in the sense that no pre-existing information is needed on the homogenized tensor to derive it. Even though this technique is not always fully mathematically correct, it provides the initial insight that allows to use more powerful and less intuitive methods (Γ-, G- or H-convergence for instance) to prove that the guess was indeed correct. Unfortunately, multiple-scale analysis does not work for non-linear materials. So, even though the theoretical material exist to deal with the upscaling of non-linear and random problems, very few explicit results can be found and numerical simulations are often the only alternative (Kouznetsova et al. 2001, Miehe and Koch 2002, Geers et al. 2010, Clément et al. 2012). Preliminary results in (Jehel and Cottereau 2015) show the influence of upscaling and heterogeneity on the apparent complexity of the constitutive relation of a concrete beam. Likewise, we illustrated in (de Abreu Corrêa et al. 2016) that apparent damping away from a ballasted railway track might be due to the influence of heterogeneity (through localization) rather than any kind of true non-linear constitutive relation. Generally, heterogeneity in the material is transferring energy from the coherent to the incoherent field, therefore creating apparent damping. It is a crucial aspect that should clearly be further analyzed.

Coupling of wave propagation and kinetic models - PMLs in random media. Most coupling techniques consider the same type of equation at both scales, with differences only in the material parameters (rapidly-fluctuating at the micro-scale and slowly-fluctuating at the macro-scale) and/or the mesh size. However, some authors tackle the more interesting case of heterogeneous models, where the variables are different for the two models. Beam models are for instance easily coupled to continuum mechanics models (see Cottereau (2014) and references therein). Shorter and Langley (2005) describe the coupling of a Statistical Energy Analysis model with a wave propagation model. Degond et al. (2006) describe the incorporation of kinetic models effects in a fluid model. General coupling of Radiative Transfer Equation, Diffusion models and wave propagation models is *a priori* possible within the Arlequin framework, and would interesting *per se* to include source or boundary details (faults for instance) in a large scale domain. Besides this direct use, a very appealing use of such a coupling technique would be the creation of an absorbing layer (similar to Perfectly Matched Layers) for wave propagation in random media. The design of absorbing layers for random media is a difficult problem because, unlike in homogeneous media, energy might be reflected back from the exterior of the domain. Some type of assumption must therefore be made to decide what energy is to be sent back and RTE or diffusion models might just provide this assumption. Such a PML would the first to be created for wave propagation in random media.

Multiscale inversion in geophysical media. The identification of mechanical properties of the Earth can be performed at different scales and using different models. For instance, inversion based on the wave equation (Fichtner 2012, Haned et al. 2016) provides detailed maps of the wave velocities at the global scale (Koelemeijer et al. 2016), based mostly on the first arrivals of the waves. Using the decay rate of the envelope of the wave fields, Radiative Transfer and diffusion models can be used to derive coda Q coefficients (Margerin et al. 1999, Takahashi et al. 2009, Calvet et al. 2013). Unfortunately, inverse problems are not well-posed, and it is difficult to obtain details on the fluctuations of the mechanical properties based only on one type of information restrained to the surface of the Earth. An interesting alternative would come from considering both informations (first arrivals and coda) to identify simultaneously the velocity field and the Q coefficient. As the theoretical relationship between the two is known (Section 3.3.4), the use of combined information is expected to improve the solvability of the inverse problem. This is similar to the approach we are currently implementing in the ANR project CouESt for the multiscale identification of models of polycrystalline materials, but in a dynamical context.

Appendices

Software list

A

The programs and libraries listed below are some of which I participated in developing. Only the software that is developed with a focus on scalability over large number of processors is listed. Most of the development was performed by Ph.D students and post-doctoral fellows (with a particular mention to T. Milanetto Schlittler for the development of CArl and L. de Carvalho Paludo for RandomField) and researchers and engineers (with a particular mention to L. Aubry at CEA for the development of SEM3D).

A.1 CArl (*Code Arlequin*)

CArl is a 2D and 3D implementation of the Arlequin framework for the numerical approximation of coupled multi-scale problems. As those problems usually involve specific parameterization and solvers, care is being take to re-use pre-existing specialized software. In particular, only the solution of the coupling equation (last line of Eq. 2.14) is actually approximated with CArl, while the solution of the other two equations is requested from model-specific software. An iterative solver, described in Néron et al. (2015), allows to decompose the process into a step that is sent to outside software for solving and a step that is solved locally. To construct the coupling matrices, which involve integration of functions over heterogeneous meshes, the meshes are intersected and quadrature rules are built on the intersected elements. The intersection is constructed with an algorithm by Gander and Japhet (2008).

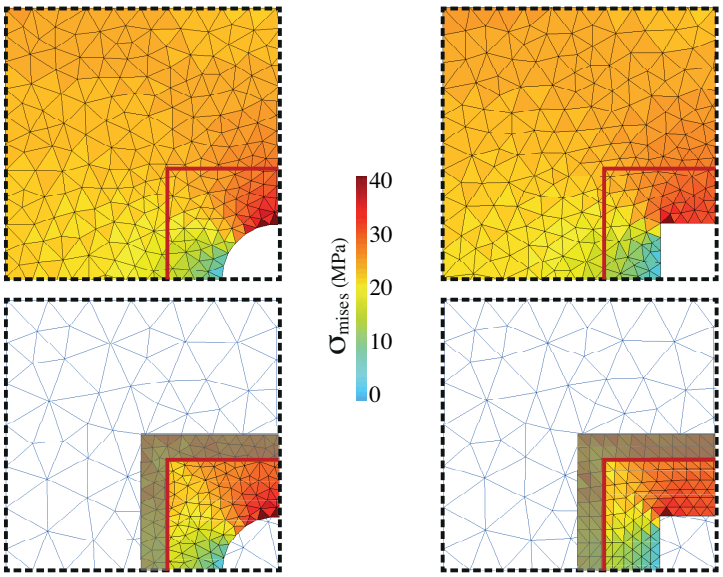

Figure A.1 – *Influence of local geometrical details on stress concentration: comparison of round shape (left column) and square shape (right column), and comparison between mono-model solutions (upper row) and CArl coupled solutions (lower row). Taken from Néron et al. (2015).*

The code is available in 2D in Matlab, with a 2D and 3D parallel C++ implementation currently under way. Fig. A.1 compares 2D results obtained with the Matlab implementation of CArl to those obtained with corresponding mono-models. Fig. A.2 presents results obtained for the

analysis of a polycrystalline material under uniform strain. It is distributed under CeCiLL C licence and freely available on GitHub. The C++ implementation uses CGAL, BLAS, HDF5 and MPI libraries. Both implementations work only for triangular and tetrahedral elements.

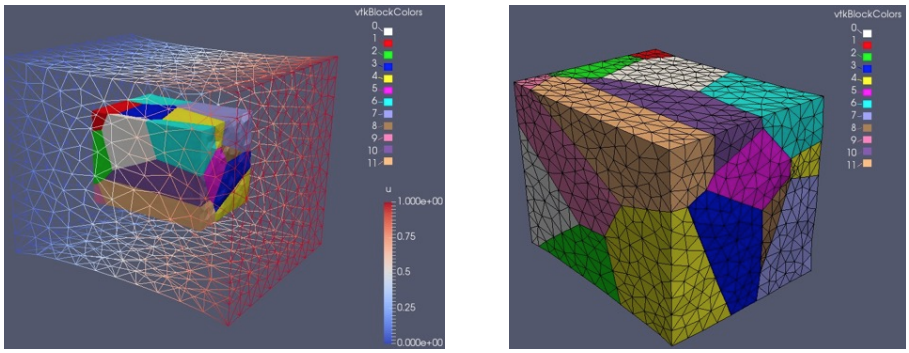

Figure A.2 – *Global (left plot) and local (right plot) models of a polycrystalline material under uniform strain.*

A.2 RandomField

There are essentially two classes of techniques to generate realizations of stationary random fields with chosen first-order marginal density and autocovariance $\mathcal{R}(\mathbf{x})$, either generating in the space domain or in the spectral domain. Both rely on the generation of a Gaussian random field $g(\mathbf{x})$ and its subsequent transformation through a point-wise non-linear map (e.g., the Rosenblatt (1952) transform) into the desired first-order marginal density. In the case of generation in the space domain (Rue 2001), a covariance matrix $\mathbf{R}$ is assembled, such that $\mathbf{R}_{ij} = \mathcal{R}(\mathbf{x}_i - \mathbf{x}_j)$, where the $\{\mathbf{x}_i\}_{1 \leq i \leq N_p}$ are the N_p points where the random field is to be generated. The most computationally intensive part of the generation algorithm in space is the Cholesky factorization of $\mathbf{R}$, which scales as $\mathcal{O}(N_p^3)$ in the general case, but can be improved to sub-$\mathcal{O}(N_p^2)$ using a polynomial approximation of the Cholesky factor (Chow and Saad 2014). On the other hand, working in the wave number domain, the spectral representation technique (Shinozuka and Deodatis 1991) expands the random field $g(\mathbf{x})$ as:

$$g(\mathbf{x}) = \sum_{\mathbf{n} \leq \mathbf{N}} \sqrt{2\mathcal{S}(\mathbf{k_n})|\Delta\mathbf{k}|} \cos\left(\mathbf{k_n} \cdot \mathbf{x} + \hat{\phi}_\mathbf{n}\right) \tag{A.1}$$

where the spectral domain $\mathbf{k}$ is discretized over a regular grid of size $\mathbf{N} = [N_x, N_y, N_z]$ and indexed by $\mathbf{n} = [n_x, n_y, n_z]$, $\mathcal{S}(\mathbf{k_n})$ is the power spectral density of the random field (Fourier transform of $\mathcal{R}(\mathbf{x})$), $|\Delta\mathbf{k}|$ is the unit volume in the spectral domain and the random variables $\hat{\phi}_\mathbf{n}$ are the independent elements of a $\mathbf{N}$-dimensional random variable with uniform density over $[0, 2\pi]$. The complexity of that generation scheme in the space domain is $\mathcal{O}(N_p^2)$ and can be improved to $\mathcal{O}(N_p \log N_p))$ using the Fast Fourier Transform (Shinozuka and Deodatis 1991).

As the generation schemes are all super-linear, they cannot generate fields that span many correlation length in every direction. The scalability issue can be solved (de Carvalho Paludo et al. 2016) by generating realizations of $g(\mathbf{x})$ over the entire domain as superpositions of I smaller independent realizations $g_i(\mathbf{x})$ supported on overlapping subdomains Ω_i of Ω:

$$g(\mathbf{x}) = \sum_{i \in I} \sqrt{\psi_i(\mathbf{x})} g_i(\mathbf{x}). \tag{A.2}$$

where the set of functions $\psi_i(\mathbf{x})$ forms a partition of unity of Ω (that is to say $\sum_{i \in I} \psi_i(\mathbf{x}) = 1$ for any $\mathbf{x} \in \Omega$), supported by the set of subdomains Ω_i. Using this approach, the complexity becomes $\mathcal{O}(n_p \log(n_p))$ where $n_p = N_p/\mathrm{P}$ and P is the number of processors. Essentially, this means that the scheme is $\mathcal{O}(1)$ when we consider a constant number of points per processor. The overlap in Eq. (A.2) involves an approximation that does not alter the average and variance of the resulting field $g(\mathbf{x})$ (de Carvalho Paludo et al. 2016). The influence on the correlation structure depends on the overlap, relative to the correlation length. Theory and numerical tests have shown (de

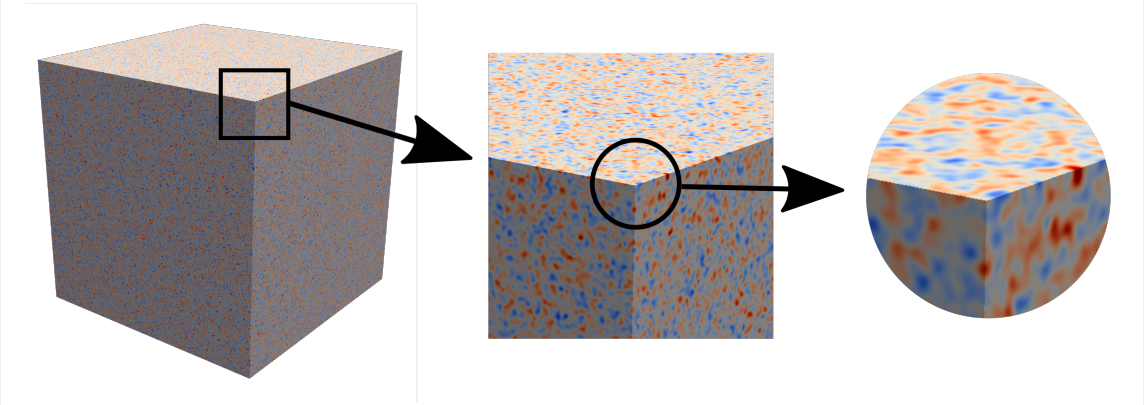

Figure A.3 – *Example of 3D random field generated over 512 processors using the localized approach. The cube edge length is 300 times the correlation length. The generation time was 30 minutes (Wall time).*

Carvalho Paludo et al. 2016) that a transition volume of 5 to 10 correlation length is enough to make statistics homogeneous over the whole domain.

An illustration of Eq. (A.2) is presented in Fig. A.4 for two processors in 1D. The first processor generates a field $g_1(\mathbf{x})$ over $[0-125]$ km, the second processor generates a field $g_2(\mathbf{x})$ over $[25-150]$ km, and the overlap is $[25-125]$ km. The partition of unity is composed of linear functions $\psi_1(\mathbf{x})$ and $\psi_2(\mathbf{x}) = 1 - \psi_1(\mathbf{x})$ in the overlap. The upper plots of Fig. A.4 present in thin continuous lines the two fields $g_1(\mathbf{x})$ (top left) and $g_2(\mathbf{x})$ (top right), as well as the functions $\sqrt{\psi_1(\mathbf{x})}$ (top left) and $\sqrt{\psi_2(\mathbf{x})}$ (top right) in dotted lines. The lower plot of Fig. A.4 presents the field $g(\mathbf{x})$ reconstructed over $[0-150]$ km using Eq. (A.2). Finally, an example of a 3D realization is presented in Figure A.3.

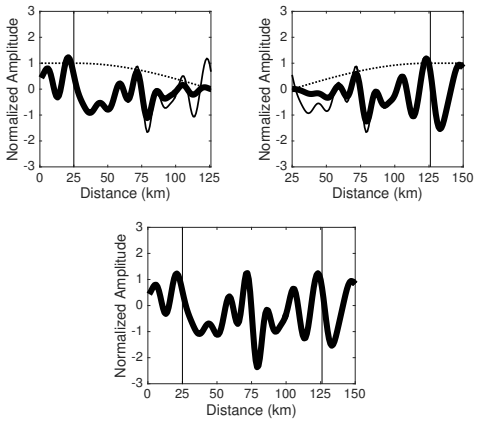

Figure A.4 – *Generation of two independent samples (thin solid lines) $g_1(\mathbf{x})$ (top left) and $g_2(\mathbf{x})$ (top right), with their respective weight functions $\sqrt{\psi_1(\mathbf{x})}$ and $\sqrt{\psi_2(\mathbf{x})}$ (dashed lines). The thick solid lines represent the products $\sqrt{\psi_1(\mathbf{x})}g_1(\mathbf{x})$ (top left) and $\sqrt{\psi_2(\mathbf{x})}g_2(\mathbf{x})$ (top left) and the reconstructed global random field $g(\mathbf{x})$ (lower plot) given by Eq. (A.2). Taken from†Camata et al. (2016).*

The library is implemented in Fortran 90, and uses MPI and HDF5 libraries. It is distributed under CeCiLL C licence and freely available on GitHub. It provides generation routines for incorporation in other software (such as SEM3D, see Sec. A.3), based on either (i) Eq. (A.1), (ii) the corresponding FFT formula or (iii) an optimized routine for isotropic correlation kernels. It allows to choose between many correlation kernels and for non-linear transformation into various first-order marginal densities. A limited scaling study is provided in Table A.1.

Table A.1 – *Weak scalability analysis for random field generation using RandomField library (performed on Igloo, an Altix ICE 8400 LX machine with 800 cores at 2.66GHZ).*

Cores	Nodes	Generation Time [s]	
		Standard	Localized
16	4×10^6	227	320
128	32×10^6	1778	375
512	13×10^7	6761	388

A.3 SEM (*Spectral Element Method*)

SEM is 2D and 3D a wave propagation solver based on the spectral element method (Cohen 2001, Canuto et al. 2006). It is mainly used for the simulation of seismic wave propagation in the Earth (within project SINAPS@, see Berge-Thierry et al. (2016) for a description of the main objectives of the project), although it is also being used for dam engineering and soil-fluid-structure interaction (through the Ph.D. thesis of M. Hammami, funded by Tractebel), and railway engineering (through the Ph.D. thesis of L. de Abreu Corrêa, funded by SNCF). The current version accounts for the propagation of wave in heterogeneous solids (elastic and viscoelastic, isotropic or anisotropic) and (acoustic) fluids. Random materials can be considered through the library RandomField (see Sec. A.2). Unbounded domains are modeled with Perfectly Matched Layers (Berenger 1994), in a stress-velocity formulation (Festa and Vilotte 2005).

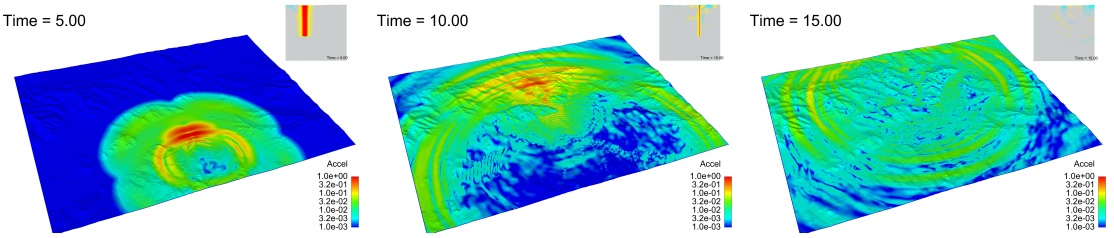

Figure A.5 – *Simulation of a kinematical fault (dislocation over* 15×15 *km*^{2}*) in a region around Ulaan Bator (Mongolia), including topography, sedimentary basin and attenuation. The simulation included* 20×10^6 *elements* (1.4×10^9 *degrees of freedom) and lasted one week over 2048 processors of machine Tera100. Taken from Guillot et al. (2014).*

A pre-processor distributed with the solver can create automatically structured meshes, and also provides the capability to use complex geometries (surface topography, material interfaces) through a reader for various classical mesh file formats, such as Abaqus or Ideas (UNV). This pre-processor provides domain decomposition capabilities, based on the METIS library, for parallel solution on large scale clusters. Note that the method is restricted to quadrilateral meshes in 2D and hexahedral meshes in 3D, both conformal. The restriction may be issue when complex geometries are considered.

In the spectral element method (SEM), the approximation in space of Eq. (1.1) is performed using Lagrange polynomials of high order (typically order 5 to 7) over each element of the mesh. The nodes of the Lagrange polynomials are those of the Gauss-Lobatto-Legendre (GLL) quadrature so that $\mathbf{N}_i(\mathbf{x}_i) = 1$, and $\mathbf{N}_i(\mathbf{x}_{j\neq i}) = 0$ for all polynomials $\mathbf{N}_i$ and quadrature points $\mathbf{x}_i$. The stiffness matrix $\mathbf{K}$ is defined by $\mathbf{K}_{ij} = \int_\Omega \nabla \mathbf{N}_i : \mathbb{C} : \nabla \mathbf{N}_j d\Omega$. The mass matrix $\mathbf{M}$ is defined by $\mathbf{M}_{ij} = \int_\Omega \rho \mathbf{N}_i \cdot \mathbf{N}_j d\Omega$. The integrals are evaluated with the GLL quadrature corresponding to the nodes of the polynomials so the mass matrix is naturally diagonal. For time discretization, we consider a second-order explicit scheme. This scheme is conditionally stable under the Courant-Friedrich-Levy (CFL) condition $\Delta t \leq \alpha h / v_P$, where h is the smallest distance between two GLL nodes, v_P is the largest wave velocity (P-wave velocity for isotropic materials), and α is a safeguard constant, usually taken as $\alpha = 0.2$ for SEM simulations (Meza Fajardo 2007, Cupillard et al. 2012). Table A.2 shows good scalability of the solver up to 4096 cores for a 3D simulation of wave propagation in a homogeneous space with 7 GLL nodes in each direction and element and with no PMLs (Camata et al. 2016).

The code is mainly written in Fortran 90, with large parts in C++ and python. It uses libraries

Table A.2 – *Weak scalability analysis for wave propagation with SEM3D (performed on Tera100, a a BULL machine equipped with almost 140,000 Intel Xeon 7500 processor cores). The time indicated are per time step.*

Cores	DOFs	Elements	Average Time [s]	Minimum Time [s]
32	36,026,967	55,296	0.204	0.198
128	141,137,643	221,184	0.212	0.200
512	558,508,233	884,736	0.256	0.208
4096	4,527,010,569	7,077,888	0.362	0.256

BLAS, MPI and HDF5. Although initially developed at Institut de Physique du Globe de Paris, this software is currently developed jointly by Commissariat à l'Énergie Atomique, Institut de Physique du Globe de Paris and CentraleSupélec. It is available under a CeCiLL C licence, but not currently distributed outside the participants to project SINAPS@. Its development is currently funded mainly by project SINAPS@.

Personal bibliography

I. Baydoun, E. Savin, R. Cottereau, D. Clouteau, and J. Guilleminot. Kinetic modeling of multiple scattering of elastic waves in heterogeneous anisotropic media. *Wave Motion*, 51(8):1325–1348, 2014. doi: 10.1016/j.wavemoti.2014.08.001.

C. Berge-Thierry, P.-Y. Bard, T. Chartier, R. Cottereau, E. Bertrand, F. Lopez-Caballero, D. Clouteau, S. Grange, S. Erlicher, F. Hollender, P. Kotronis, M. Lancieri, A. Laurendeau, A. Le Maoult, N. Moussallam, M. Nicolas, F. Ragueneau, J.-F. Semblat, and F. Voldoire. Toward an integrated seismic risk assessment for nuclear safety improving current French methodologies through the SINAPS@ research project. *Nuclear Engr. Design*, 2016. Accepted for publication.

J. J. Camata, L. de Abreu Corrêa, L. de Carvalho Paludo, L. Aubry, R. Cottereau, and A. L. G. A. Coutinho. Wave propagation in highly heterogeneous media: scalability of the mesh and random properties generator. *Comp. & Geosci.*, 2016. In preparation.

D. Clouteau and R. Cottereau. EASD review on advanced methods in structural dynamics. *J. Sound Vib.*, 332(10):2377–2378, 2013. doi: 10.1016/j.jsv.2012.11.028.

D. Clouteau, R. Cottereau, and G. Lombaert. Dynamics of structures coupled with elastic media – a review. *J. Sound Vib.*, 332(10):2415–2436, 2013. doi: 10.1016/j.jsv.2012.10.011.

R. Cottereau. Numerical strategy for the unbiased homogenization of random materials. *Int. J. Numer. Meth. Engr.*, 95(1):71–90, 2013a. doi: 10.1002/nme.4502.

R. Cottereau. A stochastic-deterministic coupling method for multiscale problems. Application to numerical homogenization of random materials. *Procedia IUTAM*, 6:35–43, 2013b. doi: 10.1016/j.piutam.2013.01.004.

R. Cottereau. A coupling method for the homogenization of stochastic structural models. In M. Papadrakakis and G. Stefanou, editors, *Multiscale modeling and uncertainty quantification of materials and structures*, volume 2, pages 35–49. Springer, 2014. doi: 10.1007/978-3-319-06331-7_3.

R. Cottereau and P. Díez. Numerical modeling of erosion using an improvement of the extended finite element method. *Europ. J. Environm. Civil Eng.*, 15(8):1187–1206, 2011. doi: 10.3166/ejece.15.1187-1206.

R. Cottereau and P. Díez. Fast r-adaptivity for multiple queries of heterogeneous stochastic material fields. *Comp. Mech.*, 56(4):601–612, 2015. doi: 10.1007/s00466-015-1190-x.

R. Cottereau, D. Clouteau, and C. Soize. Construction of a probabilistic model for the soil impedance matrix using a non-parametric method. In C. Soize and G. I. Schuëller, editors, *EURODYN 2005: Proceedings of the 6th European Conference on Structural Dynamics*, pages 841–846. Millpress Science Publishers, 2005.

R. Cottereau, D. Clouteau, C. Soize, and S. Cambier. Probabilistic nonparametric model of impedance matrices. Application to the seismic design of a structure. *Europ. J. Comput. Mech.*, 15(1-3):131–142, 2006. doi: 10.3166/remn.15.131-142.

R. Cottereau, D. Clouteau, and C. Soize. Construction of a probabilistic model for impedance matrices. *Comp. Meth. Appl. Mech. Eng.*, 196(17-20):2252–2268, 2007a. doi: 10.1016/j.cma.2006.12.001.

R. Cottereau, D. Clouteau, and C. Soize. Probabilistic impedance of foundation: impact of the seismic design on uncertain soils. *Earth. Eng. Struct. Dyn.*, 196(17-20):899–918, 2007b. doi: 10.1002/eqe.794.

R. Cottereau, D. Clouteau, and C. Soize. Parametric and nonparametric models of the impedance matrix of a random medium. *Europ. J. Comput. Mech.*, 17(5-7):881–892, 2008. doi: 10.3166/remn.17.881-892.

R. Cottereau, P. Díez, and A. Huerta. Strict error bounds for linear solid mechanics problems using a subdomain-based flux-free method. *Comp. Mech.*, 44(4):533–547, 2009. doi: 10.1007/s00466-009-0388-1.

R. Cottereau, H. Ben Dhia, and D. Clouteau. Localized modeling of uncertainty in the Arlequin framework. In A. Belyaev and R. Langley, editors, *IUTAM Symposium on the Vibration Analysis of Structures with Uncertainties*, volume 27 of *IUTAM Bookseries*, pages 477–488. Springer, 2010a. doi: 10.1007/978-94-007-0289-9_33.

R. Cottereau, L. Chamoin, and P. Díez. Strict error bounds for linear and nonlinear solid mechanics problems using a subdomain-based flux-free method. *Mécanique & Industries*, 11(3-4):249–254, 2010b. doi: 10.1051/meca/2010049.

R. Cottereau, P. Díez, and A. Huerta. Modeling, with a unified level-set representation, of the expansion of a hollow in the ground under different physical phenomena. *Comp. Mech.*, 46(2):315–327, 2010c. doi: 10.1007/s00466-009-0443-y.

R. Cottereau, D. Clouteau, H. Ben Dhia, and C. Zaccardi. A stochastic-deterministic coupling method for continuum mechanics. *Comp. Meth. Appl. Mech. Eng.*, 200(47-48):3280–3288, 2011. doi: 10.1016/j.cma.2011.07.010.

L. de Abreu Corrêa, R. Cottereau, E. Bongini, S. Costa d'Aguiar, B. Faure, and C. Voivret. Impact of the heterogeneity of the ballast on the dynamical behavior of the ballast-soil system. In *Proceedings of the CM3 Conference on Computational Transport*. Springer, 2016a. Submitted for publication.

L. de Abreu Corrêa, R. Cottereau, J. C. Quezada, S. Costa d'Aguiar, and C. Voivret. Randomly-fluctuating heterogeneous continuum model of a granular medium. *Comp. Mech.*, 2016b. In preparation.

L. de Carvalho Paludo, V. Bouvier, and R. Cottereau. Scalable parallel scheme for sampling of Gaussian random fields over large domains. *Int. J. Numer. Meth. Engr.*, 2016. In preparation.

P. Díez, S. Zlotnik, and R. Cottereau. Enforcing interface flux continuity in enhanced XFEM: stability analysis. *Reports Mathematisches Forschungsinstitut Oberwolfach*, 9(1):523–535, 2012. doi: 10.4171/OWR/2012/09.

P. Díez, R. Cottereau, and S. Zlotnik. A stable extended FEM formulation for multi-phase problems enforcing the accuracy of the fluxes through Lagrange multipliers. *Int. J. Numer. Meth. Engr.*, 96(5):303–322, 2013. doi: 10.1002/nme.4554.

P. Jehel and R. Cottereau. On damping created by heterogeneous yielding in the numerical analysis of nonlinear RC frame elements. *Comp. & Struct.*, 154:192–203, 2015. doi: 10.1016/j.compstruc.2015.03.001.

S. Khazaie, R. Cottereau, and D. Clouteau. Influence of the spatial correlation structure of an elastic random medium on its scattering properties. *J. Sound Vib.*, 370:132–148, 2016a. doi: 10.1016/j.jsv.2016.01.012.

S. Khazaie, R. Cottereau, and D. Clouteau. Numerical observation of the equipartition regime in a 3D randomly heterogeneous elastic medium, and discussion on the limiting parameters. *Comp. & Geosci.*, 2016b. Submitted for publication.

Y. Le Guennec, R. Cottereau, D. Clouteau, and C. Soize. A coupling method for stochastic continuum models at different scales. *Prob. Engr. Mech.*, 37:138–147, 2014. doi: 10.1016/j.probengmech.2013.10.005.

D. Néron, H. Ben Dhia, and R. Cottereau. A decoupled strategy to solve reduced-order multi-model problems in the PGD and Arlequin frameworks. *Comp. Mech.*, 57(4):509–521, 2015. doi: 10.1007/s00466-015-1236-0.

A. Panunzio, G. Puel, R. Cottereau, S. Simon, and X. Quost. Construction of a stochastic model of track geometry irregularities and validation through experimental measurements of dynamic loading. *Vehicle Syst. Dyn.*, 2016. Submitted for publication.

Q.-A. Ta, D. Clouteau, and R. Cottereau. Modeling of random anisotropic elastic media and impact on wave propagation. *Europ. J. Comput. Mech.*, 19(1-3):241–253, 2010a. doi: 10.3166/ejcm.19.241-253.

Q.-A. Ta, D. Clouteau, and R. Cottereau. Numerical modeling of wave propagation in random anisotropic heterogeneous elastic media. In S. Sas and B. Bergen, editors, *Proceedings of ISMA 2010 - International Conference on Noise and Vibration Engineering including USD 2010*, pages 5223–5237. Katholieke Universiteit Leuven, 2010b.

R. Taherzadeh, D. Clouteau, and R. Cottereau. Simple formulas for the dynamic stiffness of pile groups. *Earth. Eng. Struct. Dyn.*, 38(15):1665–1685, 2009. doi: 10.1002/eqe.918.

C. Zaccardi, L. Chamoin, R. Cottereau, and H. Ben Dhia. Error estimation and model adaptation for a stochastic-deterministic coupling method based on the Arlequin framework. *Int. J. Numer. Meth. Engr.*, 96(2):87–109, 2013. doi: 10.1002/nme.4540.

Bibliography

A. Abdulle and A. Nonnenmacher. A posteriori error analysis of the heterogeneous multiscale method for homogenization problems. *Comptes Rendus Acad. Sci. - Series I - Math.*, 347(17-18): 1081–1086, 2009. doi: 10.1016/j.crma.2009.07.004.

A. Abdulle, M. J. Grote, and C. Stohrer. Finite element heterogeneous multiscale method for the wave equation: long-time effects. *SIAM Multiscale Model. Simul.*, 12(3):1230–1257, 2014. doi: 10.1137/13094195X.

E. Abrahams, P. W. Anderson, D. C. Licciardello, and T. V. Ramakrishnan. Scaling theory of localization: absence of quantum diffusion in two dimensions. *Phys. Rev. Lett.*, 42(10):673–676, 1979. doi: 10.1103/PhysRevLett.42.673.

I. Agnolin and J.-N. Roux. On the elastic moduli of three-dimensional assemblies of spheres: characterization and modeling of fluctuations in the particle displacement and rotation. *Int. J. Solids Struct.*, 45(3-4):1101–1123, 2008. doi: 10.1016/j.ijsolstr.2007.07.016.

S. Ahmed, J. Harkness, L. Le Pen, W. Powrie, and A. Zervos. Numerical modelling of railway ballast at the particle scale. *Int. J. Numer. Anal. Meth. Geomech.*, 2015. doi: 10.1002/nag.2424. Accepted for publication.

M. Ainsworth and J. T. Oden. *A posteriori error estimation in finite element analysis*. Pure and Applied Mathematics. Wiley-Interscience, 2000.

K. Aki. Analysis of the seismic coda of local earthquakes as scattered waves. *J. Geophys. Res.*, 74 (2):615–631, 1969. doi: 10.1029/JB074i002p00615.

K. Aki and B. Chouet. Origin of coda waves: source, attenuation, and scattering effects. *J. Geophys. Res.*, 80(23):3322–3342, 1975. doi: 10.1029/JB080i023p03322.

K. Aki and W. H. K. Lee. Determination of three-dimensional velocity anomalies under a seismic array using first P arrival times from local earthquakes. Part I. A homogeneous initial model. *J. Geophys. Res.*, 81:4381–4399, 1976. doi: 10.1029/JB081i023p04381.

K. Aki, A. Christoffersson, and E. S. Husebye. Three-dimensional seismic structure of the lithosphere under Montana LASA. *Bull. Seism. Soc. Amer.*, 66:501–524, 1976.

P. Alart, D. Iceta, and D. Dureisseix. A nonlinear domain decomposition formulation with application to granular dynamics. *Comp. Meths. Appl. Mech. Engr.*, 205-208:59–67, 2012. doi: 10.1016/j.cma.2011.04.024.

G. Allaire. Homogenization of the Navier-Stokes equations in open sets perforated with tiny holes I. abstract framework, a volume distribution of holes. *Arch. Rational Mech. Anal.*, 113(3): 209–259, 1991a. doi: 10.1007/BF00375065.

G. Allaire. Homogenization of the Navier-Stokes equations in open sets perforated with tiny holes II. non-critical sizes of the holes for a volume distribution and a surface distribution of holes. *Arch. Rational Mech. Anal.*, 113(3):261–298, 1991b. doi: 10.1007/BF00375066.

P. W. Anderson. Absence of diffusion in certain random lattices. *Phys. Rev.*, 109(5):1492–1505, 1958. doi: 10.1103/PhysRev.109.1492.

P. W. Anderson. The question of classical localization: a theory of white paint ? *Phil. Mag. B*, 52 (3):505–509, 1985. doi: 10.1080/13642818508240619.

P. Angot, C.-H. Bruneau, and P. Fabrie. A penalization method to take into account obstacles in incompressible viscous flows. *Numer. Math.*, 81(4):497–520, 1999. doi: 10.1007/s002110050401.

P. Anugonda, J. S. Wiehn, and J. A. Turner. Diffusion of ultrasound in concrete. *Ultrasonics*, 39(6): 429–435, 2001. doi: 10.1016/S0041-624X(01)00077-4.

T. Arbogast and K. J. Boyd. Subgrid upscaling and mixed multiscale finite elements. *SIAM J. Numer. Anal.*, 44(3):1150–1171, 2006. doi: 10.1137/050631811.

D. Arjmand and O. Runborg. Analysis of heterogeneous multiscale methods for long time wave propagation problems. *SIAM Multiscale Model. Simul.*, 12(3):1135–1166, 2014. doi: 10.1137/140957573.

M. Arnst and R. G. Ghanem. Probabilistic equivalence and stochastic model reduction in multiscale analysis. *Comp. Meths. Appl. Mech. Engr.*, 197:3584–3592, 2008. doi: 10.1016/j.cma.2008.03.016.

M. Arnst, R. G. Ghanem, E. Phipps, and J. Red-Horse. Reduced chaos expansions with random coefficients in reduced-dimensional stochastic modeling of coupled problems. *Int. J. Numer. Meth. Engr.*, 97(5):352–376, 2014. doi: 10.1002/nme.4595.

J.-L. Auriault and C. Boutin. Long wavelength inner-resonance cut-off frequencies in elastic composite materials. *Int. J. Solids Struct.*, 49:3269–3281, 2012. doi: 10.1016/j.ijsolstr.2012.07.002.

J.-L. Auriault, C. Boutin, and C. Geindreau. *Homogenization of coupled phenomena in heterogeneous media*. John Wiley & Sons, 2010.

E. Azéma, F. Radjai, and G. Saussine. Quasistatic rheology, force transmission and fabric properties of a packing of irregular polyhedral particles. *Mech. Mat.*, 41:729–741, 2009. doi: 10.1016/j.mechmat.2009.01.021.

I. Babuška and J. E. Osborn. Generalized finite element methods: their performance and their relation to mixed methods. *SIAM J. Numer. Anal.*, 20(3):510–536, 1983. doi: 10.1137/0720034.

I. Babuška and W. C. Rheinboldt. Error estimates for adaptive finite element computations. *SIAM J. Numer. Anal.*, 15(4):736–755, 1978a.

I. Babuška and W. C. Rheinboldt. A posteriori error estimates for the finite element method. *Int. J. Numer. Meth. Engr.*, 12(10):1597–1615, 1978b.

I. Babuška, F. Nobile, and R. Tempone. A stochastic collocation method for elliptic partial differential equations with random input data. *SIAM Rev.*, 52(2):317–355, 2010. doi: 10.1137/100786356.

I. Babuška, M. Motamed, and R. Tempone. A stochastic multiscale method for the elastodynamic wave equation arising from fiber composites. *Comp. Meths. Appl. Mech. Engr.*, 276:190–211, 2014. doi: 10.1016/j.cma.2014.02.018.

G. E. Backus. Long-wave elastic anisotropy produced by horizontal layering. *J. Geophys. Res.*, 67 (11):4427–4440, 1962. doi: 10.1029/JZ067i011p04427.

K. Bagi. Statistical analysis of contact force components in random granular assemblies. *Granular Matter*, 5(1):45–54, 2003. doi: 10.1007/s10035-002-0123-5.

K. Bagi. Analysis of microstructural strain tensors for granular assemblies. *Int. J. Solids Struct.*, 43(10):31666–3184, 2006. doi: 10.1016/j.ijsolstr.2005.07.016.

G. Bal. Kinetics of scalar wave fields in random media. *Wave Motion*, 43(2):132–157, 2005. doi: 10.1016/j.wavemoti.2005.08.002.

G. Bal, T. Komorowski, and L. Ryzhik. Self-averaging of wigner transforms in random media. *Comm. Math. Phys.*, 242(1):81–135, 2003. doi: 10.1007/s00220-003-0937-y.

G. Bal, T. Komorowski, and L. Ryzhik. Kinetic limits for waves in random media. *Kinetic Related Models*, 3(4):529–644, 2010. doi: 10.3934/krm.2010.3.529.

A. Bamberger, B. Engquist, L. Halpern, and P. Joly. Parabolic wave equation approximation in heterogeneous media. *SIAM J. Appl. Math.*, 48(1):99–128, 1988a. doi: 10.1137/0148005.

A. Bamberger, B. Engquist, L. Halpern, and P. Joly. Higher order paraxial wave equation approximations in heterogeneous media. *SIAM J. Appl. Math.*, 48(1):129–154, 1988b.

J. P. Bardet and I. Vardoulakis. The asymetry of stress in granular media. *Int. J. Solids Struct.*, 38 (2):353–367, 2001. doi: 10.1016/S0020-7683(00)00021-4.

I. Baydoun, E. Savin, R. Cottereau, D. Clouteau, and J. Guilleminot. Kinetic modeling of multiple scattering of elastic waves in heterogeneous anisotropic media. *Wave Motion*, 51(8):1325–1348, 2014. doi: 10.1016/j.wavemoti.2014.08.001.

T. Belytschko and S. P. Xiao. Coupling methods for continuum model with molecular model. *Int. J. Multiscale Comp. Engr.*, 1(1):134–145, 2003. doi: 10.1615/IntJMultCompEng.v1.i1.100.

H. Ben Dhia. Multiscale mechanical problems: the Arlequin method. *Comptes Rendus Acad. Sci. - Series IIB - Mech.-Phys.-Astron.*, 326(12):899–904, 1998. doi: 10.1016/S1251-8069(99)80046-5.

H. Ben Dhia. Further insights by theoretical investigations of the multiscale Arlequin method. *Int. J. Multiscale Comp. Engr.*, 6(3):215–232, 2008. doi: 10.1615/IntJMultCompEng.v6.i3.30.

H. Ben Dhia and K. Abben. Une approche multi-échelle en dynamique des structures. In *Proceedings du 12ème Colloque National En Calcul des Structures (Giens 2015)*, 2015.

H. Ben Dhia and G. Rateau. Mathematical analysis of the mixed Arlequin method. *Comptes Rendus Acad. Sci. - Series I - Math.*, 332(7):649–654, 2001. doi: 10.1016/S0764-4442(01)01900-0.

H. Ben Dhia and G. Rateau. The Arlequin method as a flexible engineering design tool. *Int. J. Numer. Meth. Engr.*, 62(11):1442–1462, 2005. doi: 10.1002/nme.1229.

A. Bensoussan, J.-L. Lions, and G. Papanicolaou. *Asymptotic analysis for periodic structures*. Number 5 in Studies in Mathematics and its Applications. North Holland, 1978.

J.-P. Berenger. A perfectly matched layer for the absorption of electromagnetic waves. *J. Comp. Phys.*, 114(2):185–200, 1994. doi: 10.1006/jcph.1994.1159.

A. Bespalov, C. E. Powell, and D. Silvester. A priori error analysis of stochastic Galerkin mixed approximations of elliptic PDEs with random data. *SIAM J. Numer. Anal.*, 50(4):2039–2063, 2012. doi: 10.1137/110854898.

F. Birch. The velocity of compressional waves in rocks to 10 kilobars: part 2. *J. Geophys. Res.*, 66 (7):2199–2224, 1961. doi: 10.1029/JZ066i007p02199.

J. E. Bishop, J. M. Emery, R. V. Field, C. R. Weinberger, and D. J. Littlewood. Direct numerical simulations in solid mechanics for understanding the macroscale effects of microscale material variability. *Comp. Meths. Appl. Mech. Engr.*, 287:262–289, 2015. doi: 10.1016/j.cma.2015.01.017.

X. Blanc, C. Le Bris, and P.-L. Lions. Stochastic homogenization and random lattices. *Journal Mathématiques Pures Appliquées*, 88(1):34–63, 2007. doi: 10.1016/j.matpur.2007.04.006.

A. Bourgeat and A. Piatnitski. Approximations of effective coefficients in stochastic homogenization. *Ann. Inst. Henri Poincaré*, 40:153–165, 2004. doi: 10.1016/j.anihpb.2003.07.003.

A. Bourgeat, A. Mikelić, and S. Wright. Stochastic two-scale convergence in the mean and applications. *Journal Reine Angewandte Mathematik*, 1994(456):19–52, 1994. doi: 10.1515/crll.1994.456.19.

R. C. Bourret. Stochastically perturbed fields, with applications to wave propagation in random media. *Il Nuovo Cimento*, 26(1):1–31, 1962. doi: 10.1007/BF02754339.

C. Boutin. Acoustics of porous media with inner resonators. *J. Acoust. Soc. Amer.*, 134:4717, 2013. doi: 10.1121/1.4824965.

C. Boutin and J.-L. Auriault. Rayleigh scattering in elastic composite materials. *Int. J. Engr. Sci.*, 31(12):1669–1689, 1993. doi: 10.1016/0020-7225(93)90082-6.

C. Boutin, A. Rallu, and S. Hans. Large scale modulation of high frequency acoustics fields in porous media. In *Proceedings of Acoustics 2012*, pages 1895–1901. Société Française d'Acoustique, 2012.

C. Boutin, J. Soubestre, L. Schwan, and M. Dietz. Multi-scale modeling for dynamics of structure-soil-structure interactions. *Acta Geophys.*, 62(5):1005–1024, 2014. doi: 10.2478/s11600-014-0230-9.

A. Brandt. Multiscale scientific computation: review 2001. In *Multiscale and multiresolution methods*, volume 20 of *Lecture Notes in Computational Science and Engineering*, pages 3–95, 2002.

H. Brandt. A study of the speed of sound in porous granular media. *J. Appl. Mech.*, 22:479–186, 1955.

M. E. Brewster and G. Beylkin. A multiresolution strategy for numerical homogenization. *Appl. Comp. Harmonic Anal.*, 2(4):327–349, 1995. doi: 10.1006/acha.1995.1024.

F. Brezzi and A. Russo. Choosing bubbles for advection-diffusion problems. *Math. Models Meth. Appl. Sci.*, 4(4):571–587, 1994. doi: 10.1142/S0218202594000327.

T. Butler, C. Dawson, and T. Wildey. A posteriori error analysis of stochastic differential equations using polynomial chaos expansions. *SIAM J. Sci. Comp.*, 33(3):1267–1291, 2011. doi: 10.1137/100795760.

R. E. Caflisch. Monte Carlo and quasi-Monte Carlo methods. *Acta Numer.*, 7:1–49, 1998. doi: 10.1017/S0962492900002804.

B. Cairns and E. Wolf. Comparison of the Born and the Rytov approximations for scattering on quasi-homogeneous media. *Optics Comm.*, 74(5):284–289, 1990. doi: 10.1016/0030-4018(90)90384-6.

M. Calvet, M. Sylvander, L. Margerin, and A. Villaseñor. Spatial variations of seismic attenuation and heterogeneity in the Pyrenees: Coda Q and peak delay time analysis. *Tectonophys.*, 608:428–439, 2013. doi: 10.1016/j.tecto.2013.08.045.

J. J. Camata, L. de Abreu Corrêa, L. de Carvalho Paludo, L. Aubry, R. Cottereau, and A. L. G. A. Coutinho. Wave propagation in highly heterogeneous media: scalability of the mesh and random properties generator. *Comp. & Geosci.*, 2016. In preparation.

B. Cambou, M. Chaze, and F. Dedecker. Change of scale in granular materials. *Europ. J. Mech. A/Solids*, 19(6):999–1014, 2000. doi: 10.1016/S0997-7538(00)01114-1.

E. Cancès, V. Ehrlacher, F. Legoll, and B. Stamm. An embedded corrector problem to approximate the homogenized coefficients of an elliptic equation. *Comptes Rendus Math.*, 353(9):801–806, 2015. doi: 10.1016/j.crma.2015.06.019.

C. Canuto and T. Kozubek. A fictitious domain approach to the numerical solution of PDEs in stochastic domains. *Numer. Math.*, 107(2):257–293, 2007. doi: 10.1007/s00211-007-0086-x.

C. Canuto, M. Y. Hussaini, A. Quarteroni, and T. A. Zang. *Spectral methods. Fundamentals in single domains*. Scientific Computation. Springer-Verlag, 2006.

Y. Capdeville and P. Cance. Residual homogenization for elastic wave propagation in complex media. *Geophys. J. Int.*, 200:986–999, 2015. doi: 10.1093/gji/ggu452.

Y. Capdeville and J.-J. Marigo. Second order homogenization of the elastic wave equation for non-periodic layered media. *Geophys. J. Int.*, 170(2):823–838, 2007. doi: 10.1111/j.1365-246X.2007.03462.x.

Y. Capdeville and J.-J. Marigo. A non-periodic two scale asymptotic method to take account of rough topographies for 2-D elastic wave propagation. *Geophys. J. Int.*, 192:163–189, 2013. doi: 10.1093/gji/ggs001.

Y. Capdeville, E. Chaljub, J.-P. Vilotte, and J.-P. Montagner. Coupling the spectral element method with a modal solution for elastic wave propagation in global earth models. *Geophys. J. Int.*, 152 (1):34–67, 2003. doi: 10.1046/j.1365-246X.2003.01808.x.

Y. Capdeville, L. Guillot, and J.-J. Marigo. 2D non-periodic homogenization to upscale elastic media for P-SV waves. *Geophys. J. Int.*, 182(2):903–922, 2010. doi: 10.1111/j.1365-246X.2010.04636.x.

Y. Capdeville, E. Stutzmann, N. Wang, and J.-P. Montagner. Residual homogenization for seismic forward and inverse problems in layered media. *Geophys. J. Int.*, 198(2):470–487, 2013. doi: 10.1093/gji/ggt102.

F. Chabas and Christian Soize. Modeling mechanical subsystems by boundary impedance in the finite element method. *La Recherche Aérospatiale (English version)*, 5:59–75, 1987.

L. Chamoin, J. T. Oden, and S. Prudhomme. A stochastic coupling method for atomic-to-continuum Monte-Carlo simulations. *Comp. Meths. Appl. Mech. Engr.*, 197(43-44):3530–3546, 2008. doi: 10.1016/j.cma.2008.04.013.

L. Chamoin, S. Prudhomme, H. Ben Dhia, and J. T. Oden. Ghost forces and spurious effects in atomic-to-continuum coupling methods by the Arlequin approach. *Int. J. Numer. Meth. Engr.*, 83(8-9):1081–1113, 2010. doi: 10.1002/nme.2879.

L. Chamoin, E. Florentin, S. Pavot, and V. Visseq. Robust goal-oriented error estimation based on the constitutive relation error for stochastic problems. *Comp. & Struct.*, 106-107:189–195, 2012. doi: 10.1016/j.compstruc.2012.05.002.

C. S. Chang and M. Lun. Elastic material constants for isotropic granular solids with particle rotation. *Int. J. Solids Struct.*, 29(8):1001–1018, 1992. doi: 10.1016/0020-7683(92)90071-Z.

C. S. Chang, S. J. Chao, and Y. Chang. Estimates of elastic moduli for granular material with anisotropic random packing structure. *Int. J. Solids Struct.*, 32(14):1989–2008, 1995. doi: 10.1016/0020-7683(94)00225-L.

K. Charles. Mother Earth gets undressed. *Nature News*, 2008. doi: 10.1038/news.2008.1001.

J. Charrier. Strong and weak error estimates for elliptic partial differential equations with random coefficients. *SIAM J. Numer. Anal.*, 50(1):216–246, 2012. doi: 10.1137/100800531.

K.-S. Cheong and E. P. Busso. Discrete dislocation density modelling of single phase FCC polycrystal aggregates. *Acta Mater.*, 52(19):5665–5675, 2004. doi: 10.1016/j.actamat.2004.08.044.

L. A. Chernov. *Wave propagation in a random medium*. McGraw-Hill, 1960.

N. Cherroret and S. E. Skipetrov. Microscopic derivation of self-consistent equations of Anderson localization in a disordered medium of finite size. *Phys. Rev. E*, 77(046608):1–9, 2008. doi: 10.1103/PhysRevE.77.046608.

C. Chesnais, C. Boutin, and S. Hans. Effects of the local resonance on the wave propagation in periodic frame structures: generalized Newtonian mechanics. *J. Acoust. Soc. Amer.*, 132(4):2873–2887, 2012. doi: 10.1121/1.4744975.

J. Chessa and T. Belytschko. An extended finite element method for two-phase fluids: flow simulation and modeling. *J. Appl. Mech.*, 70(1):10–17, 2003. doi: 10.1115/1.1526599.

M. Chevreuil, A. Nouy, and E. Safatly. A multiscale method with patch for the solution of stochastic partial differential equations with localized uncertainties. *Comp. Meths. Appl. Mech. Engr.*, 255:255–274, 2013. doi: 10.1016/j.cma.2012.12.003.

P. D. Chinh. New estimates for macroscopic elastic moduli of random polycrystalline aggregates. *Phil. Mag. A*, 86(2):205–226, 2006. doi: 10.1080/14786430500343876.

E. Chow and Y. Saad. Preconditioned Krylov subspace methods for sampling multivariate Gaussian distributions. *SIAM J. Sci. Comp.*, 36(2):A588–A608, 2014. doi: 10.1137/130920587.

N. Christensen. Poisson's ratio and crustal seismology. *J. Geophys. Res.*, 101:3139–3156, 1996. doi: 10.1029/95JB03446.

N. Christensen and W. Mooney. Seismic velocity structure and composition of the continental crust: a global view. *J. Geophys. Res.*, 100:9761–9788, 1995. doi: 10.1029/95JB00259.

A. Clément, C. Soize, and J. Yvonnet. Computational nonlinear stochastic homogenization using a nonconcurrent multiscale approach for hyperelastic heterogeneous microstructures analysis. *Int. J. Numer. Meth. Engr.*, 91(8):799–824, 2012.

G. Cohen. *Higher-order numerical methods for transient wave equations*. Scientific Computation. Springer, 2001.

D. P. Connolly, G. Kouroussis, O. Laghrouche, C. L. Ho, and M. C. Forde. Benchmarking railway vibrations – track, vehicle, ground and building effects. *Construction Building Mater.*, 2014. doi: 10.1016/j.conbuildmat.2014.07.042. In press.

R. Costaouec, C. Le Bris, F. Legoll, and X. Blanc. Variance reduction using antithetic variables: applications to stochastic homogenization. *Markov Proc. Rel. Fields*, 2011. Submitted for publication.

R. Cottereau. Numerical strategy for the unbiased homogenization of random materials. *Int. J. Numer. Meth. Engr.*, 95(1):71–90, 2013. doi: 10.1002/nme.4502.

R. Cottereau and P. Díez. Numerical modeling of erosion using an improvement of the extended finite element method. *Europ. J. Environm. Civil Eng.*, 15(8):1187–1206, 2011. doi: 10.3166/ejece.15.1187-1206.

R. V. Craster, J. Kaplunov, and A. V. Pichugin. High frequency homogenization for periodic media. *Proc. Royal Soc. London A*, 466:2341–2362, 2010.

A. M. Cuitiño and M. Ortiz. Computational modelling of single crystals. *Modelling Simul. Mat. Sci. Engng.*, 1(3):225–263, 1993. doi: 10.1088/0965-0393/1/3/001.

P. A. Cundall and O. D. L. Strack. A discrete numerical model for granular assemblies. *Géotechnique*, 29(1):47–65, 1979. doi: 10.1680/geot.1979.29.1.47.

P. Cupillard, E. Delavaud, G. Burgos, G. Festa, J.-P. Vilotte, Y. Capdeville, and J.-P. Montagner. RegSEM: a versatile code based on the spectral element method to compute seismic wave propagation at the regional scale. *Geophys. J. Int.*, 188(3):1203–1220, 2012. doi: 10.1111/j.1365-246X.2011.05311.x.

W. A. Curtin and R. E. Miller. Atomistic/continuum coupling in computational materials science. *Modelling Simul. Mat. Sci. Engng.*, 11:R33, 2003. doi: 10.1088/0965-0393/11/3/201.

G. Dal Maso. *An Introduction to Γ-convergence*, volume 8 of *Progress in Nonlinear Differential Equations and Their Applications*. Birkhäuser, 1993. doi: 10.1007/978-1-4612-0327-8.

H. Darcy. *Les Fontaines Publiques de la Ville de Dijon*. Dalmon, Paris, 1856.

L. de Abreu Corrêa, R. Cottereau, J. C. Quezada, S. Costa d'Aguiar, and C. Voivret. Randomly-fluctuating heterogeneous continuum model of a granular medium. *Comp. Mech.*, 2016. In preparation.

L. de Carvalho Paludo, V. Bouvier, and R. Cottereau. Scalable parallel scheme for sampling of Gaussian random fields over large domains. *Int. J. Numer. Meth. Engr.*, 2016. In preparation.

G. de Saxcé, J. Fortin, and O. Millet. About the numerical simulation of the dynamics of granular media and the definition of the mean stress tensor. *Mech. Mat.*, 36(12):1175–1184, 2004. doi: 10.1016/j.mechmat.2003.01.002.

M. K. Deb, I. M. Babuška, and J. T. Oden. Solution of stochastic partial differential equations using Galerkin finite element techniques. *Comp. Meths. Appl. Mech. Engr.*, 190(48):6359–6372, 2001. doi: 10.1016/S0045-7825(01)00237-7.

P. Degond and S. Jin. A smooth transition model between kinetic and diffusion equations. *SIAM J. Numer. Anal.*, 42(6):2671–2687, 2005. doi: 10.1137/S0036142903430414.

P. Degond, J.-G. Liu, and L. Mieussens. Macroscopic fluid models with localized kinetic upscaling effects. *SIAM Multiscale Model. Simul.*, 5(3):940–979, 2006. doi: 10.1137/060651574.

B. Devincre, R. Madec, G. Monnet, S. Queyreau, R. Gatti, and L. Kubin. Modeling crystal plasticity with dislocation dynamics simulations: the MicroMegas code. In O. Thomas, A. Ponchet, and S. Forest, editors, *Mechanics of nano-objects*, pages 81–100. Les Presses des Mines, 2011.

A. Devulder, D. Aubry, and G. Puel. Two-time scale fatigue modelling: application to damage. *Comp. Mech.*, 45(6):637–646, 2010. doi: 10.1007/s00466-010-0476-2.

P. J. Digby. The effective elastic moduli of porous granular rocks. *J. Appl. Mech.*, 48(4):803–808, 1981. doi: 10.1115/1.3157738.

V. Dolean, P. Jolivet, and F. Nataf. *An introduction to Domain Decomposition Methods. Algorithms, Theory, and Parallel implementation*. Society for Industrial and Applied Mathematics (SIAM), 2015.

M. Dorobantu and B. Engquist. Wavelet-based numerical homogenization. *SIAM J. Numer. Anal.*, 35(2):540–559, 1998. doi: 10.1137/S0036142996298880.

A. Drescher and G de Josselin de Jong. Photoelastic verification of a mechanical model for the flow of a granular material. *J. Mech. Phys. Solids*, 20(5):337–340, 1972. doi: 10.1016/0022-5096(72)90029-4.

M. Dubois, A. Moreau, M. Militzer, and J. F. Bussière. Laser-ultrasonic monitoring of phase transformations in steels. *Scripta Materialia*, 39(6):735–741, 1998. doi: 10.1016/S1359-6462(98)00179-1.

O. Durán, N. P. Kruyt, and S. Luding. Analysis of three-dimensional micro-mechanical strain formulations for granular materials: evaluation of accuracy. *Int. J. Solids Struct.*, 47(2):251–260, 2010. doi: 10.1016/j.ijsolstr.2009.09.035.

F. J. Dyson. The radiation theories of Tomonaga, Schwinger, and Feynman. *Phys. Rev.*, 75(3):486–502, 1949a. doi: 10.1103/PhysRev.75.486.

F. J. Dyson. The S matrix in quantum electrodynamics. *Phys. Rev.*, 75(11):1736–1755, 1949b. doi: 10.1103/PhysRev.75.1736.

W. E. *Principles of multiscale modeling*. Cambridge University Press, 2011.

W. E and B. Engquist. The heterogeneous multiscale methods. *Comp. Mat. Sci.*, 1(1):87–132, 2003. doi: 10.4310/CMS.2003.v1.n1.a8.

W. E, P. Ming, and P. Zhang. Analysis of the heterogeneous multiscale method for elliptic homogenization problems. *J. Amer. Math. Soc.*, 18:121–156, 2005. doi: 10.1090/S0894-0347-04-00469-2.

Y. Efendiev and T. Y. Hou. *Multiscale finite element methods. Theory and applications*, volume 4 of *Surveys and Tutorials in the Applied Mathematical Sciences*. Springer, 2009.

Y. Efendiev, J. Galvis, and T. Y. Hou. Generalized multiscale finite-element methods (GMsFEM). *J. Comp. Phys.*, 251:116–135, 2013. doi: 10.1016/j.jcp.2013.04.045.

K. Emoto, H. Sato, and T. Nishimura. Synthesis of vector wave envelopes on the free surface of a random medium for the vertical incidence of a plane wavelet based on the Markov approximation. *J. Geophys. Res.: Solid Earth*, 115(B08306):1–15, 2010. doi: 10.1029/2009JB006955.

B. Engquist and O. Runborg. Wavelet-based numerical homogenization with applications. In T. J. Barth, T. F. Chan, and R. Haimes, editors, *Multiscale and Multiresolution methods: theory and applications*, Lecture Notes in Computational Science and Engineering, pages 97–148. Springer-Verlag, 2001. doi: 10.1007/978-3-642-56205-1_2.

B. Engquist, H. Holst, and O. Runborg. Multiscale methods for the wave equation. *Comp. Mat. Sci.*, 9(1):33–56, 2011.

B. Engquist, H. Holst, and O. Runborg. Multiscale methods for wave propagation in heterogeneous media over long time. In B. Engquist, O. Runborg, and Y.-H. R. Tsai, editors, *Numerical analysis of multiscale computations*, volume 82 of *Lecture Notes in Computational Science and Engineering*, pages 167–186. Springer, 2012. doi: 10.1007/978-3-642-21943-6_8.

L. P. Evers, D. M. Parks, W. A. M. Brekelmans, and M. G. D. Geers. Crystal plasticity model with enhanced hardening by geometrically necessary dislocation accumulation. *J. Mech. Phys. Solids*, 50(11):2403–2424, 2002. doi: 10.1016/S0022-5096(02)00032-7.

N. Fang, D. Xi, J. Xu, M. Ambati, W. Srituravanich, C. Sun, and X. Zhang. Ultrasonic metamaterials with negative modulus. *Nature Mater.*, 5:452–456, 2006. doi: 10.1038/nmat1644.

C. Farhat and F.-X. Roux. A method of finite element tearing and interconnecting and its parallel solution algorithm. *Int. J. Numer. Meth. Engr.*, 32(6):1205–1227, 1991. doi: 10.1002/nme.1620320604.

M. Fehler, H. Sato, and L.-J. Huang. Envelope broadening of outgoing waves in 2D random media: a comparison between the Markov approximation and numerical simulations. *Bull. Seism. Soc. Amer.*, 90(4):914–928, 2000. doi: 10.1785/0119990143.

D. M. Feiner and J. H. Griffin. Mistuning identification of bladed disks using a fundamental mistuning model – Part I: theory. *J. Turbomach.*, 126(1):150–158, 2004. doi: 10.1115/1.1643913.

G. A. Fenton. Random field modeling of CPT data. *J. Geotech. Geoenv. Engr.*, 125(6):486–498, 1999. doi: 10.1061/(ASCE)1090-0241(1999)125:6(486).

G. Festa and J.-P. Vilotte. The Newmark scheme as velocity-stress time-staggering: an efficient PML implementation for spectral element simulations of elastodynamics. *Geophys. J. Int.*, 161: 789–812, 2005.

F. Feyel. Multiscale FE^2 elastocviscoplastic analysis of composite structures. *Comp. Mat. Sci.*, 16 (1-4):344–354, 1999. doi: 10.1016/S0927-0256(99)00077-4.

F. Feyel and J.-L. Chaboche. FE^2 multiscale approach for modelling the elastoviscoplastic behaviour of long fibre SiC/Ti composite materials. *Comp. Meths. Appl. Mech. Engr.*, 183(3-4): 309–330, 2000. doi: 10.1016/S0045-7825(99)00224-8.

A. Fichtner. *Full seismic waveform modelling and inversion*. Advances in Geophysical and Environmental Mechanics and Mathematics. Springer, 2012.

M. Filoche and S. Mayboroda. Universal mechanism for Anderson and weak localization. *Proc. Nat. Acad. Sci. USA*, 109(37):14761–14766, 2012. doi: 10.1073/pnas.1120432109.

J. Fish. *Practical multiscaling*. John Wiley & Sons, 2014.

J. Fish, M. Bailakanavar, L. Powers, and T. Cook. Multiscale fatigue life prediction model for heterogeneous materials. *Int. J. Numer. Meth. Engr.*, 91(10):1087–1104, 2012. doi: 10.1002/nme.4307.

M. Fivel and S. Forest. Plasticité cristalline et transition d'échelle: cas du monocristal. In *Etude des métaux et des alliages: état métallique*. Techniques de l'Ingénieur, 2004. in French.

S. M. Flatté, R. Dashen, W. H. Munk, K. M. Watson, and F. Zachariasen. *Sound transmission through a fluctuating ocean*. Cambridge University Press, 1979.

E. Florentin and P. Diez. Adaptive reduced basis strategy based on goal oriented error assessment for stochastic problems. *Comp. Meths. Appl. Mech. Engr.*, 225-228:116–127, 2012. doi: 10.1016/j.cma.2012.03.016.

J. Foo, X. Wan, and G. E. Karniadakis. The multi-element probabilistic collocation method (ME-PCM): Error analysis and applications. *J. Comp. Phys.*, 227(22):9572–9595, 2008. doi: 10.1016/j.jcp.2008.07.009.

J.-P. Fouque, J. Garnier, G. Papanicolaou, and K. Solna. *Wave propagation and time reversal in randomly layered media*, volume 56 of *Stochastic Modelling and Applied Probability*. Springer, 2007.

L. Frenje and C. Juhlin. Scattering attenuation: 2-D and 3-D finite difference simulations vs. theory. *J. Appl. Geophys.*, 44(1):33–46, 2000. doi: 10.1016/S0926-9851(00)00003-3.

U. Frisch. La propagation des ondes en milieu aléatoire et les équations stochastiques. *Annales Astrophysique*, 29:645–682, 1966.

U. Frisch. La propagation des ondes en milieu aléatoire et les équations stochastiques. II. applications. *Annales Astrophysique*, 30:565–601, 1967.

P. J. Gaebler, T. Eulenfeld, and U. Wegler. Seismic scattering and absorption parameters in the W-Bohemia/Vogtland region from elastic and acoustic radiative transfer theory. *Geophys. J. Int.*, 201:1471–1481, 2015. doi: 10.1093/gji/ggv393.

D. Galluzzo, M. La Rocca, L. Margerin, E. Del Pozzo, and R. Scarpa. Attenuation and velocity structure from diffuse coda waves: constraints from underground array data. *Phys. Earth Planetary Interiors*, 240:34–42, 2015. doi: 10.1016/j.pepi.2014.12.004.

B. Ganapathysubramanian and N. Zabaras. Modeling diffusion in random heterogeneous media: data-driven models, stochastic collocation and the variational multiscale method. *J. Comp. Phys.*, 226(1):326–353, 2007. doi: 10.1016/j.jcp.2007.04.009.

B. Ganapathysubramanian and N. Zabaras. A stochastic multiscale framework for modeling flow through random heterogeneous porous media. *J. Comp. Phys.*, 228(2):591–618, 2009. doi: 10.1016/j.jcp.2008.10.006.

M. J. Gander and C. Japhet. An algorithm with optimal complexity for non-matching grid projections. In M. Bercovier, M. J. Gander, R. Kornhuber, and O. Widlund, editors, *Domain Decomposition Methods in Science and Engineering XVIII*. Springer, 2008.

K. Gao, S. Fu, R. L. Gibson Jr., E. T. Chung, and Y. Efendiev. Generalized Multiscale Finite-Element Method (GMsFEM) for elastic wave propagation in heterogeneous, anisotropic media. *J. Comp. Phys.*, 295:161–188, 2015. doi: 10.1016/j.jcp.2015.03.068.

B. Garber, M. Cahay, and G. E. W. Bauer. Localization of Rayleigh waves. *Phys. Rev. B*, 62(19): 12831, 2000. doi: 10.1103/PhysRevB.62.12831.

S. Gavoille, C. Rey, C. Mariotti, and A. Delaplace. Stratégie de résolution en dynamique combinant des champs discret et continu. In *Proceedings of the 18th Conférence Française de Mécanique*, 2007.

M. G. D. Geers, V. G. Kouznetsova, and W. A. M. Brekelmans. Multi-scale computational homogenization: trends and challenges. *J. Comp. Appl. Math.*, 234(7):2175–2182, 2010. doi: 10.1016/j.cam.2009.08.077.

P. Gérard, P. A. Markowich, N. J. Mauser, and F. Poupaud. Homogenization limits and Wigner transforms. *Comm. Pure Appl. Math.*, 4:323–379, 1997.

A. Ghanem, M. Torkhani, N. Mahjoubi, T. N. Baranger, and A. Combescure. Arlequin framework for multi-model, multi-time scale and heterogeneous time integrators for structural transient dynamics. *Comp. Meths. Appl. Mech. Engr.*, 254:292–308, 2013. doi: 10.1016/j.cma.2012.08.019.

R. G. Ghanem and W. Brzakala. Stochastic finite-element analysis of soil layers with random interface. *J. Engr. Mech.*, 122(4):361–369, 1996. doi: 10.1061/(ASCE)0733-9399(1996)122:4(361).

D. Givon and I. G. Kevrekidis. Multiscale integration schemes for jump-diffusion systems. *SIAM Multiscale Model. Simul.*, 7(2):495–516, 2008. doi: 10.1137/070693473.

O. A. Grigorev and T. D. Shemergor. The scattering of ultrasonic waves by polycrystals. *Physica Status Solidi (a)*, 64(1):385–394, 1981. doi: 10.1002/pssa.2210640142.

J. M. Guedes and N. Kikuchi. Preprocessing and postprocessing for materials based on the homogenization method with adaptive finite element methods. *Comp. Meths. Appl. Mech. Engr.*, 83(2):143–198, 1990. doi: 10.1016/0045-7825(90)90148-F.

T. Guenounni and D. Aubry. Réponse homogénéisée en temps de structures sous chargements cycliques. *Comptes Rendus Acad. Sci. - Series IIB - Mech.-Phys.-Astron.*, 303(20):1765–1768, 1986.

J. Guilleminot, A. Noshadravan, C. Soize, and R. G. Ghanem. A probabilistic model for bounded elasticity tensor random fields with application to polycrystalline microstructures. *Comp. Meths. Appl. Mech. Engr.*, 200(17-20):1637–1648, 2011. doi: 10.1016/j.cma.2011.01.016.

L. Guillot, L. Aubry, F. Le Piver, C. Mariotti, O. Sèbe, E. Thauvin, C. Odonbaatar, M. Ulziibat, S. Demberel, and S. Sukhbaatar. Numerical simulation of seismic wave propagation: site effects. *Chocs*, 45:29–36, 2014.

C. B. Guo, P. Höller, and K. Goebbels. Scattering of ultrasonic waves in anisotropic polycrystalline metals. *Acustica*, 59(2):112–120, 1985.

A. A. Gusev. Representative volume element size for elastic composites: a numerical study. *J. Mech. Phys. Solids*, 45(9):1449–1459, 1997. doi: 10.1016/S0022-5096(97)00016-1.

A. A. Gusev and I. R. Abubakirov. Simulated envelopes of non-isotropically scattered body waves as compared to observed ones: another manifestation of fractal heterogeneity. *Geophys. J. Int.*, 127(1):49–60, 1996. doi: 10.1111/j.1365-246X.1996.tb01534.

H. Haddadi, C. Teodosiu, S. Héraud, L. Allais, and A. Zaoui. A "numerical mesoscope" for the investigation of local fields in rate-dependent elastoplastic materials at finite strain. In C. Miehe, editor, *IUTAM Symposium on Computational Mechanics of Solid Materials at Large Strains*, pages 311–320. Kluwer Academic Publishers, 2003.

M. Hadigol, A. Doostan, H. G. Matthies, and R. Niekamp. Partitioned treatment of uncertainty in coupled domain problems: a separated representation approach. *Comp. Meths. Appl. Mech. Engr.*, 274:103–124, 2014. doi: 10.1016/j.cma.2014.02.004.

A. Haned, E. Stutzmann, M. Schimmel, S. Kiselev, A. Davaille, and A. Yelles-Chaouche. Global tomography using seismic hum. *Geophys. J. Int.*, 204(2):1222–1236, 2016. doi: 10.1093/gji/ggv516.

S. Hartzell, S. Harmsen, and A. Frankel. Effects of 3D random correlated velocity perturbations on predicted ground motions. *Bull. Seism. Soc. Amer.*, 100(4):1415–1426, 2010. doi: 10.1785/0120090060.

M. Heckl, G. Hauck, and R. Wettschureck. Structure-borne sound and vibration from rail traffic. *J. Sound Vib.*, 193(1):175–184, 1996. doi: 10.1006/jsvi.1996.0257.

K. Helbig. Anisotropy and dispersion in periodically layered media. *Geophys.*, 49(4):364–373, 1984. doi: 10.1190/1.1441672.

K. Helbig and L. Thomsen. 75-plus years of anisotropy in exploration and reservoir seismics: a historical review of concepts and methods. *Geophys.*, 70(6):9–23, 2005. doi: 10.1190/1.2122407.

R. Hennino, N. Trégourès, N. M. Shapiro, L. Margerin, M. Campillo, B. A. van Tiggelen, and R. L. Weaver. Observation of equipartition of seismic waves. *Phys. Rev. Lett.*, 86(15):3447–3450, 2001. doi: 10.1103/PhysRevLett.86.3447.

S. Héraud, L. Allais, H. Haddadi, B. Marini, C. Teodosiu, and A. Zaoui. Du polycristal au multicristal: vers un mésoscope numérique. *Journal Physique IV*, 8(Pr4):27–32, 1998. doi: 10.1051/jp4:1998403.

M. Herraiz and A. F. Espinosa. Coda waves: a review. *Pure Appl. Geophys.*, 125(4):499–577, 1987. doi: 10.1007/BF00879572.

G. Hillers, M. Campillo, Y. Ben-Zion, and P. Roux. Seismic fault zone trapped noise. *J. Geophys. Res.: Solid Earth*, 119(7):5786–5799, 2014. doi: 10.1002/2014JB011217.

S. Hirsekorn. The scattering of ultrasonic waves in polycrystalline materials with texture. *J. Acoust. Soc. Amer.*, 77(3):832–843, 1985. doi: 10.1121/1.392052.

S. Hirsekorn. Elastic properties of polycrystals. *Textures Microstruct.*, 12(1-3):1–14, 1990. doi: 10.1155/TSM.12.1.

J. P. Hirth and J. Lothe. *Theory of dislocations*. Krieger Publications, second edition, 1982.

C. H. Hodges and J. Woodhouse. Theories of noise and vibration transmission in complex structures. *Rep. Progress Phys.*, 49(2):107–170, 1986. doi: 10.1088/0034-4885/49/2/001.

K. Holliger. Upper-crustal seismic velocity heterogeneity as derived from a variety of P-wave sonic logs. *Geophys. J. Int.*, 125(3):813–829, 1996. doi: 10.1111/j.1365-246X.1996.tb06025.x.

T.-K. Hong, R.-S. Wu, and B. L. N. Kennett. Stochastic features of scattering. *Phys. Earth Planetary Interiors*, 148(2-4):131–148, 2005. doi: 10.1016/j.pepi.2004.08.002.

U. Hornung. *Homogenization and porous media*. Springer, 2012.

T. Y. Hou and X.-H. Wu. A multiscale finite element method for elliptic problems in composite materials and porous media. *J. Comp. Phys.*, 134(1):169–189, 1997. doi: 10.1006/jcph.1997.5682.

T. Y. Hou, X.-H. Wu, and Z. Cai. Convergence of a multiscale finite element method for elliptic problems with rapidly oscillating coefficients. *Math. Comp.*, 68:913–943, 1999. doi: 10.1090/S0025-5718-99-01077-7.

H. Hu, A. Strybulevych, J. H. Page, S. E. Skipetrov, and B. A. van Tiggelen. Localization of ultrasound in a three-dimensional elastic network. *Nature Phys.*, 4:945–948, 2008. doi: 10.1038/nphys1101.

X. Huang and A. A. Maradudin. Propagation of surface acoustic waves across random gratings. *Phys. Rev. B*, 36(15):7827–2839, 1987. doi: 10.1103/PhysRevB.36.7827.

J. A. Hudson. A parabolic approximation for elastic waves. *Wave Motion*, 2(3):207–214, 1980. doi: 10.1016/0165-2125(80)90002-5.

T. J. R. Hughes. Multiscale phenomena: Green's functions, the Dirichlet-to-Neumann formulation, subgrid scale models, bubbles and the origins of stabilized methods. *Comp. Meths. Appl. Mech. Engr.*, 127(1-4):387–401, 1995. doi: 10.1016/0045-7825(95)00844-9.

T. J. R. Hughes, G. R. Feijóo, L. Mazzei, and J.-B. Quincy. The variational multiscale method – a paradigm for computational mechanics. *Comp. Meths. Appl. Mech. Engr.*, 166(1-2):3–24, 1998. doi: 10.1016/S0045-7825(98)00079-6.

H. Igel, G. Jahnke, and Y. Ben-Zion. Numerical simulation of fault zone guided waves: accuracy and 3-D effects. *Pure Appl. Geophys.*, 159:2067–2083, 2002.

W. Imperatori and P. M. Mai. Broad-band near-field ground motion simulations in 3-dimensional scattering media. *Geophys. J. Int.*, 192(2):725–744, 2013. doi: 10.1093/gji/ggs041.

B. Indraratna, W. Salim, and C. Rujikiatkamjorn. *Advanced rail geotechnology. Ballasted track*. CRC Press, 2011.

A. F. Ioffe and A. R. Regel. Non-crystalline, amorphous, and liquid electronic semiconductors. *Progress Semiconductors*, 4:237, 1960.

A. Ishimaru. *Wave propagation and scattering in random media*, volume 1-2. Academic Press, 1978.

E. T. Jaynes. Information theory and statistical mechanics. *Phys. Rev.*, 106(4):620–630, 1957. doi: 10.1103/PhysRev.106.620.

J. Jenkins, D. Johnson, L. La Ragione, and H. Makse. Fluctuations and the effective moduli of an isotropic, random aggregate of identical, frictionless spheres. *J. Mech. Phys. Solids*, 53(1):197–225, 2005. doi: 10.1016/j.jmps.2004.06.002.

X. Jia, C. Caroli, and B. Velicky. Ultrasound propagation in exernally stressed granular media. *Phys. Rev. Lett.*, 82(9):1863–1866, 1999. doi: 10.1103/PhysRevLett.82.1863.

X. Jing, P. Sheng, and M. Zhou. Theory of acoustic excitations in colloidal suspensions. *Phys. Rev. Lett.*, 66(9):1240–1243, 1991. doi: http://dx.doi.org/10.1103/PhysRevLett.66.1240.

X. Jing, P. Sheng, and M. Zhou. Acoustic and electromagnetic quasimodes in dispersed random media. *Phys. Rev. A*, 46(10):6513–6534, 1992. doi: 10.1103/PhysRevA.46.6513.

T. Kanit, S. Forest, I. Galliet, V. Mounoury, and D. Jeulin. Determination of the size of the representative volume element for random composites: statistical and numerical approach. *Int. J. Solids Struct.*, 40(13-14):3647–3679, 2003. doi: 10.1016/S0020-7683(03)00143-4.

F. C. Karal and J. B. Keller. Elastic, electromagnetic, and other waves in a random medium. *J. Math. Phys.*, 5(4):537–547, 1964. doi: 10.1063/1.1704145.

J. B. Keller. Accuracy and validity of the Born and Rytov approximations. *J. Opt. Soc. Amer.*, 59 (8):1003–1004, 1969. doi: 10.1364/JOSA.59.001003.

J. Kenter, H. Braaksma, K. Verwer, and X. van Lanen. Acoustic behavior of sedimentary rocks: geologic properties versus Poisson's ratios. *The Leading Edge*, 26(4):436–444, 2007. doi: 10.1190/1.2723206.

S. Khazaie, R. Cottereau, and D. Clouteau. Numerical observation of the equipartition regime in a 3D randomly heterogeneous elastic medium, and discussion on the limiting parameters. *Comp. & Geosci.*, 2016. Submitted for publication.

V. I. Klyatskin and V. I. Tatarskii. The parabolic equation approximation for propagation of waves in a medium with random inhomogeneities. *Soviet Physics JETP*, 31(2):335–339, 1970.

G. Kneib. The statistical nature of the upper continental crystalline crust derived from *in situ* seismic measurements. *Geophys. J. Int.*, 122(2):594–616, 1995. doi: 10.1111/j.1365-246X.1995.tb07015.x.

P. Koelemeijer, J. Ritsema, A. Deuss, and H.-J. van Heijst. SP12RTS: a degree-12 model of shear- and compressional-wave velocity for Earth's mantle. *Geophys. J. Int.*, 204(2):1024–1039, 2016. doi: 10.1093/gji/ggv481.

M. Korn and H. Sato. Synthesis of plane vector wave envelopes in two-dimensional random elastic media based on the Markov approximation and comparison with finite-difference simulations. *Geophys. J. Int.*, 161(3):839–848, 2005. doi: 10.1111/j.1365-246X.2005.02624.x.

V. G. Kouznetsova, W. A. M. Brekelmans, and F. P. T. Baaijens. An approach to micro-macro modeling of heterogeneous materials. *Comp. Mech.*, 27(1):37–48, 2001. doi: 10.1007/s004660000212.

S. M. Kozlov. Averaging of random operators. *Math. USSR Sbornik*, 37(2):167–180, 1980. doi: 10.1070/SM1980v037n02ABEH001948.

M. R. Kuhn. Structured deformation in granular materials. *Mech. Mat.*, 31(6):407–429, 1999. doi: 10.1016/S0167-6636(99)00010-1.

H. Kumagai, T. Saito, G. S. O'Brien, and T. Yamashina. Characterization of scattered seismic wavefields simulated in heterogeneous media with topography. *J. Geophys. Res.: Solid Earth*, 116(B03308):1–13, 2011. doi: 10.1029/2010JB007718.

P. Ladevèze and E. Florentin. Verification of stochastic models in uncertain environments using the constitutive relation error method. *Comp. Meths. Appl. Mech. Engr.*, 196(1-3):225–234, 2006. doi: 10.1016/j.cma.2006.03.006.

P. Ladevèze and J.-P. Pelle. *Mastering calculations in linear and nonlinear mechanics*. Mechanical Engineering. Springer, 2005.

A. Lagendijk, B. A. van Tiggelen, and D. S. Wiersma. Fifty years of Anderson localization. *Phys. Today*, 62(8):24–29, 2009. doi: 10.1063/1.3206091.

T. Landers and J. F. Claerbout. Numerical calculations of elastic waves in laterally inhomogeneous media. *J. Geophys. Res.*, 77(8):1476–1482, 1972. doi: 10.1029/JB077i008p01476.

V. D. Laptev. Construction and practical use of two-scaled extensions for rapidly oscillating functions. *J. Math. Sci.*, 158(2):211–218, 2009. doi: 10.1007/s10958-009-9384-4.

E. Larose, L. Margerin, B. A. van Tiggelen, and M. Campillo. Weak localization of seismic waves. *Phys. Rev. Lett.*, 93(4):048501, 2004. doi: 10.1103/PhysRevLett.93.048501.

C. Le Bris. Some numerical approaches for weakly random homogenization. In G. Kreiss, P. Lötstedt, A. Målqvist, and M. Neytcheva, editors, *Numerical Mathematics and Advanced Applications 2009*, pages 29–45. Springer-Verlag, 2010. doi: 10.1007/978-3-642-11795-4_3.

Y. Le Guennec, R. Cottereau, D. Clouteau, and C. Soize. A coupling method for stochastic continuum models at different scales. *Prob. Engr. Mech.*, 37:138–147, 2014. doi: 10.1016/j.probengmech.2013.10.005.

F-M. Li and Y.-S. Wang. Wave localization in randomly disordered multi-coupled multi-span beams on elastic foundations. *Waves Random Complex Media*, 16(3):261–279, 2006. doi: 10.1080/17455030600758552.

J. Li and S. I. Rokhlin. Propagation and scattering of ultrasonic waves in polycrystals with arbitrary crystallite and macroscopic texture symmetries. *Wave Motion*, 58:145–164, 2015. doi: 10.1016/j.wavemoti.2015.05.004.

W. L. Lim and G. R. McDowell. Discrete element modelling of railway ballast. *Granular Matter*, 7 (1):19–29, 2005. doi: 10.1007/s10035-004-0189-3.

C.-H. Liu, S. R. Nagel, D. A. Schecter, S. N. Coopersmith, S. Majumdar, O. Narayan, and T. A. Witten. Force fluctuations in bead packs. *Science*, 269(5223):513–515, 1995. doi: 10.1126/science.269.5223.513.

D. Liu. Analysis of multiscale methods for stochastic dynamical systems with multiple time scales. *SIAM Multiscale Model. Simul.*, 8(3):944–964, 2010. doi: 10.1137/090750664.

X. N. Liu, G. K. Hu, G. L. Huang, and C. T. Sun. An elastic metamaterial with simultaneously negative mass density and bulk modulus. *Appl. Phys. Lett.*, 98:251907, 2011. doi: 10.1063/1.3597651.

O. I. Lobkis and R. L. Weaver. Anderson localization of ultrasound in plates: further experimental results. *J. Acoust. Soc. Amer.*, 124(6):3528–3533, 2008. doi: 10.1121/1.2999345.

K. Lochmann, L. Oger, and D. Stoyan. Statistical analysis of random sphere packings with variable radius distribution. *Solid State Sci.*, 8(12):1397–1413, 2006. doi: 10.1016/j.solidstatesciences.2006.07.011.

G. Lombaert and D. Clouteau. Resonant multiple wave scattering in the seismic response of a city. *Waves Random Complex Media*, 16(3):205–230, 2006. doi: 10.1080/17455030600703574.

G. Lombaert, G. Degrande, J. Kogut, and S. François. The experimental validation of a numerical model for the prediction of railway induced vibrations. *J. Sound Vib.*, 297(3-5):512–535, 2006. doi: 10.1016/j.jsv.2006.03.048.

M. Lu and G. R. McDowell. The importance of modelling ballast particle shape in the discrete element method. *Granular Matter*, 9:69–80, 2007. doi: 10.1007/s10035-006-0021-3.

V. Lucas, J.-C. Golinval, S. Paquay, V.-D. Nguyen, L. Noels, and L. Wu. A stochastic computational multiscale approach: application to MEMS resonators. *Comp. Meths. Appl. Mech. Engr.*, 294:141–167, 2015. doi: 10.1016/j.cma.2015.05.019.

R. H. Lyon and R. G. DeJong. *Theory and application of statistical energy analysis*. Butterworth-Heinemann, 1995.

A. Ma, F. Roters, and D. Raabe. A dislocation density based constitutive model for crystal plasticity FEM including geometrically necessary dislocations. *Acta Mater.*, 54(8):2169–2179, 2006. doi: 10.1016/j.actamat.2006.01.005.

A. MacKinnon and B. Kramer. The scaling theory of electrons in disordered solids – additional numerical results. *Zeitschrift Physik B*, 53(1):1–13, 1983. doi: 10.1007/BF01578242.

F. Magoulès and I. Harari. Absorbing boundary conditions. *Comp. Meths. Appl. Mech. Engr.*, 195 (29-32):3551–3902, 2006.

J. Marchais, C. Rey, and L. Chamoin. Representation of localized phenomena in dynamics using multi-scale coupling. In B. H. V. Topping, editor, *Proceedings of the Eleventh International Conference on Computational Structures Technology*, number 252, pages 1–12, 2012.

L. Margerin. Attenuation, transport and diffusion of scalar waves in textured random media. *Tectonophys.*, 416(1-4):229–244, 2006. doi: 10.1016/j.tecto.2005.11.011.

L. Margerin, M. Campillo, N. M. Shapiro, and B. A. van Tiggelen. Residence time of diffuse waves in the crust as a physical interpretation of coda Q: application to seismograms recorded in Mexico. *Geophys. J. Int.*, 138(2):343–352, 1999. doi: 10.1046/j.1365-246X.1999.00897.x.

G. S. Martin, R. Wiley, and K. J. Marfurt. Marmousi2: an elastic upgrade for Marmousi. *Leading Edge*, 25(2):156–166, 2006. doi: 10.1190/1.2172306.

A. Martinez. *An introduction to semiclassical and microlocal analysis*. Springer, 2002.

W. P. Mason and H. J. McSkimin. Attenuation and scattering of high frequency sound waves in metals and glasses. *J. Acoust. Soc. Amer.*, 19(3):464–473, 1947.

L. Mathelin and O. le Maître. Dual-based *a posteriori* error estimate for stochastic finite element methods. *Comm. Appl. Math. Comp. Sci.*, 2(1):83–115, 2007. doi: 10.2140/camcos.2007.2.83.

H. G. Matthies. Stochastic finite elements: computational approaches to stochastic partial differential equations. *ZAMM - J. Appl. Math. Mech.*, 88(11):849–873, 2008. doi: 10.1002/zamm.200800095.

J. J. McCoy. A parabolic theory of stress wave propagation through inhomogeneous linearly elastic solids. *J. Appl. Mech.*, 44(3):462–468, 1977. doi: 10.1115/1.3424101.

S. Meille and E. J. Garboczi. Linear elastic properties of 2D and 3D models of porous materials made from elongated objects. *Modelling Simul. Mat. Sci. Engng.*, 9(5):371, 2001. doi: 10.1088/0965-0393/9/5/303.

J. M. Melenk and I. Babuška. The partition of unity finite element method: basic theory and applications. *Comp. Meths. Appl. Mech. Engr.*, 139(1-4):289–314, 1996. doi: 10.1016/S0045-7825(96)01087-0.

M. Meschede and B. Romanowicz. Lateral heterogeneity scales in regional and global upper mantle shear velocity models. *Geophys. J. Int.*, 200:1076–1093, 2015. doi: 10.1093/gji/ggu424.

K. C. Meza Fajardo. *Numerical simulation of wave propagation in unbounded elastic domains using the spectral element method*. PhD thesis, Università degli Studi di Pavia, Italy, 2007.

C. Miehe and A. Koch. Computational micro-to-macro transitions of discretized microstructures undergoing small strains. *Arch. Appl. Mech.*, 72(4):300–317, 2002. doi: 10.1007/s00419-002-0212-2.

G. W. Milton. *The theory of composites*. Cambridge Monographs on Applied and Computational Mechanics. Cambridge University Press, 2002.

N. Moës, J. Dolbow, and T. Belytschko. A finite element method for crack growth without remeshing. *Int. J. Numer. Meth. Engr.*, 46(1):131–150, 1999. doi: 10.1002/(SICI)1097-0207(19990910)46:1<131::AID-NME726>3.0.CO;2-J.

D. Moos and M. D. Zoback. In situ studies of velocity in fractured crystalline rocks. *J. Geophys. Res.: Solid Earth*, 88(B3):2345–2358, 1983. doi: 10.1029/JB088iB03p02345.

J. J. Moreau. Unilateral contact and dry friction in finite freedom dynamics. In J. J. Moreau and P. D. Panagiotopoulos, editors, *Nonsmooth mechanics and applications*, volume 302 of *CISM Courses and Lectures*, pages 1–81, 1989.

J. J. Moreau. The stress tensor in granular media and in other mechanical collections. In B. Cambou, M. Jean, and F. Radjaï, editors, *Micromechanics of granular materials*. Wiley, 2001.

H. Moulinec and P. Suquet. A numerical method for computing the overall response of nonlinear composites with complex microstructures. *Comp. Meths. Appl. Mech. Engr.*, 157(1-2):69–94, 1998. doi: 10.1016/S0045-7825(97)00218-1.

O. Mouraille and S. Luding. Sound wave propagation in weakly polydisperse granular materials. *Ultrasonics*, 48(6-7):498–505, 2008. doi: 10.1016/j.ultras.2008.03.009.

P. Mu. *Study of crack initiation in low-cycle fatigue of an austenitic stainless steel*. PhD thesis, École Centrale de Lille, France, 2011.

S. R. Murthy. A study of ultrasonic velocity and attenuation on polycrystalline Ni-Zn ferrites. *Bull. Mater. Sci.*, 24(6):611–616, 2001. doi: 10.1007/BF02704009.

N. Nakata and G. C. Beroza. Stochastic characterization of mesoscale seismic velocity heterogeneity in Long Beach, California. *Geophys. J. Int.*, 203:2049–2054, 2015. doi: 10.1093/gji/ggv421.

D. Néron, H. Ben Dhia, and R. Cottereau. A decoupled strategy to solve reduced-order multimodel problems in the PGD and Arlequin frameworks. *Comp. Mech.*, 57(4):509–521, 2015. doi: 10.1007/s00466-015-1236-0.

N.-S. Nguyen, H. Magoariec, and B. Cambou. Local stress analysis in granular materials at a mesoscale. *Int. J. Numer. Anal. Meth. Geomech.*, 36:1609–1635, 2012. doi: 10.1002/nag.1063.

K. Nishigami. Deep crustal heterogeneity along and around the San Andreas fault system in central California and its relation to the segmentation. *J. Geophys. Res.: Solid Earth*, 105(B4): 7983–7998, 2000. doi: 10.1029/1999JB900381.

J. Nolen, G. C. Papanicolaou, and O. Pironneau. A framework for adaptive multiscale methods for elliptic problems. *SIAM Multiscale Model. Simul.*, 7(1):171–196, 2008. doi: 10.1137/070693230.

G. Nolet. *A breviary of seismic tomography: imaging the interior of the Earth and sun*. Cambridge University Press, 2008.

A. N. Norris. Diffuse wave density and directionality in anisotropic solids. *J. Acoust. Soc. Amer.*, 123(3):1399–1408, 2008. doi: 10.1121/1.2836755.

A. Nouy. Recent developments in spectral stochastic methods for the numerical solution of stochastic partial differential equations. *Arch. Comp. Meths. Engr.*, 16(3):251–285, 2009. doi: 10.1007/s11831-009-9034-5.

A. Nouy and A. Clément. Extended stochastic finite element method for the numerical simulation of heterogeneous materials with random material interfaces. *Int. J. Numer. Meth. Engr.*, 83(10): 1312–1344, 2010. doi: 10.1002/nme.2865.

G. S. O'Brien and C. J. Bean. Volcano topography, structure and intrinsic attenuation: their relative influences on a simulated 3D visco-elastic wavefield. *J. Volcan. Geotherm. Res.*, 183(1-2): 122–136, 2009. doi: 10.1016/j.jvolgeores.2009.03.004.

J. T. Oden, I. Babuška, F. Nobile, Y. Feng, and R. Tempone. Theory and methodology for estimation and control of errors due to modeling, approximation, and uncertainty. *Comp. Meths. Appl. Mech. Engr.*, 194(2-5):195–204, 2005. doi: 10.1016/j.cma.2003.06.003.

M. L. Oristaglio. Accuracy of the Born and Rytov approximations for reflection and refraction at a plane interface. *J. Opt. Soc. Amer.*, 2(11):1987–1992, 1985. doi: 10.1364/JOSAA.2.001987.

M. Ostoja-Starzewski. *Microstructural randomness and scaling in mechanics of materials*. CRC Press, 2007.

J. C. J. Paasschens. Solution of the time-dependent Boltzmann equation. *Phys. Rev. E*, 56(1): 1135–1141, 1997. doi: 10.1103/PhysRevE.56.1135.

J. H. Page, P. Sheng, H. P. Schriemer, I. Jones, X. Jing, and D. A. Weitz. Group velocity in strongly scattering media. *Science*, 271(5249):634–637, 1996. doi: 10.1126/science.271.5249.634.

R. Paolucci, A. Maffeis, L. Scandella, M. Stupazzini, and M. Vanini. Numerical prediction of low-frequency ground vibrations induced by high-speed trains at Ledsgaard, Sweden. *Soil Dyn. Earthquake Engr.*, 23(6):425–433, 2003. doi: 10.1016/S0267-7261(03)00061-7.

E. P. Papadakis. Ultrasonic attenuation and velocity in three transformation products in steel. *J. Appl. Phys.*, 35(5):1474–1482, 1964. doi: 10.1063/1.1713652.

E. P. Papadakis. Ultrasonic attenuation caused by scattering in polycrystalline metals. *J. Acoust. Soc. Amer.*, 37(4):711–717, 1965. doi: 10.1121/1.1909401.

G. C. Papanicolaou and S. R. S. Varadhan. Boundary value problems with rapidly oscillating random coefficients. In J. Fritz and J. L. Lebowitz, editors, *Proceedings of the Conference on Random Fields*, volume 2 of *Seria Colloquia Mathematica Societatis Janos Bolyai*, pages 835–873. North Holland, 1981.

R. Paroni. Homogenization of polycrystalline aggregates. *Arch. Rational Mech. Anal.*, 151(4):311–337, 2000. doi: 10.1007/s002050050199.

A. Paul, M. Campillo, L. Margerin, E. Larose, and A. Derode. Empirical synthesis of time-asymmetrical Green functions from the correlation of coda waves. *J. Geophys. Res.: Solid Earth*, 110(B08302):1–13, 2005. doi: 10.1029/2004JB003521.

K.-K. Phoon and F. H. Kulhawy. Characterization of geotechnical variability. *Canadian Geotech. J.*, 36(4):612–624, 1999. doi: 10.1139/t99-038.

C. Pierre. Weak and strong vibration localization in disordered structures: a statistical investigation. *J. Sound Vib.*, 139(1):111–132, 1990. doi: 10.1016/0022-460X(90)90779-Y.

A. Pitarka and G. Ichinose. Simulating forward and backward scattering in viscoelastic 3D media with random velocity variations and basin structure. Technical Report 06HQGR0042, USGS, 2009.

G. W. Postma. Wave propagation in a stratified medium. *Geophys.*, 20(4):780–806, 1955. doi: 10.1190/1.1438187.

G. L. Povirk. Incorporation of microstructural information into models of two-phase materials. *Acta Metall. Mater.*, 43(8):3199–3206, 1995. doi: 10.1016/0956-7151(94)00487-3.

F. Radjai, M. Jean, J.-J. Moreau, and S. Roux. Force distributions in dense two-dimensional granular systems. *Phys. Rev. Lett.*, 77(2):274–277, 1996. doi: 10.1103/PhysRevLett.77.274.

F. Radjai, D. Wolf, M. Jean, and J. J. Moreau. Bimodal character of stress transmission in granular packings. *Phys. Rev. Lett.*, 80:61–64, 1998. doi: 10.1103/PhysRevLett.80.61.

C. Redenbach. Microstructure models for cellular materials. *Comp. Mat. Sci.*, 44(4):1397–1407, 2009. doi: 10.1016/j.commatsci.2008.09.018.

J. Renard and M. F. Marmonier. Étude de l'initiation de l'endommagement dans la matrice d'un matériau composite par une méthode d'homogénéisation. *La Recherche Aérospatiale*, 6:43–51, 1987.

M. Renouf, F. Dubois, and P. Alart. A parallel version of the non smooth contact dynamics algorithm applied to the simulation of granular media. *J. Comp. Appl. Math.*, 168(1-2):375–382, 2004. doi: 10.1016/j.cam.2003.05.019.

A. P. Roberts and E. J. Garboczi. Elastic properties of model porous ceramics. *J. Amer. Ceramic Soc.*, 83(12):3041–3048, 2000. doi: 10.1111/j.1151-2916.2000.tb01680.x.

P. Ropars and C. Desceliers. A modal strategy devoted to the hidden state variables method with large interfaces. *Comp. Mech.*, 55(5):805–818, 2015. doi: 10.1007/s00466-015-1148-z.

M. Rosenblatt. Remarks on a multivariate transformation. *Annals Math. Stat.*, 23(3):470–472, 1952.

F. Roters, P. Eisenlohr, T. R. Bieler, and D. Raabe. *Crystal plasticity finite element methods in materials science and engineering*. John Wiley and Sons, 2011.

L. Rothenburg and N. P. Kruyt. Micromechanical definition of an entropy for quasi-static deformation of granular materials. *J. Mech. Phys. Solids*, 57(3):634–655, 2009. doi: 10.1016/j.jmps.2008.09.018.

H. Rue. Fast sampling of Gaussian Markov random fields. *J. Roy. Stat. Soc.*, B63:325–338, 2001.

S. M. Rytov, Y. A. Kravtsov, and V. I. Tatarskii. *Principles of statistical radiophysics: wave propagation through random media*. Springer, 1989.

L. Ryzhik, G. Papanicolaou, and J. B. Keller. Transport equations for elastic and other waves in random media. *Wave Motion*, 24:327–370, 1996. doi: 10.1016/S0165-2125(96)00021-2.

K. Sab. On the homogenization and the simulation of random materials. *Europ. J. Mech. A/Solids*, 11(5):585–607, 1992.

T. Saito, H. Sato, and M. Ohtake. Envelope broadening of spherically outgoing waves in three-dimensional random media having power-law spectra. *J. Geophys. Res.: Solid Earth*, 107(B5): 1–15, 2002. doi: 10.1029/2001JB000264.

T. Saito, H. Sato, M. Fehler, and M. Ohtake. Simulating the envelope of scalar waves in 2D random media having power-law spectra of velocity fluctuation. *Bull. Seism. Soc. Amer.*, 93(1): 240–252, 2003. doi: 10.1785/0120020105.

E. E. Salpeter and H. A. Bethe. A relativistic equation for bound-state problems. *Phys. Rev.*, 84(6): 1232–1242, 1951. doi: 10.1103/PhysRev.84.1232.

Y. Samuelides. Velocity shift using the Rytov approximation. *J. Acoust. Soc. Amer.*, 104:2596, 1998.

M. Satake. Some considerations on the mechanics of granular materials. In E. Kröner, editor, *Proceedings of the IUTAM Symposium on the Generalized Cosserat Continuum and the Continuum Theory of Dislocations with Applications*, 1968. doi: 10.1007/978-3-662-30257-6_19.

H. Sato. Attenuation and envelope formation of three-component seismograms of small local earthquakes in randomly inhomogeneous lithosphere. *J. Geophys. Res.*, 89:1221–1241, 1984. doi: 10.1029/JB089iB02p01221.

H. Sato. Broadening of seismogram envelopes in the randomly inhomogeneous lithosphere based on the parabolic approximation: Southeastern Honshu, Japan. *J. Geophys. Res.: Solid Earth*, 94 (17):735–747, 1989. doi: 10.1029/JB094iB12p17735.

H. Sato. Energy transportation in one- and two-dimensional scattering media: analytic solutions of the multiple isotropic scattering model. *Geophys. J. Int.*, 112(1):141–146, 1993. doi: 10.1111/j.1365-246X.1993.tb01443.x.

H. Sato. Multiple isotropic scattering model including P-S conversions for the seismogram envelope formation. *Geophys. J. Int.*, 117:487–494, 1994. doi: 10.1111/j.1365-246X.1994.tb03946.x.

H. Sato and M. C. Fehler. Synthesis of seismogram envelopes in heterogeneous media. *Adv. Geophys.*, 48:561–596, 2007. doi: 10.1016/S0065-2687(06)48010-9.

H. Sato, M. C. Fehler, and T. Maeda. *Seismic wave propagation and scattering in the heterogeneous earth*. Springer, second edition, 2012.

E. Savin. Propagation d'ondes élastiques hautes fréquences en milieux hétérogènes. Rapport d'habilitation à diriger des recherches, Université Pierre et Marie Curie, 2010.

E. Savin. High-frequency dynamics of heterogeneous slender structures. *J. Sound Vib.*, 332(10): 2461–2487, 2013. doi: 10.1016/j.jsv.2012.10.009.

C. M. Sayers. Scattering of ultrasound by minority phases in polycrystalline metals. *Wave Motion*, 7(1):95–104, 1985. doi: 10.1016/0165-2125(85)90029-0.

M. Schevenels, G. Lombaert, G. Degrande, and S. François. A probabilistic assessment of resolution in the SASW test and its impact on the prediction of ground vibrations. *Geophys. J. Int.*, 172(1):262–275, 2008. doi: 10.1111/j.1365-246X.2007.03626.x.

S. Schilt, J. Oliver, L. Brown, S. Kaufman, D. Albauch, J. Brewer, F. Cook, L. Jensen, P. Krumhansl, G. Long, and D. Steiner. The heterogeneity of the continental crust: results from deep crustal reflection profiling using the Vibroseis technique. *Rev. Geophys.*, 17(2):354–368, 1979. doi: 10.1029/RG017i002p00354.

E. Schisselé, S. Gaffet, and Y. Cansi. Characterization of regional and local scattering effects from small-aperture seismic array recordings. *J. Seismology*, 9(2):137–149, 2005. doi: 10.1007/s10950-005-8234-1.

J. Schwartz. *Approche non locale en plasticité cristalline: application à l'étude du comportement mécanique de l'acier AISI 316LN en fatigue oligocyclique*. PhD thesis, École Centrale Paris, 2011. in French.

J. F. M. Scott. The statistics of waves propagating in a one-dimensional random medium. *Proc. Royal Soc. A*, 398(1815):341–363, 1985. doi: 10.1098/rspa.1985.0038.

R. Sepehrinia, A. Bahraminasab, M. Sahimi, and M. Reza Rahimi Tabar. Dynamic renormalization group analysis of propagation of elastic waves in two-dimensional heterogeneous media. *Phys. Rev. B*, 77(014203):1–12, 2008. doi: 10.1103/PhysRevB.77.014203.

T. Shang and L. Gao. Transportation theory of multiple scattering and its application to seismic coda waves of impulsive source. *Scientia Sinica (series B, China)*, 31:1503–1514, 1988.

C. E. Shannon. A mathematical theory of communication. *Bell Syst. Techn. J.*, 27:379–423;623–656, 1948. doi: 10.1145/584091.584093.

N. M. Shapiro, M. Campillo, L. Margerin, S. K. Singh, V. Kostoglodov, and J. Pacheco. The energy partitioning and the diffusive character of the seismic coda. *Bull. Seism. Soc. Amer.*, 90 (3):655–665, 2000. doi: 10.1785/0119990021.

S. A. Shapiro and G. Kneib. Seismic attenuation by scattering: theory and numerical results. *Geophys. J. Int.*, 114(2):373–391, 1993. doi: 10.1111/j.1365-246X.1993.tb03925.x.

P. Shearer. Seismic scattering in the deep Earth. In G. Schubert, editor, *Treatise on geophysics*, volume 1: Deep Earth Structure, pages 695–730, 2007.

P. Sheng. *Introduction to wave scattering, localization and mesoscopic phenomena*. Springer Series in Materials Science. Springer, second edition, 2006.

W. Shi and C. Zhang. Error analysis of generalized polynomial chaos for nonlinear random ordinary differential equations. *Appl. Numer. Math.*, 62(12):1954–1964, 2012. doi: 10.1016/j.apnum.2012.08.007.

H. Shin and J. Santamarina. Role of particle angularity on the mechanical behavior of granular mixtures. *J. Geotech. Geoenv. Engr.*, 139(2):353–355, 2013. doi: 10.1061/(ASCE)GT.1943-5606.0000768.

M. Shinozuka and G. Deodatis. Simulation of stochastic processes by spectral representation. *Appl. Mech. Rev.*, 44(4):191–205, 1991. doi: 10.1115/1.3119501.

K. Shiomi, H. Sato, and M. Ohtake. Broad-band power-law spectra of well-log data in Japan. *Geophys. J. Int.*, 130:57–64, 1997. doi: 10.1111/j.1365-246X.1997.tb00987.x.

P. J. Shorter and R. S. Langley. Vibro-acoustic analysis of complex systems. *J. Sound Vib.*, 288: 669–699, 2005. doi: 10.1016/j.jsv.2005.07.010.

G. Simmons and H. Wang. *Single crystal elastic constants and calculated aggregate properties: a handbook*. MIT Press, 1971.

C. Soize. A nonparametric model of random uncertainties for reduced matrix models in structural dynamics. *Prob. Engr. Mech.*, 15:277–294, 2000.

C. Soize. Maximum entropy approach for modeling random uncertainties in transient elastodynamics. *J. Acoust. Soc. Amer.*, 109(5):1979–1996, 2001.

C. Soize. Random matrix theory for modeling uncertainties in computational mechanics. *Comp. Meths. Appl. Mech. Engr.*, 194:1333–1366, 2005.

F. E. Stanke and G. S. Kino. A unified theory for elastic wave propagation in polycrystalline materials. *J. Acoust. Soc. Amer.*, 75(3):665–681, 1984. doi: 10.1121/1.390577.

Q.-A. Ta, D. Clouteau, and R. Cottereau. Modeling of random anisotropic elastic media and impact on wave propagation. *Europ. J. Comput. Mech.*, 19(1-3):241–253, 2010. doi: 10.3166/ejcm.19.241-253.

E. B. Tadmor, M. Ortiz, and R. Philipps. Quasicontinuum analysis of defects in solids. *Phil. Mag. A*, 73(6):1529–1563, 1996. doi: 10.1080/01418619608243000.

T. Takahashi, H. Sato, T. Nishimura, and K. Obara. Tomographic inversion of the peak delay times to reveal random velocity fluctuations in the lithosphere: method and application to northestearn Japan. *Geophys. J. Int.*, 178(3):1437–1455, 2009. doi: 10.1111/j.1365-246X.2009.04227.x.

S. Takemura and T. Furumura. Scattering of high-frequency p wavefield derived by dense hi-net array observations in japan and computer simulations of seismic wave propagations. *Geophys. J. Int.*, 193(1):421–436, 2013. doi: 10.1093/gji/ggs127.

S. Takemura, T. Furumura, and T. Maeda. Scattering of high-frequency seismic waves caused by irregular surface topography and small-scale velocity inhomogeneity. *Geophys. J. Int.*, 201: 459–474, 2015. doi: 10.1093/gji/ggv038.

F. D. Tappert. The parabolic approximation method. In J. B. Keller and J. S. Papadakis, editors, *Wave Propagation and Underwater Acoustics*, volume 70 of *Lecture Notes in Physics*, pages 224–287, 1977. doi: 10.1007/3-540-08527-0_5.

L. Tartar. *The general theory of homogenization: a personalized introduction*, volume 7 of *Lecture notes of the Unione Matematica Italiana*. Springer, 2009.

K. Teferra and L. Graham-Brady. Tesselation growth models for polycrystalline microstructures. *Comp. Mat. Sci.*, 102:57–67, 2015. doi: 10.1016/j.commatsci.2015.02.006.

H. Thi Minh Phuong, P. Alart, D. Dureisseix, and G. Saussine. A domain decomposition method for granular dynamics using discrete elements and application to railway ballast. *Ann. Solid Struct. Mech.*, 2(2-4):87–98, 2011. doi: 10.1007/s12356-011-0020-x.

S. Torquato. *Random heterogeneous materials. Microstructure and macroscopic properties*. Springer, 2001.

V. Tournat and V. E. Gusev. Nonlinear effects for coda-type elastic waves in stressed granular media. *Phys. Rev. E*, 80(011306):1–11, 2009. doi: 10.1103/PhysRevE.80.011306.

N. P. Trégourès and B. A. van Tiggelen. Generalized diffusion equation for multiple scattered elastic waves. *Waves Random Media*, 12(1):21–38, 2002. doi: 10.1088/0959-7174/12/1/302.

T. Tsuchikura and M. Satake. Statistical measure tensors and their application to computer simulation analysis of biaxial compression text. In H. Murakami and J. E. Luco, editors, *Engineering Mechanics: a Force for 21st Century*, pages 1732–1735. ASCE, 1998.

I. Tsvankin, J. Gaiser, V. Grechka, M. van der Baan, and L. Thomsen. Seismic anisotropy in exploration and reservoir characterization: an overview. *Geophys.*, 75(5):15–29, 2010.

J. A. Turner. Scattering and diffusion of seismic waves. *Bull. Seism. Soc. Amer.*, 88(1):276–283, 1998.

J. A. Turner and R. L. Weaver. Radiative transfer and multiple scattering of diffuse ultrasound in polycrystalline media. *J. Acoust. Soc. Amer.*, 96(6):3675–3683, 1994. doi: 10.1121/1.410587.

L. F. Uhrig and F. A. van Melle. Velocity anisotropy in stratified media. *Geophys.*, 20(4):774–779, 1955. doi: 10.1190/1.1438185.

M. C. W. van Rossum and T. M. Nieuwenhuizen. Multiple scattering of classical waves: microscopy, mesoscopy, and diffusion. *Rev. Modern Phys.*, 71(1):313–371, 1999. doi: 10.1103/RevModPhys.71.313.

A. Vattré, B. Devincre, F. Feyel, R. Gatti, S. Groh, O. Jamond, and A. Roos. Modelling crystal plasticity by 3D dislocation dynamics and the finite element method: the Discrete-Continuous Model revisited. *J. Mech. Phys. Solids*, 63:491–505, 2014. doi: 10.1016/j.jmps.2013.07.003.

V. Červený. *Seismic Ray Theory*. Cambridge University Press, 2005.

V. Červený, L. Klimeš, and I. Pšenčík. Seismic ray method: recent developments. *Adv. Geophys.*, 48:1–126, 2007. doi: 10.1016/S0065-2687(06)48001-8.

B. Velamur Asokan and N. Zabaras. Variational multiscale stabilized FEM formulations for transport equations: stochastic advection-diffusion and incompressible stochastic Navier-Stokes equations. *J. Comp. Phys.*, 202(1):94–133, 2005. doi: 10.1016/j.jcp.2004.06.019.

B. Velamur Asokan and N. Zabaras. A stochastic variational multiscale method for diffusion in heterogeneous random media. *J. Comp. Phys.*, 218(2):654–676, 2006. doi: 10.1016/j.jcp.2006.02.026.

D. Vollhardt and P. Wölfle. Diagrammatic, self-consistent treatment of the Anderson localization problem in $d \leq 2$ dimensions. *Phys. Rev. B*, 22(10):4666–4679, 1980. doi: 10.1103/PhysRevB.22.4666.

S. C. Wales and J. J. McCoy. A comparison of parabolic waves theories for linearly elastic solids. *Wave Motion*, 5(2):99–113, 1983. doi: 10.1016/0165-2125(83)90027-6.

K. Walton. The effective elastic moduli of a random packing of spheres. *J. Mech. Phys. Solids*, 35 (2):213–226, 1987. doi: 10.1016/0022-5096(87)90036-6.

R. L. Weaver. Diffusivity of ultrasound in polycrystals. *J. Mech. Phys. Solids*, 38(1):55–86, 1990a. doi: 10.1016/0022-5096(90)90021-U.

R. L. Weaver. Anderson localization of ultrasound. *Wave Motion*, 12(2):129–142, 1990b. doi: 10.1016/0165-2125(90)90034-2.

R. L. Weaver and W. Sachse. Diffusion of ultrasound in glass bead slurry. *J. Acoust. Soc. Amer.*, 97 (4):2094, 1995. doi: 10.1121/1.412002.

J. Weber. Recherches concernant les contraintes intergranulaires dans les milieux pulvérulents. *Bulletin Liaison Ponts Chaussées*, 1966.

M. Weber and U. Münch, editors. *Tomography of the Earth's crust: from geophysical sounding to real-time monitoring*. Number 21 in GEOTECHNOLOGIEN Science Report. Springer, 2014.

C. Wellmann and P. Wriggers. A two-scale model of granular materials. *Comp. Meths. Appl. Mech. Engr.*, 205-208:46–58, 2012. doi: 10.1016/j.cma.2010.12.023.

N.-E. Wiberg and P. Díez. Adaptive modeling and simulation. *Comp. Meths. Appl. Mech. Engr.*, 195(4-6):205–480, 2006.

J. R. Willis. Dynamics of composites. In P. Suquet, editor, *Continuum micromechanics*, International Centre for Mechanical Sciences, pages 265–290. CISM Udine, Springer, 1997. doi: 10.1007/978-3-7091-2662-2_5.

J. R. Willis. The construction of effective relations for waves in a composite. *Comptes Rendus Mécanique*, 340(4-5):181–192, 2012. doi: 10.1016/j.crme.2012.02.001.

M. J. Woodward. A qualitative comparison of the first-order Born and Rytov approximations. Report SEP-60, Stanford Exploration Project, 1989.

R.-S. Wu. Attenuation of short period seismic waves due to scattering. *Geophys. Res. Lett.*, 9(1): 9–12, 1982. doi: 10.1029/GL009i001p00009.

R.-S. Wu. Multiple scattering and energy transfer of seismic waves - separation of scattering effects from intrinsic attenuation. I. theoretical modelling. *Geophys. J. Int.*, 82(1):57–80, 1985. doi: 10.1111/j.1365-246X.1985.tb05128.x.

R.-S. Wu and K. Aki. Multiple scattering and energy transfer of seismic waves - separation of scattering effects from intrinsic attenuation. II. Application of the theory to Hindu-Kush region. *Pure Appl. Geophys.*, 128:49–80, 1988a. doi: 10.1007/BF01772590.

R.-S. Wu and K. Aki. Introduction: seismic wave scattering in three-dimensionally heterogeneous Earth. *Pure Appl. Geophys.*, pages 1–6, 1988b. doi: 10.1007/978-3-0348-7722-0_1. Pageoph Topical Volume "Scattering and Attenuations of Seismic Waves".

R.-S. Wu, Z. Xu, and X. P. Li. Heterogeneity spectrum and scale-anisotropy in the upper crust revealed by the German Continental Deep-Drilling (KTB) holes. *Geophys. Res. Lett.*, 21:911–914, 1994. doi: 10.1029/94GL00772.

S. P. Xiao and T. Belytschko. A bridging domain method for coupling continua with molecular dynamics. *Comp. Meths. Appl. Mech. Engr.*, 193(17-20):1645–1669, 2004. doi: 10.1016/j.cma.2003.12.053.

D. B. Xiu and D. M. Tartakovsky. Numerical methods for differential equations in random domains. *SIAM J. Sci. Comp.*, 28(3):1167–1185, 2006. doi: 10.1137/040613160.

X. F. Xu. A multiscale stochastic finite element method on elliptic problems involving uncertainties. *Comp. Meths. Appl. Mech. Engr.*, 196(25-28):2723–2736, 2007. doi: 10.1016/j.cma.2007.02.002.

Z. Yang, J. Mei, M. Yang, N. H. Chan, and P. Sheng. Membrane-type acoustic metamaterials with negative dynamic mass. *Phys. Rev. Lett.*, 101(20):204301, 2008. doi: 10.1103/PhysRevLett.101.204301.

T. Yu and X. Y. Yue. Residual-free bubble methods for numerical homogenization of elliptic problems. *Comp. Mat. Sci.*, 9(4):1163–1176, 2011. doi: 10.4310/CMS.2011.v9.n4.a12.

V. V. Yurinskii. Averaging an elliptic boundary-value problem with random coefficients. *Siberian Math. J.*, 21(3):470–482, 1980. doi: 10.1007/BF00968192.

J. Yvonnet and G. Bonnet. Nonlocal/coarse-graining homogenization of linear elastic media with non-separated scales using least-square polynomial filters. *Int. J. Multiscale Comp. Engr.*, 12(5): 375–395, 2014. doi: 10.1615/IntJMultCompEng.2014010414.

J. Zeman and M. Šejnoha. Numerical evaluation of effective elastic properties of graphite fiber tow impregnated by polymer matrix. *J. Mech. Phys. Solids*, 49(1):69–90, 2001. doi: 10.1016/S0022-5096(00)00027-2.

Y. Zeng. Compact solutions for multiple scattered wave energy in time domain. *Bull. Seism. Soc. Amer.*, 81(3):1022–1029, 1991.

G. Zhang and M. Gunzburger. Error analysis of a stochastic collocation method for parabolic partial differential equations with random input data. *SIAM J. Numer. Anal.*, 50(4):1922–1940, 2012. doi: 10.1137/11084306X.

H. Zhang and C. Thurber. Double-difference tomography: the method and its application to the Hayward fault, California. *Bull. Seism. Soc. Amer.*, 93(5):1875–1889, 2003. doi: 10.1785/0120020190.

D. Zhao, Z. Wang, N. Umino, and A. Hasegawa. Mapping the mantle wedge and interplate thrust zone of the northeast Japan arc. *Tectonophys.*, 467(1-4):89–106, 2009. doi: 10.1016/j.tecto.2008.12.017.

N. I. Zheludev and Y. S. Kivshar. From metamaterials to metadevices. *Nature Mater.*, 11:917–924, 2012. doi: 10.1038/nmat3431.

Y. Zheng, F. Su, and K. Aki. Scattering wave energy propagation in a random isotropic scattering medium. 1. Theory. *J. Geophys. Res.*, 96:607–619, 1991. doi: 10.1029/90JB02012.

V. V. Zhikov, S. M. Kozlov, O. A. Oleinik, and K. T. Ngoan. Averaging and G-convergence of differential operators. *Russian Math. Surv.*, 34:69, 1979. doi: 10.1070/RM1979v034n05ABEH003898.

O. C. Zienkiewicz and J. Z. Zhu. A simple error estimator and adaptive procedure for practical engineering analysis. *Int. J. Numer. Meth. Engr.*, 24:337–357, 1987.